Design of Nanoparticles That Cross the Blood-Brain Barrier by Receptor Mediated Transcytosis

Thesis by

Devin Thomas Wiley

In Partial Fulfillment of the Requirements

for the Degree of

Doctor of Philosophy

California Institute of Technology

Pasadena, California

2013

(Defended May 1, 2013)

Acknowledgements

I must first acknowledge my wife, Jill Craven. I can't say how much I appreciate her support of my decision to pursue an MD/PhD program, and the patience she has shown for the long hours I have spent in both medical school and in the lab while at Caltech. I am forever grateful to Jill for staying at my side through this experience, and for always supporting and loving me.

Next, I would like to thank my advisor Mark Davis for his academic support and mentorship. I am grateful that Mark has proven to me that a chemical engineer can be successful in the field of medical translational research. Because of him I know that chemical engineers have much to offer medicine, and I hope that I can offer as much to medicine in my career as he already has. I thank him for all of the collaborations he facilitated and all of the financial support he provided.

I would like to thank Yashodan Bhawe, my office mate of four years, and Jonathan Zuckerman for their friendship, all of the laughs we shared, and for making the workday enjoyable. I want to thank Yasho for helping me become a little more computer savvy and for teaching me Matlab. I would like to thank John Zuckerman for all of our stimulating discussions and for his moral support as I attempted to break out of my comfort zone of chemical engineering.

I would like to thank all of my collaborators who were immensely helpful and who taught me the many scientific techniques that I now take for granted. I would like to thank Dr. David Stout, Dr. Waldemar Ladno, Graciella Flores, and Jeff Collins at UCLA for helping me execute the ^{64}Cu and PET/CT studies. I thank Dr. Rex Moats and Dr. Gevorg Karapetyan at CHLA for their help with the MRI, Fluorescence Xenogen

imaging and SPECT/CT studies. I thank Dr. Towhid Salam at USC for his help with biostatistics. I thank Dr. Yen Yuan and Dr. Joseph Chao at City of Hope for their guidance and warm conversation about translational medicine. At Caltech I thank Dr. Nathan Dalleska for his help with the ICP-MS studies, Dr. Mona Shahgholi for her help with MALDI-TOF, Dr. Carol Garland and Dr. Alasdair McDowell for their help with TEM and cryo TEM respectively, Gwen Williams and Dr. Laura Parsley for their help with animal handling (especially the perfusion fixation experiments), and Dr. Thai Truong for his time teaching me and training me on the confocal microscope. I would like to thank Alexey Fedorov and Benjamin Sveinbjornsson for the extensive amount of time they spent helping me learn organic synthesis, and David Vander Velde for his time teaching me and helping me with my NMR experiments. I also thank Aaron Gale for his help with tissue processing and being a great person with which to throw around ideas.

I also would like to say a special thank you to Dr. Paul Webster for being so kind and helping me on many different levels. I thank him for teaching me nearly everything I know about processing biological tissues for TEM, taking TEM images from biological samples, and understanding the limitations of TEM imaging. Also, in Paul's lab, I would like to thank Dr. Debbie Guerrero and Dr. Siva Wu for their help with processing tissues for TEM.

I would like to thank the other professors and administration at Caltech who have been so encouraging to me throughout my PhD. Notably Dr. Rick Flagan who always provided good advice and was always a wonderful and willing resource. Also, I would like to thank Rick for helping Matt Coggon and me start the Caltech Paddling Club and encouraging us to start kayaking on the Kern River. I would like to thank Dr. Dave

Tirrell for being so supportive and serving on both my PhD thesis committee and my candidacy committee. I would like to thank Martha Hepworth, Kathy Bubash, Karen Baumgartner, Anne Hormann, and Yvette Grant for their help with administrative work, and Suresh Guptha for his immense amount of IT help.

I would like to thank my classmates from the chemical engineering incoming class of 2009. I thank them for being such a wonderful and supportive group, and I give special thanks to Tristan Day who kept me laughing during some very rough times, and who always found time for Amigos margaritas and T-Boyles beers. I would like to thank my class also for being so supportive in creating the first generation of Big Sibs in the Big Sib Little Sib mentoring program. Their willingness to 'pay it forward' shows their true character, and has made possible a program that I hope will help generations of first year chemical engineering students to come.

I would also like to thank Felicia Hunt, Sue Chiarchiaro, Andy Downard, Emily Warren, Christine Morrison, and Swarnima Manohar for their friendship in the RA program. I thank Felicia for being a source of moral support and for being such a warm, wonderful, and positive person. I am grateful I was given the opportunity to serve as an RA, as it gave me a real connection to people and to my MD training during my mostly bench-top PhD work in the basement of Spalding.

Finally I would like to thank the USC/Caltech MD/PhD program. Most notably I would like to thank Dr. Robert Chow who believed in me and helped admit me into the program. I would like to thank Dr. Paul Patterson for being a good resource at Caltech for the MD/PhD program and for his moral and scientific support. I am grateful to Sandy Mosteller for her work in putting together all of the wonderful dinners and support

meetings during this very long program. Finally, I thank Roland Rappaport at USC who has been a constant friendly face and a great help over the last six years.

Abstract

The primary objective of my thesis work is to establish a set of design criteria for nanoparticles whose purpose is to safely and efficiently access the brain after systemic injection. Nanoparticles that can access the brain may be able to deliver therapeutic molecules to the brain that otherwise would be excluded by the blood-brain barrier.

E. coli glycoprotein 96 (Ecgp96) is explored as a candidate receptor on the blood-brain barrier that could potentially facilitate nanoparticle-receptor mediated transcytosis into the brain. Results from studies utilizing PET/CT, SPECT/CT, MRI, Xenogen fluorescence imaging, and confocal microscopy conclude that Ecgp96 is observed in the blood-brain barrier endothelial cells, but is not accessible from the blood of adult or neonatal mice under normal, non-pathological conditions.

Transferrin receptor is a well-characterized receptor on the blood-brain barrier that is accessible from the blood and known to transcytose transferrin. I focused on this receptor and on synthesizing and characterizing a well-defined set of transferrin containing gold nanoparticles of various sizes and transferrin compositions that would be investigated during *in-vivo* studies. Nanoparticle sizes were measured by DLS and nanoparticle tracking analysis. Zeta potentials were also measured. Nanoparticle transferrin content was directly measured by labeling transferrin with ^{64}Cu and measuring the nanoparticle associated gamma activity. The nanoparticle binding avidities to mouse transferrin receptors were ranked by a silver enhancement fluorescence-based method using the mouse Neruo2A cell line.

Each nanoparticle formulation was systemically injected into mice, and localization in the mouse brain was observed by silver enhancement light microscopy, and TEM. The quantitation of the gold was determined by ICP-MS. Nanoparticles with large amounts of transferrin remain strongly attached to brain endothelial cells, while nanoparticles with less transferrin are capable of both interacting with transferrin receptor on the luminal side of the blood-brain barrier and detaching from transferrin receptor on the brain side of the blood-brain barrier. These results highlight the fact that the nanoparticle avidity must be tuned to maximize the number of nanoparticles exiting the endothelial cells and entering the brain tissue. Lanthanum nitrate perfusion-fixation studies demonstrate that the nanoparticle formulations investigated do not degrade the blood-brain barrier integrity and enter the brain by transferrin receptor-mediated transcytosis. The results from these studies provide initial design criteria for creating nanoparticle therapeutics for delivery to the brain from systemic administrations.

Table of Contents

List of Figures

List of Tables

Chapter 1: Introduction

Cardiovascular diseases and cancers have been a major focus of biomedical research over the past several decades as these diseases have been the predominant cause of morbidity and mortality in the United States [1]. The next major focus of biomedical research will likely be on diseases of the brain, such as Alzheimer's disease. The baby boomer generation is quickly reaching advanced age (65 and over) and therefore a concurrent increase in the incidence of diseases of the elderly such as Alzheimer's Disease is expected [2]. In 2012, 5.4 million Americans above the age of 65 had Alzheimer's disease, and by 2050, as many as 16 million will have the disease [3].

Treating Alzheimer's disease and other related diseases of the brain has recently become a national priority. In addition to the estimated 200 billion dollars spent by families in 2012, 200 billion dollars was spent by the federal government on Alzheimer's disease care (roughly five percent of the federal budget) [3]. To establish a national initiative and help direct researchers in finding solutions to Alzheimer's disease, in January 2011 the National Alzheimer's Project Act (NAPA) was signed into law. Included in the goals of NAPA is the development of effective prevention and treatment approaches for Alzheimer's disease and related dementias by 2025 [4].

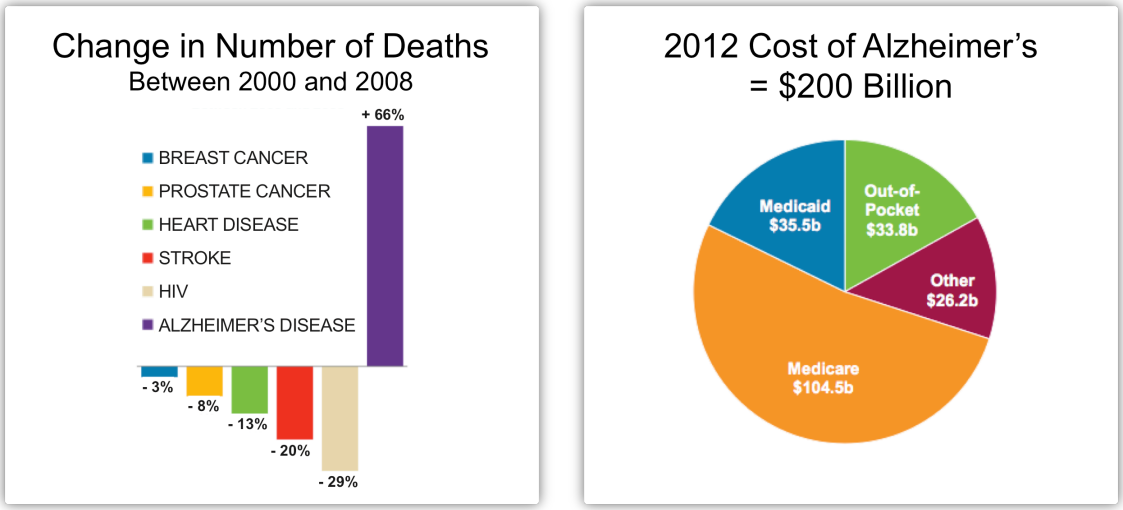

Figure 1.1: Statistics on Alzheimer's Disease – figure from [3]. (Left Panel) Rates of mortality due to cancers, cardiovascular diseases, and infectious diseases have decreased over the last decade. Deaths due to brain diseases such as Alzheimer's Disease are on the rise. (Right Panel) The costs associated with treating and caring for patients with brain diseases is reaching five percent of the federal budget, and costs are continuing to rise as the population continues to age.

In order to meet the goals of NAPA, new strategies for treating brain diseases must be approached. Traditionally, brain diseases have been treated by oral administration of small molecule therapeutics that distribute throughout the body and indiscriminately flood the brain. During a 2013 lecture at Caltech's TEDx *The Brain*, Caltech professor David Anderson eloquently composed an analogy describing this current strategy for treating brain diseases and the problems that arise from it:

> *"…A lot of people won't take them [medications]…because of their unpleasant side effects. These drugs have so many side effects, because using them to treat a complex psychiatric disorder is a bit like trying to change your engine oil by opening a can and pouring it all over the engine block. Some of it will drip into the right place, but a lot of it will do more harm than good."*

This highlights the major issues that must be addressed when designing the next generation of therapeutics for brain diseases. New therapeutics need to be developed with reduced side effects, and these therapeutics need to be delivered specifically to the sites of pathology in the brain. The next generation of brain therapeutics is likely to be made of larger molecules, such as siRNA [5, 6], that contain more chemical information and can more specifically treat a disease with reduced side effects. However, these large molecule therapeutics may be ineffective at treating brain diseases because they cannot access the brain due to the blood-brain barrier (see below).

There are currently four cholinesterase inhibitor-based medications approved for the treatment of Alzheimer's disease (donepezil, galantamine, rivastigmine, and tacrine – memantine is an NMDA receptor antagonist also approved for the treatment of the disease). These medications are used only to treat the memory loss symptoms of Alzheimer's disease and do not treat the underlying cause of the disease. Also, these therapeutics are prescribed when the patients already exhibit the most crippling symptom of the disease – memory loss. Therefore there is great need for developing therapeutics that treat the underlying pathology of Alzheimer's disease and significantly delay the onset of the disease and its memory loss symptoms. Decreasing the overall prevalence of Alzheimer's disease by delaying its onset will be paramount to geriatric quality of life, and significant in offsetting the financial burden felt by individual families and the economic burden felt by the nation [7].

To accomplish this, the disease must first be diagnosed and treated well before the onset of symptoms. Improved imaging studies including positron emission tomography of amyloid beta aggregate binding-Pittsburgh compound B (PIB) are quickly advancing

and could potentially make pre-mortem diagnoses possible well before the onset of memory loss [8-10]. New therapeutics designed to target the underlying pathophysiology of Alzheimer's Disease (amyloid beta aggregation and resulting neuronal cell death) are also being tested in clinical trials [11]. Amongst the recently completed phase III clinical trials, two therapeutics were tested that targeted amyloid beta aggregation in the brain (gamma secretase inhibitor Ly450139, and 'selective amyloid beta 42 lowering agent' MPC-7869 (or tarenflurbil)). Both therapeutics failed to continue beyond phase III trials.

Like the current FDA approved drugs for Alzheimer's disease, Ly450139 and MPC-7869 are both small molecules below 400 Da [12, 13]). Medications currently on the market for brain diseases and therapeutics that target a pathology within the brain are limited to small (molecular weight less than 400 Da) lipophilic molecules because these molecules can cross the blood-brain barrier (see below) [14]. One of the largest difficulties in therapeutic development for diseases of the brain is that any therapeutic currently developed to reach the brain must meet these criteria: they must be small molecules and have chemical compositions that allow passage across the blood-brain barrier. Any therapeutic currently being tested to treat a brain disease is therefore highly limited in chemical composition by these requirements.

The Blood-Brain Barrier

The blood-brain barrier is composed of brain microvascular endothelial cells, the tight junctions between those cells, cell efflux pump systems, and supporting cells such as astrocytes and their foot processes [15]. The blood-brain barrier was initially observed by Paul Ehlrich in 1885 after systemically injecting vital dyes into animals and observing that these dyes distributed throughout the body, except for the brain [16]. The blood-

brain barrier is important to tightly regulating the brain's microenvironment and protecting the brain from harmful outside agents [15]. In certain conditions such as cases of juvenile bacterial meningitis, medical emergencies are indicated when the blood-brain barrier is breached and bacteria are found on cerebral spinal fluid cultures [17]. It is therefore important that the blood-brain barrier functions well at excluding foreign agents from entering the brain in order to protect the brain. Though isolating the brain from the external environment and protecting the brain from foreign agents is vitally important, it is also a major problem when developing new therapeutics for brain diseases, as potentially functional therapeutics will be excluded from the brain by the blood-brain barrier.

An exceptional pharmaceutical success story in the treatment of Parkinson's disease is that of L-DOPA, which is a prodrug and precursor to dopamine. The pharmacologic mechanism of L-DOPA is a triumph in blood-brain barrier related chemistries and highlights the necessity for developing therapeutics whose chemical composition allows passage across the blood-brain barrier as well as contains functionality in targeting a molecular pathophysiologic mechanism. L-DOPA is administered to Parkinson's disease patients to increase the concentration of dopamine in the brain, especially at the point of pathology in the substantia nigra. Dopamine itself does not cross the blood-brain barrier, however L-DOPA contains an extra carboxylic acid group on its terminal carbon that allows it to cross the blood-brain barrier through receptor mediated transcytosis [18]. Once in the brain, the carboxylic acid is cleaved from L-DOPA by DOPA decarboxylase to form dopamine [19]. In addition to L-DOPA, carbidopa can be concurrently administered to the patient. Carbidopa is an analogue of

L-DOPA that does not cross the blood-brain barrier and can inhibit DOPA decarboxylase in the peripheral circulation [19]. This increases the concentration of available L-DOPA to cross the blood-brain barrier where it then can be converted to dopamine by brain associated DOPA decarboxylase.

Designing therapeutics such as L-DOPA that contain chemical compositions that allow passage across the blood-brain barrier is problematic as this is highly difficult to accomplish and greatly reduces the number of potential therapeutics that otherwise would contain good therapeutic functionality. Though a solution for delivering dopamine to the brain was found, the story of L-DOPA is more the exception than the rule. Therefore new approaches must be considered to circumvent the blood-brain barrier that do not involve modifying the chemistries of the therapeutic molecules so they contain blood-brain barrier permeability properties. This means that a new approach must be developed that can deliver any therapeutic molecule into the brain, regardless of the molecular size or chemical composition.

Numerous multidisciplinary-based strategies to transport therapeutic agents from the blood into the brain have been proposed [20]. Among the strategies currently being explored to deliver therapeutics into the brain include blood-brain barrier disruption (mannitol [21], ultrasound [22], adenosine [23]), antibody-drug conjugate systems [24], and various types of targeted and untargeted nanoparticle systems (liposomes [25], PBCA [26], and targeted exosomes [27]). The strategy taken in this thesis work is of receptor-mediated transcytosis of nanoparticle drug delivery vehicles. Receptor mediated transcytosis naturally occurs at the blood brain barrier, and is responsible for delivering a

variety of proteins to the brain that are necessary for the brain to function properly, such as the iron-carrying protein, transferrin [28].

Receptor mediated transcytosis at the blood-brain barrier takes advantage of receptors on the endothelial cells that bind to their ligand from the blood, aid in internalizing their ligand into vesicles that are transported to the brain side of the endothelial cell, and release the protein into the brain once the vesicle fuses with the cell membrane on the brain side of the endothelial cell (Figure 1.2). These receptors that facilitate receptor-mediated transcytosis can be tricked into carrying nanoparticles across the blood-brain barrier by coating the nanoparticles with the protein that normally is transcytosed (Figure 1.3 and 1.4). Several receptors have been reported to facilitate receptor mediated transcytosis at the blood-brain barrier, most notably the transferrin receptor [28, 29], insulin receptor [30, 31], and low density lipoprotein receptor-related protein [32]. In addition, phage libraries have been employed to find new ligands to unknown blood-brain barrier receptors that could potentially facilitate receptor-mediated transcytosis *in-vivo*[33, 34].

Receptor mediated transcytosis of antibodies [35] and nanoparticles [26] across the blood brain barrier have been reported. Of interest concerning the transferrin receptor (the receptor of focus in this thesis work), Friden et al. report of a low affinity (nearly identical to transferrin-transferrin receptor interaction strength) antibody that significantly accumulated in the brain parenchyma after receptor mediated transcytosis [35]. Also lactoferrin modified nanoparticles (lactoferrin binds to transferrin receptor) were shown by TEM to be transported into the brain parenchyma through receptor-mediated transcytosis [36].

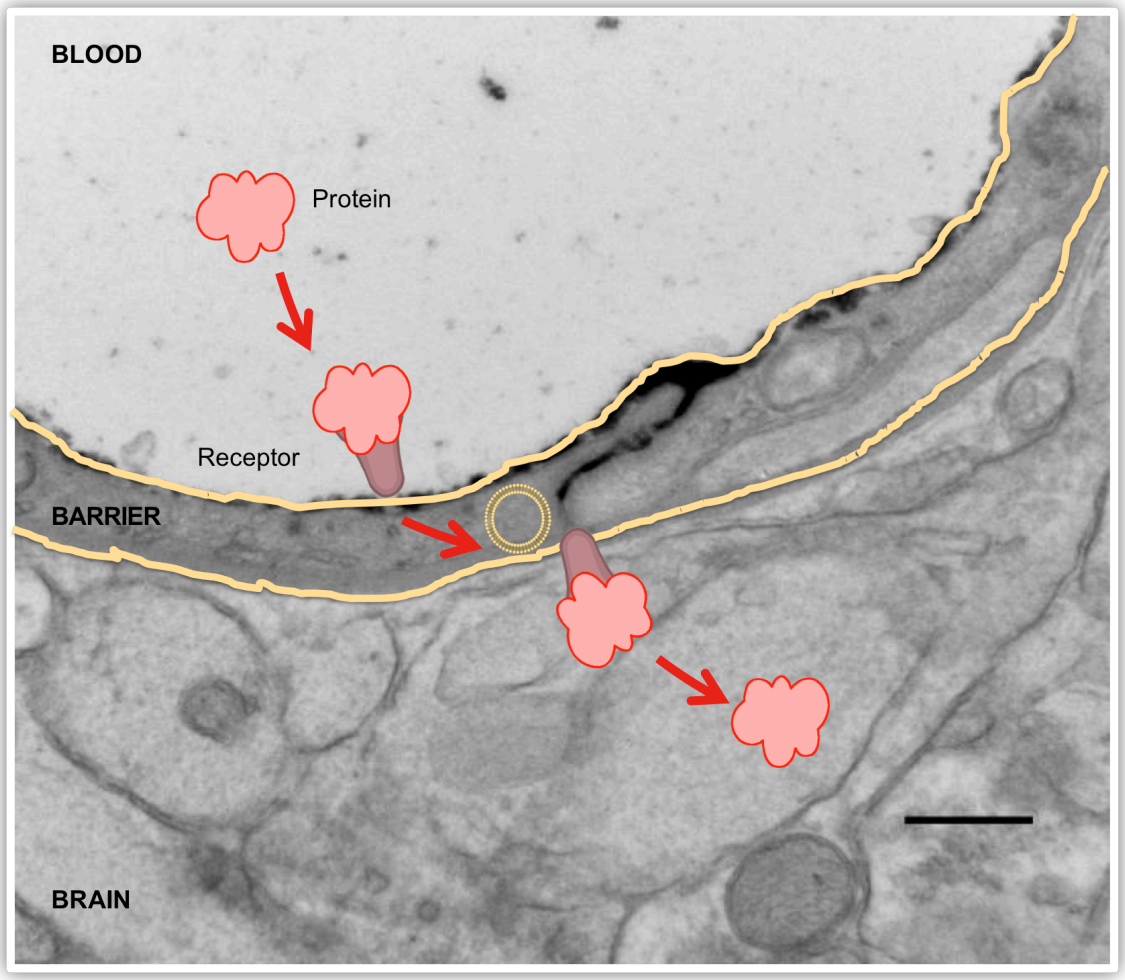

Figure 1.2: Schematic of receptor-mediated transcytosis of a protein. A protein in the blood attaches to its receptor on the surface of the blood-brain barrier and is endocytosed into vesicle of the endothelial cell. The endocytic vesicle is transported across the endothelial cell, and once it arrives on the brain side of the blood-brain barrier, the vesicle fuses with the cell membrane and the protein is released into the brain parenchyma.

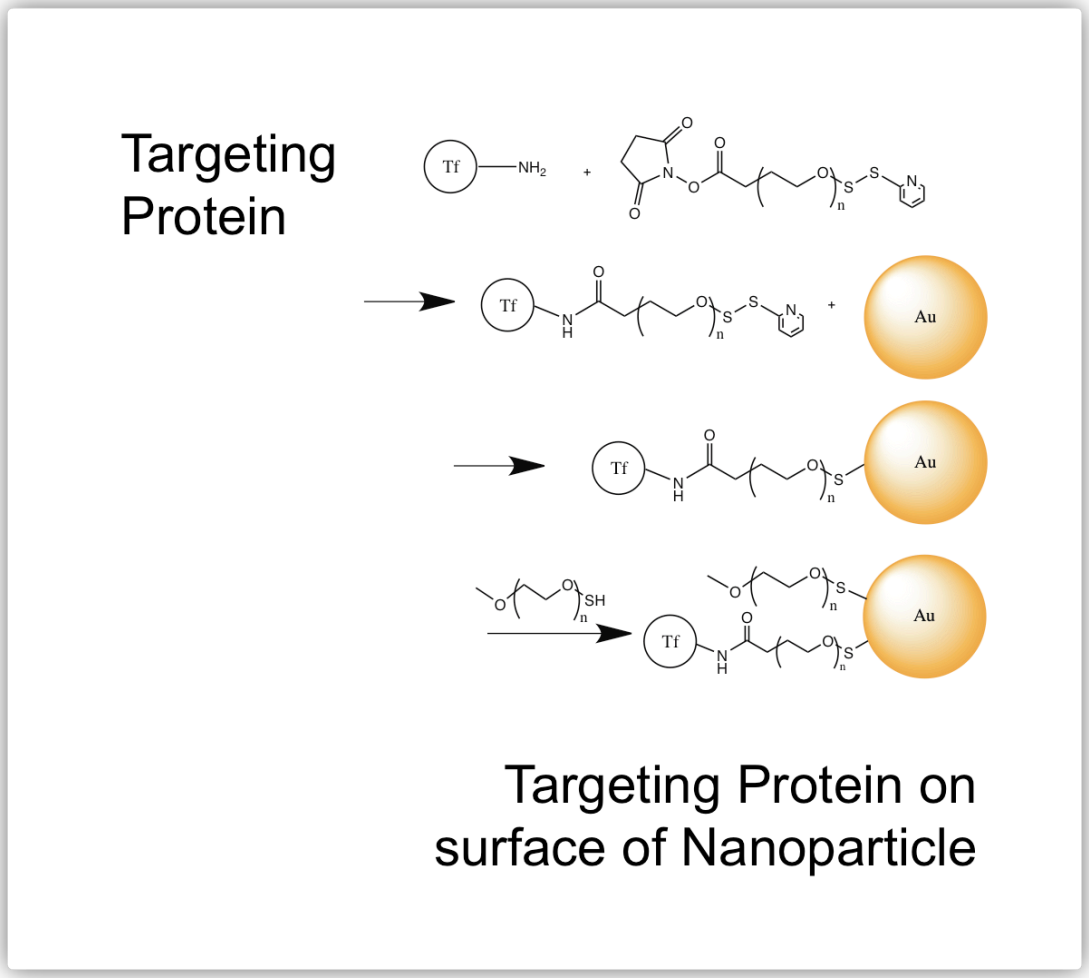

Figure 1.3: Nanoparticles can be created to contain protein that binds to receptors on the blood-brain barrier. The protein is attached to the surface of the nanoparticles through a polyethylene glycol (PEG) polymer. Additional PEG is added to the surface of the nanoparticles (PEGylation) in order to provide stability in high ionic solutions such as blood.

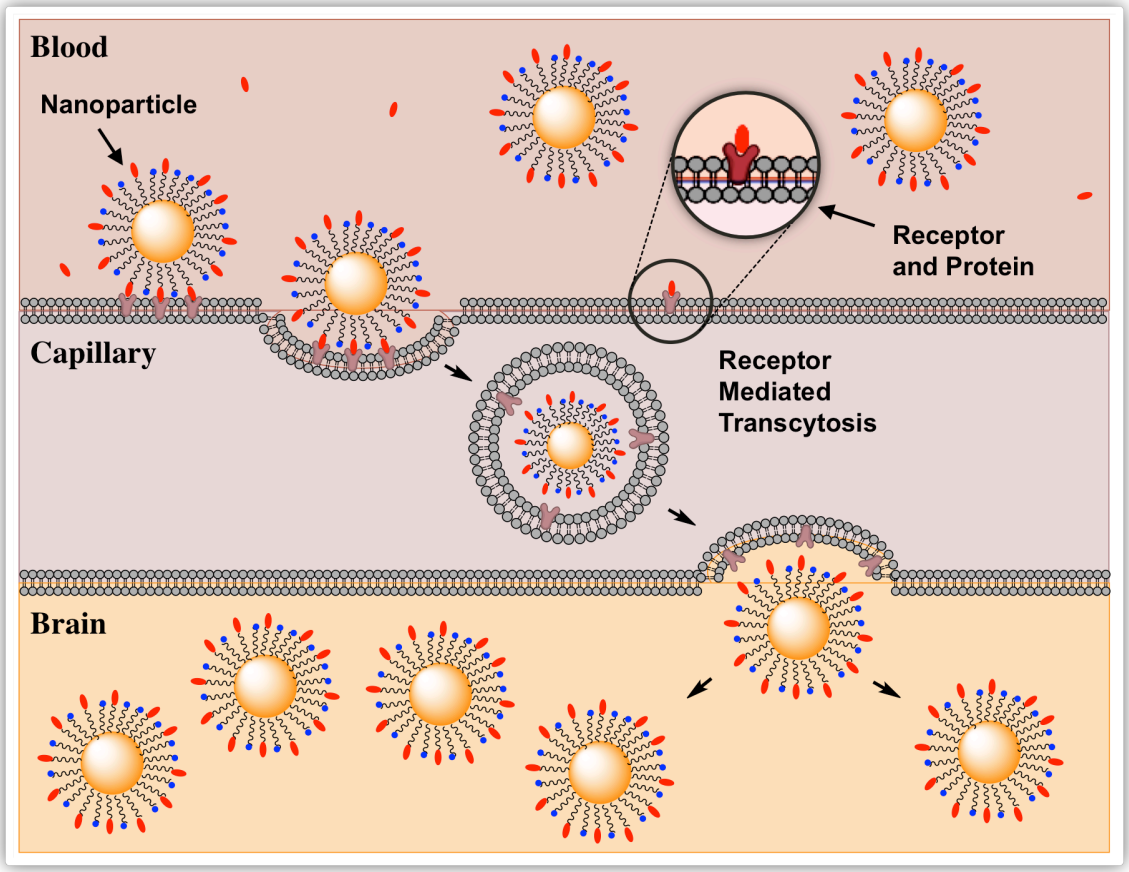

Figure 1.4: Receptor mediated transcytosis of nanoparticles. Nanoparticles containing protein that attaches to receptors on the blood side of the blood-brain barrier can be endocytosed into vesicles and transported across the endothelial cells (denoted capillary in this figure), and once on the brain side of the blood-brain barrier, can be released into the brain parenchyma.

Nanoparticles for Delivery of Therapeutics across the Blood-Brain Barrier

Nanoparticles have many advantages for drug delivery on which comprehensive reviews have been written [37]. Most relevant for delivery to brain, they mask (but do not alter) the chemical composition of the therapeutic being delivered, which reduces toxicity and eliminates the need for designing small (<400 Da) molecules with highly specific chemistries for blood-brain barrier passage [14]. Nanoparticles also shield the small molecule therapeutics from p-glycoprotein efflux pump systems in the blood-brain barrier, which eliminates endothelial cell rejection of drug back into the blood [38-40].

Most importantly for drug delivery to the brain by receptor-mediated transcytosis, the nanoparticle provides a platform on which ligands can be attached that specifically target transcytosing receptors on the blood-brain barrier. These ligands have been shown to trick receptors into carrying a nanoparticle with payload of interest through the endothelial cell where the therapeutic can be released by the nanoparticle into the brain parenchyma [41].

Targeted nanoparticles are finding application for the delivery of a wide variety of therapeutic agents, and several have already reached clinical testing in humans[42, 43]. For example, a transferrin-containing nanoparticle was used to deliver siRNA to cancer patients in a Phase I clinical trial, and shown to deliver functional siRNA to melanoma tumors in a dose dependent manner [44]. Those results demonstrate that transferrin-containing nanoparticles can be safely administered to humans. There are a number of nanoparticle based therapeutics that have already reached clinic trials as wells as a few that are now commercially available (e.g. liposome based Doxil) [42].

Multiple nanoparticle studies of receptor mediated transcytosis across the blood brain barrier have shown that nanoparticles can accumulate in the brain when they contain a ligand for blood-brain barrier receptor targeting [45-47]. Targeted nanoparticles have also been shown to facilitate internalization of nanoparticles into tumor cells, but the addition of targeting ligand does not significantly change the overall biodistribution of the nanoparticles [48]. Targeted ligand therefore affects the ability of the nanoparticle to be internalized by tumor cells *in-vivo* and also affects the ability of nanoparticles to be internalized by blood-brain barrier endothelial cells *in-vivo*.

Proof of nanoparticle accumulation in the brain parenchyma is normally

accomplished by TEM imaging of the nanoparticles in the brain parenchyma as well as the blood-brain barrier endothelial cells [26, 36, 46]. In-vivo confocal microscopy has also shown evidence that certain types nanoparticles can enter the brain parenchyma [26, 49]. Many nanoparticle studies of the blood-brain barrier quantitate the accumulation of nanoparticles in the brain by perfusing the animal with a saline solution post-mortem to remove blood-associated nanoparticles and measuring the bulk brain nanoparticle content by various methods[45, 46].

This perfusion method has been a mainstay in providing evidence that the addition of targeting ligand to the nanoparticle increases the accumulation of the nanoparticle in the brain. However it has yet to be shown that these nanoparticles accumulate in the brain parenchyma as opposed to remaining stuck in the vasculature, which would be consistent with the analysis provided by Paris-Robidas [50] that focuses on antibodies attaching to the blood-brain barrier transferrin receptors. The accumulation of nanoparticles in the vasculature would also be more consistent with the long-standing dogma that the blood-brain barrier is effective at keeping most foreign agents from entering the brain.

In this thesis work, silver enhanced light microscopy (previously unused in nanoparticle-based brain studies) was developed in order to quantitate the number of nanoparticles that remain associated with the blood-brain barrier endothelial cells as opposed to the number of nanoparticles which release from the endothelial cells and enter the brain parenchyma. This work gives first insights into the design criteria necessary for maximizing the number of nanoparticles that reach the brain parenchyma as opposed to maximizing the number of nanoparticles that accumulate in the bulk of the brain mainly

by remaining stuck to the blood-brain barrier endothelial cells. In addition, nanoparticle safety is a concern, as nanoparticles with certain characteristics (nanoparticles that are highly positively charged) degrade the blood-brain barrier [51]. Studies to prove that the blood-brain barrier remains intact have been performed by various methods, including lanthanum nitrate perfusion fixation [52]. These blood-brain barrier integrity studies are also employed in this thesis work.

Thesis Objectives and Organization

The main objective of this thesis work is to establish a set of design criteria for nanoparticles whose main purpose is to safely and efficiently access the brain after systemic injection. Nanoparticles that can access the brain may be able to deliver therapeutic molecules to the brain that otherwise would be excluded from the brain by the blood-brain barrier. Therefore, nanoparticles may become a key element for a new strategy in treating brain diseases by acting as therapeutic delivery vehicles that can cross the blood-brain barrier.

This thesis is written in three main parts. The first part explores a candidate receptor on the endothelial cells of the blood-brain barrier that could potentially facilitate nanoparticle-receptor mediated transcytosis through the blood brain barrier. This candidate receptor is E. coli glycoprotein 96 (Ecgp96). The potential importance of this candidate is that it was proposed to be accessible from the blood only at the blood-brain barrier and nowhere else in the body. Therefore it had the potential to deliver nanoparticles only to the brain; otherwise the nanoparticles would be removed from the blood circulation through normal filtration routes such as the liver and kidney. After

several imaging studies using five different imaging modalities, it was concluded that Ecgp96 was located inside the blood brain barrier endothelial cells, but was not accessible from the blood *in-vivo* as originally proposed.

The second part of this thesis work focuses on synthesizing and characterizing a well-defined set of nanoparticles that would be investigated during *in-vivo* blood-brain barrier receptor mediated transcytosis studies. These nanoparticles are composed of gold and contain transferrin that is used to target the transferrin receptor at the blood-brain barrier. Unlike Ecgp96, the transferrin receptor is expressed throughout the body and is also well accepted to exist on the blood-brain barrier and facilitate receptor mediated transcytosis of iron into the brain facilitated by the iron binding protein transferrin. Gold nanoparticles of increasing sizes were coupled with increasing amounts of transferrin. The transferrin contents of each nanoparticle formulation were directly measured through ^{64}Cu quantitative studies, the sizes were measured through dynamic light scattering and nanoparticle tracking analysis, the zeta potentials were measured with a Brookhaven Instruments ZetaPals, and the binding avidities to transferrin receptor (or effective nanoparticle binding strength to mouse cell associated transferrin receptors) were measured using a silver enhancement fluorescence-based method. Nanoparticle avidity was found to increase with increasing transferrin content, and a weak effect of increasing size on increased binding was observed.

The third part of this work was focused on understanding how each nanoparticle synthesized interacted with the blood-brain barrier *in-vivo*. Each nanoparticle formulation was systemically injected by lateral tail vein injection, and its behavior in the brain was observed by silver-enhancement light microscopy, and transmission electron

microscopy (TEM). Bulk amounts of gold in the brain were measured by ICP-MS. Nanoparticles with high transferrin content accumulated more in the bulk of the brain (as measured by ICP-MS) as well as in the blood vessels/endothelial cells (as measured by silver enhancement light microscopy and TEM). Most importantly, it was shown by silver-enhancement light microscopy that nanoparticle avidity must be tuned to maximize the number of nanoparticles exiting the endothelial cells and entering the brain tissue (called the 'brain parenchyma' or just 'parenchyma').

Nanoparticles of both 45 nm and 80 nm diameter reached the brain parenchyma, and their accumulation there was observed to depend on transferrin content. Nanoparticles with large amounts of transferrin remain strongly attached to brain endothelial cells, while nanoparticles with less transferrin are capable of both interacting with transferrin receptor on the luminal side of the blood-brain barrier and detaching from transferrin receptor on the brain side of the blood-brain barrier. TEM imaging of brain sections from mice perfused with lanthanum nitrate provided evidence that nanoparticles did not degrade the blood-brain barrier integrity, and that transferrin-containing nanoparticles reached the parenchyma via a receptor-mediated transcytosis pathway.

References

1. National Center for Health Statistics. NCHS Data Brief 90, Number 88, March 2012. 1–8 (2012).
2. Vincent, G. K. & Velkoff, V. A. The next four decades - The older population in the United States: 2010 to 2050. *US Census Bureau* 1–16 (2010).
3. Adamec, C. 2012 facts figures fact sheet. *alz.org* 1–2 (2012).
4. Khachaturian, Z. S., Khachaturian, A. S. & Thies, W. The draft "National Plan" to address Alzheimer's disease - National Alzheimer's Project Act (NAPA). *Alzheimers Dement* **8,** 234–236 (2012).
5. Ballarín-González, B. & Howard, K. A. Polycation-based nanoparticle delivery of RNAi therapeutics: Adverse effects and solutions. *Advanced Drug Delivery Reviews* **64,** 1717–1729 (2012).
6. Barros, S. A. & Gollob, J. A. Safety profile of RNAi nanomedicines. *Advanced Drug Delivery Reviews* **64,** 1730–1737 (2012).
7. Brookmeyer, R., Gray, S. & Kawas, C. Projection of Alzheimer's disease in the United Sates and the public health impact of delaying disease onset. *American Journal of Public Health* **88,** 1137–1342 (1998).
8. Shaffer, J. L. *et al.* Predicting cognitive decline in subjects at risk for Alzheimer disease by using combined cerebrospinal fluid, MR imaging, and PET biomarkers. *Radiology* **266,** 583–591 (2013).
9. Borson, S. *et al.* Improving dementia care: The role of screening and detection of cognitive impairment. *Alzheimer's & Dementia* 1–9 (2013).
10. Lehmann, M. *et al.* Diverging patterns of amyloid deposition and hypometabolism

in clinical variants of probable Alzheimer's disease. *Brain* **136,** 844–858 (2013).

11. Misra, S. & Medhi, B. Drug development status for Alzheimer's disease: present scenario. *Neurol Sci* (2013).
12. Hopkins, C. R. ACS chemical neuroscience molecule spotlight on semagacestat (LY450139). *ACS Chem Neurosci* **1,** 533–534 (2010).
13. Marder, K. Tarenflurbil in patients with mild Alzheimer's disease. *Curr Neurol Neurosci Rep* **10,** 336–337 (2010).
14. Hitchcock, S. A. Blood–brain barrier permeability considerations for CNS-targeted compound library design. *Current Opinion in Chemical Biology* **12,** 318–323 (2008).
15. Nico, B. & Ribatti, D. Morphofunctional aspects of the blood-brain barrier. *Curr. Drug Metab.* **13,** 50–60 (2012).
16. Ehrlich. Das Sauerstoff-Bedurfnis des Organismus: eine farbenalytische Studie. *Berlin: Hirschward* 1–85 (1885).
17. Sáez-Llorens, X. & McCracken, G. H. Bacterial meningitis in children. *The Lancet* **361,** 2139–2148 (2003).
18. Wade, L. A. & Katzman, R. Synthetic amino acids and the nature of L-DOPA transport at the blood-brain barrier. *J Neurochem* **25,** 837–842 (1975).
19. Gilbert, J. A., Frederick, L. M. & Ames, M. M. The aromatic-L-amino acid decarboxylase inhibitor carbidopa is selectively cytotoxic to human pulmonary carcinoid and small cell lung carcinoma cells. *Clin Cancer Res* **6,** 4365–4372 (2000).
20. Neuwelt, E. *et al.* Strategies to advance translational research into brain barriers.

Lancet Neurol **7,** 84–96 (2008).

21. Doolittle, N. D. *et al.* Safety and efficacy of a multicenter study using intraarterial chemotherapy in conjunction with osmotic opening of the blood-brain barrier for the treatment of patients with malignant brain tumors. *Cancer* **88,** 637–647 (2000).
22. Yang, F. Y. *et al.* Focused ultrasound and interleukin-4 receptor-targeted liposomal doxorubicin for enhanced targeted drug delivery and antitumor effect in glioblastoma multiforme. *Journal of Controlled Release* 1–7 (2012).
23. Carman, A. J., Mills, J. H., Krenz, A., Kim, D. G. & Bynoe, M. S. Adenosine receptor signaling modulates permeability of the blood-brain barrier. *Journal of Neuroscience* **31,** 13272–13280 (2011).
24. Pardridge, W. M. & Boado, R. J. Reengineering biopharmaceuticals for targeted delivery across the blood-brain barrier. *Protein Engineering for Therapeutics Part B* **503,** 269–292 (Elsevier Inc., 2012).
25. Geldenhuys, W., Mbimba, T., Bui, T., Harrison, K. & Sutariya, V. Brain-targeted delivery of paclitaxel using glutathione-coated nanoparticles for brain cancers. *Journal of Drug Targeting* **19,** 837–845 (2011).
26. Koffie, R. M. *et al.* Nanoparticles enhance brain delivery of blood-brain barrier-impermeable probes for in vivo optical and magnetic resonance imaging. *Proceedings of the National Academy of Sciences* (2011).
27. Alvarez-Erviti, L. *et al.* Delivery of siRNA to the mouse brain by systemic injection of targeted exosomes. *Nature Biotechnology* 1–7 (2011).
28. Deane, R., Zheng, W. & Zlokovic, B. V. Brain capillary endothelium and choroid plexus epithelium regulate transport of transferrin-bound and free iron into the rat

brain. *J Neurochem* **88,** 813–820 (2004).

29. Burdo, J. R. & Connor, J. R. Brain iron uptake and homeostatic mechanisms: an overview. *Biometals* **16,** 63–75 (2003).

30. Pardridge, W. M., Eisenberg, J. & Yang, J. Human blood-brain barrier insulin receptor. *J Neurochem* **44,** 1771–1778 (1985).

31. Duffy, K. R. & Pardridge, W. M. Blood-brain barrier transcytosis of insulin in developing rabbits. *Brain Research* **420,** 32–38 (1987).

32. Jones, A. & Shusta, E. Blood–brain barrier transport of therapeutics via receptor-mediation. *Pharm Res* **24,** 1759–1771 (2007).

33. Rooy, I. *et al.* Identification of Peptide Ligands for Targeting to the Blood-Brain Barrier. *Pharm Res* **27,** 673–682 (2010).

34. Wang, X. X., Cho, Y. K. & Shusta, E. V. Mining a yeast library for brain endothelial cell-binding antibodies. *Nat Meth* **4,** 143–145 (2007).

35. Friden, P. M., Olson, T. S., Obar, R., Walus, L. R. & Putney, S. D. Characterization, receptor mapping and blood-brain barrier transcytosis of antibodies to the human transferrin receptor. *J Pharmacol Exp Ther* **278,** 1491–1498 (1996).

36. Huang, R. *et al.* Lactoferrin-modified nanoparticles could mediate efficient gene delivery to the brain in vivo. *Brain Research Bulletin* **81,** 600–604 (2010).

37. Heidel, J. D. & Davis, M. E. Clinical Developments in Nanotechnology for Cancer Therapy. *Pharm Res* **28,** 187–199 (2010).

38. Banks, W. A. Characteristics of compounds that cross the blood-brain barrier. *BMC Neurol* **9,** S3 (2009).

39. Kabanov, A. V., Batrakova, E. V. & Miller, D. W. Pluronic block copolymers as modulators of drug efflux transporter activity in the blood-brain barrier. *Advanced Drug Delivery Reviews* **55,** 151–164 (2003).

40. Schluep, T. *et al.* Preclinical efficacy of the camptothecin-polymer conjugate IT-101 in multiple cancer models. *Clinical Cancer Research* **12,** 1606 (2006).

41. Pardridge, W. M. Molecular Trojan horses for blood-brain barrier drug delivery. *Curr Opin Pharmacol* **6,** 494–500 (2006).

42. Davis, M. E., Chen, Z. G. & Shin, D. M. Nanoparticle therapeutics: an emerging treatment modality for cancer. *Nat Rev Drug Discov* **7,** 771–782 (2008).

43. Kamaly, N., Xiao, Z., Valencia, P. M., Radovic-Moreno, A. F. & Farokhzad, O. C. Targeted polymeric therapeutic nanoparticles: design, development and clinical translation. *Chem. Soc. Rev.* **41,** 2971 (2012).

44. Davis, M. E. *et al.* Evidence of RNAi in humans from systemically administered siRNA via targeted nanoparticles. *Nature* **464,** 1067–1070 (2010).

45. Agyare, E. *et al.* Development of a smart nano-vehicle to target cerebrovascular amyloid deposits and brain parenchymal plaques observed in Alzheimer's disease and cerebral amyloid angiopathy. *Pharm Res* **25,** 2674–2684 (2008).

46. Giralt, R. *et al.* Delivery of gold nanoparticles to the brain by conjugation with a peptide that recognizes the transferrin receptor. *Biomaterials* **33,** 7194–7205 (2012).

47. Korkusuz, H. *et al.* Transferrin-coated gadolinium nanoparticles as MRI contrast agent. *Mol Imaging Biol* (2012).

48. Choi, C. H. J., Alabi, C. A., Webster, P. & Davis, M. E. Mechanism of active

targeting in solid tumors with transferrin-containing gold nanoparticles. *Proceedings of the National Academy of Sciences* **107,** 1235–1240 (2010).

49. Henrich-Noack, P. *et al.* In vivo visualisation of nanoparticle entry into central nervous system tissue. *Arch Toxicol* **86,** 1099–1105 (2012).

50. Paris-Robidas, S., Emond, V., Tremblay, C., Soulet, D. & Calon, F. In vivo labeling of brain capillary endothelial cells after intravenous injection of monoclonal antibodies targeting the transferrin receptor. *Mol. Pharmacol.* **80,** 32–39 (2011).

51. Lockman, P. R., Koziara, J. M., Mumper, R. J. & Allen, D. D. Nanoparticle surface charges alter blood-brain barrier integrity and permeability. *Journal of Drug Targeting* **12,** 635–641 (2004).

52. Zensi, A. *et al.* Human serum albumin nanoparticles modified with apolipoprotein A-I cross the blood-brain barrier and enter the rodent brain. *Journal of Drug Targeting* **18,** 842–848 (2010).

Chapter 2: E. coli Glycoprotein 96

Introduction

Current targeted delivery of nanoparticles into the brain takes advantage of blood-brain barrier receptors that are ubiquitously expressed such as the transferrin receptor, lipoprotein receptors (ApoE), and insulin receptors [1]. Our lab was approached by a group at Children's Hospital Los Angeles headed by Dr. Nemani Prasadarao who suggested investigating a new protein that had not previously been studied for targeted delivery of nanoparticles to the brain. This protein was a neonatal E. coli meningitis associated protein, E. coli glycoprotein 96 (Ecgp96), which interacts with E. coli on the surface of brain endothelial cells. Dr. Prasadarao proposed the development of a nanoparticle that would target Ecgp96 for receptor-mediated transcytosis across the blood-brain barrier *in-vivo*. The novelty of targeting the Ecgp96 receptor was that it was thought to be surface expressed only on endothelial cells of the blood-brain barrier; therefore, targeted delivery through Ecgp96 should only send nanoparticles to the brain - otherwise the nanoparticles should be cleared by the body's normal filtration process through kidney and liver.

In 1997, Dr. Prasadarao and co-workers first proposed that Ecgp96 was located on endothelial cells only in the brain [2]. They since have proposed that Ecgp96 is the receptor that facilitates E. Coli meningitis in new-born infants. Prasadarao et al. demonstrated that E. coli outer membrane protein A (OmpA), which is characteristic to the strain of E. coli that causes meningitis in newborn infants, binds to a 95 kDa glycoprotein-type receptor (Ecgp) on human brain microvascular endothelial cells (HBMECs) [3]. In this work, Prasadarao et al. demonstrated that Ecgp clustered on

HBMEC at the site of OmpA+ E. coli invasion but no clustering occurred with OmpA- E. coli. Ecgp was later positively identified as a glycoprotein 96 homologue by screening an HBMEC cDNA expression library with an anti-Ecgp96 antibody [4].

Ecgp96 (also known as grp94) is a member of the heat shock protein (hsp90) family, which is responsible for a number of important molecular processes including the insurance of correct protein folding [5]. Grp94 is the most abundant chaperone protein inside the endoplasmic reticulum [6], and is believed to be mainly located within the lumen of the endoplasmic reticulum [7]. Under conditions of stress, grp94 has been shown to be transported to the outer surface of the plasma membrane through the loss of its endoplasmic reticulum retention signal KDEL [8]. In a paramount review of hsp90 and grp94, Csermely, et al., noted that easy mobility seems to be a phenomenon of endoplasmic reticulum lumen proteins, which makes grp94 versatile by its facile ability to redistribute to different cellular compartments [5]. Though the roles of Ecgp96 are many, it is yet to be proven that Ecgp96 is directly responsible for transporting E. coli across the blood-brain barrier via receptor-mediated transcytosis *in-vivo*.

Ecgp96 was described to be only on endothelial cells of the blood-brain barrier through screening endothelial cells from four locations in the body: HBMEC, human umbilical vein, human aortic arterial, and human iliac vein endothelial cells [2]. Confirmation that Ecgp96 is exclusively on brain endothelium and is accessible from the blood *in-vivo* remains to be completed, and is the first focus of this thesis work. Though direct evidence supporting the use of Ecgp96 for nanoparticle delivery across the blood-brain barrier *in-vivo* is needed, there are studies that indirectly support the idea of targeting nanoparticles to Ecgp96 for delivery to the brain. These papers demonstrate the

OmpA/Ecgp96 interaction is essential for the invasion of E. coli across the blood-brain barrier not only in-vitro but also in-vivo [9, 10]. In these studies OmpA mutant E. coli that are less able to interact with Ecgp96 were found to be less invasive in HBMEC *in-vitro* and were also found to be significantly less able to penetrate into the central nervous system *in-vivo* as measured by cerebral spinal fluid cultures.

OmpA positive E. coli have been shown to degrade blood-brain barrier integrity in-vitro as measured by trans-endothelial electrical resistance (TEER) [11]. Thus safety concerns may preclude developing nanoparticle drug delivery vehicles targeted to Ecgp96 for use in humans. Tight junction degradation was hypothesized to occur via OmpA mediated stimulation of iNOS (inducible nitric oxide synthase), generation of cGMP, and induction of αPKC (alpha protein kinase C). Results from the same paper show that OmpA+ E. coli are capable of increasing HBMEC surface expression of Ecgp96 by twofold, presumably through the same proposed mechanism. This suggests OmpA+ E. coli could be crossing the blood-brain barrier not by Ecgp96 receptor mediated transcytosis, but instead by passing through the paracellular pathway after OmpA mediated tight junction degradation. This would lead to acute inflammation that would be harmful to the patient [12] and is therefore not ideal for a well engineered nanoparticle drug delivery system that would be administered in patients with chronic neuropathological conditions.

Organization and Summary of Results

The first step in developing a nanoparticle targeted to Ecgp96 for delivery to the brain was to confirm that Ecgp96 is located on the surface of brain endothelial cells and

accessible from the blood *in-vivo*. After four experiments using four different imaging modalities, the evidence was clear that the Ecgp96 receptor was not accessible from the blood on the brain endothelium luminal surface. Ecgp96 was found to be present *in* brain endothelial cells by confocal microscopy, however it was not accessible via the blood and thus not available for therapeutic delivery across the blood-brain barrier.

The first experiment probed for Ecgp96 expression on the blood-brain barrier through systemic injection of a ^{64}Cu radiolabeled antibody against Ecgp96 into an adult mouse followed by imaging the brain using Positron Emission Tomography/Computed Tomography (PET/CT). PET is a highly sensitive method for locating radioactive signal in-vivo. No positron signal from Ecgp96 antibody was seen in the brain by PET, though antibody was observed to circulate in the blood and accumulate in the liver. Further experimentation with additional imaging modalities were chosen to confirm that Ecgp96 was not located on the blood-brain barrier of the mouse and that antibodies to Ecgp96 did not accumulate in the brain.

The next experiment was to systemically inject a fluorophore labeled antibody to Ecgp96 and monitor for accumulated signal in the brain using fluorescence Xenogen imaging. This modality does not provide three-dimensional images like PET, and unlike PET, fluorescence Xenogen imaging is limited in sensitivity by the tissue penetration depth the emitted light must travel through. After injection and imaging, the bulk signal from the Ecgp96 antibody-treated brain was no different from the non-injected control brain, indicating no observable accumulation of the antibody in the brain.

It was concluded from the PET and Xenogen imaging biodistribution studies that

Ecgp96 was not accessible from the blood on the blood-brain barrier of adult mice. Since E. coli meningitis is a disease of neonatal infants and Dr. Prasadarao's research focused on neonatal mice, it was hypothesized that Ecgp96 would be expressed on neonatal mouse brain endothelium but not on adult mouse brain endothelium. The UCLA veterinarian did not work with neonatal mice, so PET scan biodistribution studies could not be employed on neonatal mice there. SPECT/CT imaging could be carried out on neonatal mice at the Small Animal Imaging Research Center (SAIRC) at Children's Hospital Los Angeles. A biodistribution study of Ecgp96 in neonatal mice utilizing SPECT/CT after injection of an ^{111}In radiolabeled antibody against Ecgp96 was therefore employed. SPECT is very similar to PET in that three-dimensional images can be generated from *in-vivo* signal, however SPECT is less sensitive and has lower spatial resolution.

In this experiment, a lead shield was placed around the body of the mouse to eliminate washout signal from non-brain regions (heart and liver) so that a high instrument detection gain could be used to pick up any small amount of gamma-radiation that may be present in the brain. The brain of the neonatal mouse was imaged after an intracardiac injection of radiolabeled antibody. At near maximum gamma-radiation detection gain, there was no signal due to Ecgp96 in the brain, indicating no accumulation of antibody in the brain. Therefore, Ecgp96 was concluded to not be accessible from the blood on the blood-brain barrier of neonatal mice. In addition, after imaging a neonatal mouse brain, extra radioactive antibody was available, so the mother of the neonatal mouse was imaged to confirm via SPECT/CT that Ecgp96 is not accessible from the blood on adult mouse blood-brain barrier. At a near maximum

gamma-radiation detection gain, there was still no observable signal in the brain of the adult mouse.

Confocal microscopy imaging was performed on sections of mouse brain resected a day after the mouse received a systemic dose of fluorescently labeled anti-Ecgp96 antibody. This imaging modality only has an advantage over PET in that signal can be located at the tissue level. Though PET is a sensitive method for determining if antibody accumulates in the bulk of the brain, it is possible that confocal microscopy could better detect signal from smaller quantities of labeled antibody when focused on a small section of tissue, such as an individual blood vessel. No fluorescent signal was seen by confocal microscopy in the brain from the systemically injected anti-Ecgp96 antibody. Therefore, it was concluded that the Ecgp96 protein is not accessible from the blood on the surface of brain endothelial cells.

To determine if Ecgp96 is associated with brain endothelial cells *in-vivo* as suggested by the work of Dr. Prasadarao, a normal mouse brain was resected, and tissue sections were stained with the antibody to Ecgp96 followed by a fluorophore-labeled secondary antibody for signal enhancement. Specific Ecgp96 signal was seen in the vessels of the resulting images. Therefore it was concluded that in normal mouse adult brain, Ecgp96 is expressed inside the endothelial cells, though not on the surface of the endothelial cells. That Ecgp96 is not accessible from the blood negates its usefulness as a receptor target for the purpose of delivering nanoparticles from the blood into the brain.

Confocal imaging of cultured HBMEC cells probed with antibody to Ecgp96 suggested that Ecgp96 may be located on the surface of HBMEC cells *in-vitro*.

Incubating HBMEC cells with recombinant OmpA increased the expression of Ecgp96 by twofold as measured by flow cytometry. Because E. coli meningitis is a disease of neonatal infants, these cell culture results along with our in-vivo biodistribution studies suggest that neonatal blood-brain barrier endothelial cells *in-vivo* are stimulated by OmpA positive E. coli to express Ecgp96 on their surface when E. coli reach pathologically significant quantities in the blood. This may facilitate the interaction of E. coli OmpA with endothelial cell Ecgp96, which further facilitates the passage of the E. coli across the blood-brain barrier. The exact mechanism of E. coli passage across the neonatal blood-brain barrier through this interaction is yet to be determined by an infectious disease lab.

Methods and Experimental Results

PET/CT Imaging

Positron Emission Tomography (PET) is able to localize signal in three-dimensional space from an injected radiolabeled biomolecule, and Computed Tomography generates a three-dimensional picture of the anatomy, which gives a reference for where the biomolecule localizes in-vivo. PET has several advantages to imaging biodistribution of biomolecules [13]: PET has a resolution of 3-10 mm and is capable of resolving signal at the organ level in mice, PET isotope ^{64}Cu has a half-life of 12.7 hours - excellent for radiolabeling and imaging over a 24 hour period, and coupling ^{64}Cu to antibody via chelator DOTA maintains ^{64}Cu-antibody complexation to greater than 99% over a 24 hour period allowing for highly specific signal due to the location of the biomolecule of interest. PET/CT is a proven method for measuring real time

biodistribution of injected biomolecules [14], and was therefore employed here as the main method for investigating the presence of Ecgp96 on brain endothelium. Antibody to Ecgp96 was labeled with ^{64}Cu through chelating agent DOTA, and injected into a mouse to monitor the biodistribution of Ecgp96 (Figure 2.1).

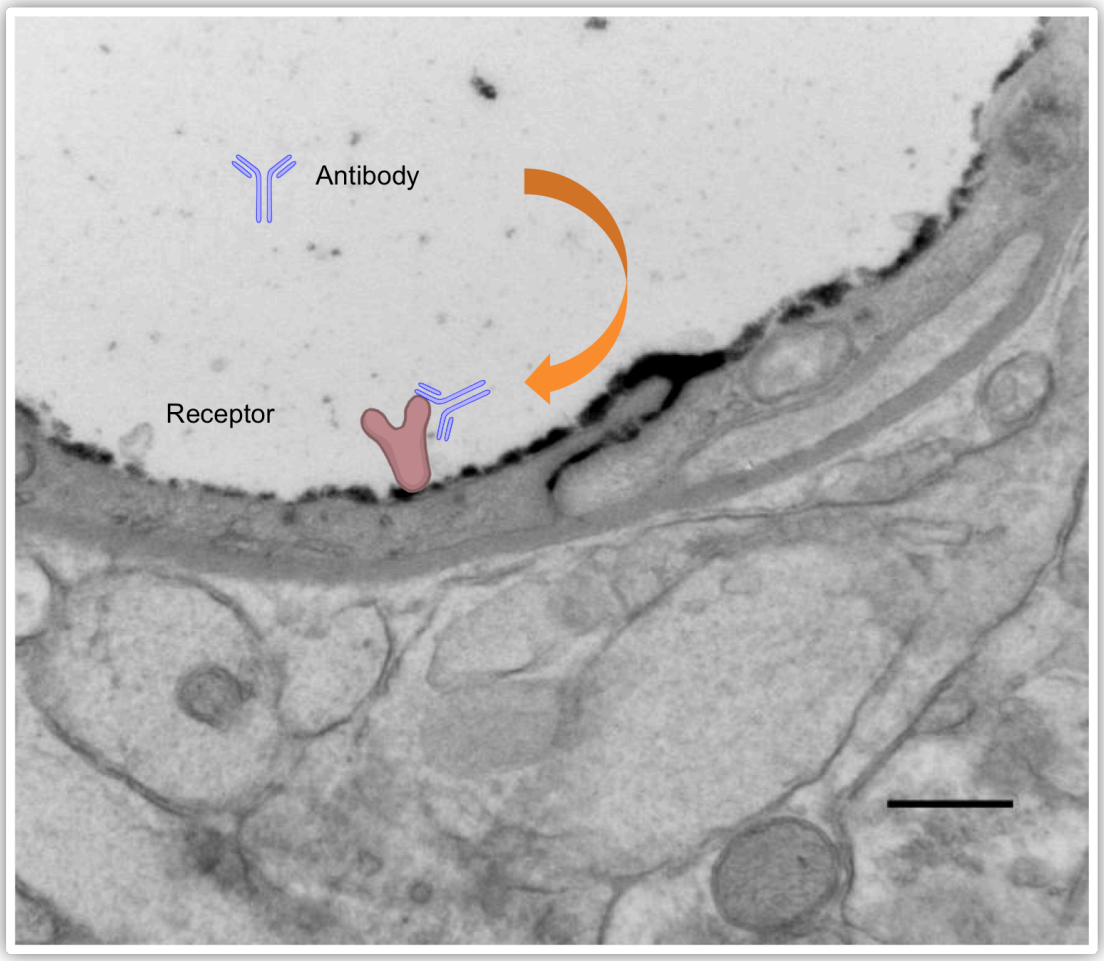

Figure 2.1: Schematic of antibody to Ecgp96 attaching to Ecgp96. Antibody labeled with ^{64}Cu can be monitored in vivo by PET/CT. Tissues in the body that contain Ecgp96 accessible from the blood will be bound by the antibody, and the accumulation of the antibody in the tissues can be observed through PET.

Conjugation of DOTA to Antibody

Both DOTA (1,4,7,10-tetraazacyclododecane-1,4,7,10-tetraacetic acid) conjugation to antibody and the evaluation of conjugation efficiency was performed as previously reported [15]. Briefly, DOTA-N-Hydroxysuccinimide (NHS)-ester was dissolved in dimethyl sulfoxide (DMSO) at 25 mg/ml. IgG was buffer exchanged into 0.1 M sodium phosphate/0.1 M sodium bicarbonate buffer (pH 8.6) at 2 mg/ml and reacted for 2 hours at room temperature with a 100 fold molar excess of DOTA-NHS-ester. Unreacted DOTA and hydroxysuccinimide byproduct was removed by filtration through a 50 kDa MWCO filter, and IgG-DOTA resided in a final metal free PBS solution. All buffers were either made with metal-free water, or treated with Chelex to remove trace metals. NHS-esters bind non-specifically to exposed primary amines on the antibody, therefore it was expected that the antibody binding efficiency to its receptor (as measured by binding dissociation constant K_d) would be decreased.

The degree of DOTA labeling was measured by determining the total DOTA content in solution and dividing by the total protein content in solution. A control antibody to be injected (normal mouse antibody) had 16 DOTA per IgG, and the antibody to Ecgp96 had 14 DOTA per IgG. Antibody content was measured using the Bradford method. DOTA content was measured by an Arsenazo III based spectrophotometric method. This is a simple non-radioactive method based on an exchange equilibrium of copper between arsenazo III reagent (red) and the copper complex of arsenazo III (purple) - absorbance changes measured at 580 nm. Previous studies have confirmed the degree of labeling values obtained by UV/Vis spectroscopy matches that found by radiolabeling [16]. Much like the Bradford method, a standard curve of DOTA concentrations allows for the calculation of the concentration of DOTA in the sample of

interest. Increasing DOTA ligand concentration at the beginning of the conjugation reaction lead to increased degree of labeling (Figure 2.2).

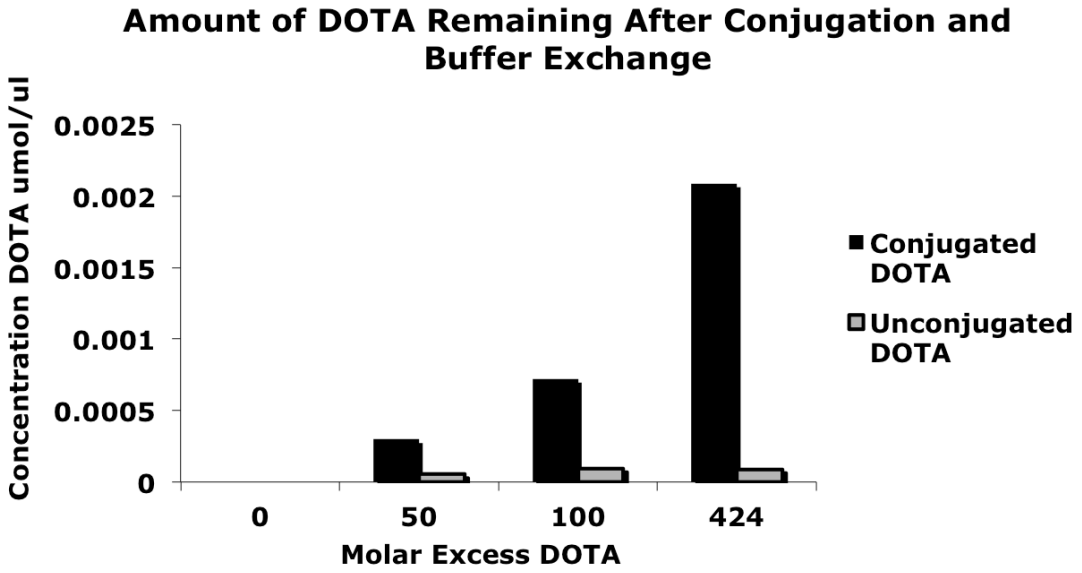

Figure 2.2: Arsenazo assay on copper solutions mixed with DOTA-antibody ('conjugated DOTA') and free DOTA ('unconjugated DOTA'). DOTA-antibody was placed in 50 kDa MWCO spin filters, and free DOTA that did not couple to antibody was removed by filtration. As a control, identical concentrations of DOTA that were not reacted with antibody were also processed by spin filtration, and the retentate was also added to the Cu-arsenazo assay ('unconjugated DOTA' data series). These data show that unreacted DOTA are efficiently removed by spin filtration, and that increasing the molar excess of DOTA during the reaction with antibody increases the degree of labeling of DOTA to antibody.

The Ecgp96 antibody used for DOTA conjugation was generously supplied by Dr. Prasadarao. This antibody was produced in the late 1990's, and gel electrophoresis with Comassie Blue staining of the IgG revealed there was a significant amount of antibody degradation over this time (data not shown). Size exclusion HPLC was performed to confirm the removal of these degradation productions during the 50 kDa MWCO filtration steps. Note in Figure 2.3 the large peak at 28 minutes in the unconjugated

antibody due to degradation products of the antibody (peaks seen near 50 kDa on gel). This peak is greatly diminished in the 'DOTA conjugated' HPLC spectra. Though most of the 50 kDa fragment was filtered, some remained and was injected in the PET/CT imaging experiment. Also, as a confirmation of successful DOTA coupling to antibody, DOTA conjugated antibody had a retention time less than 20 minutes while the unconjugated antibody had a retention time greater than 20 minutes. This is consistent with a larger molecular weight of the DOTA conjugated antibody.

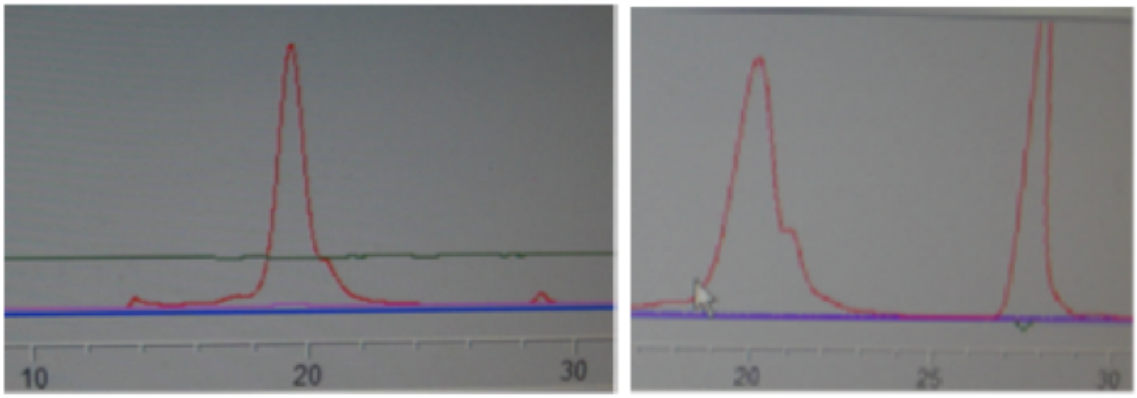

Figure 2.3: HPLC spectra of Ecgp96 antibody conjugated to DOTA (left panel) and unmodified Ecgp96 antibody (right panel). The antibody-DOTA conjugate has an elution time less than 20 minutes, while the unmodified antibody has an elution time greater than 20 minutes. Also, on first pass of the unmodified antibody through the HPLC, there is a significant amount of degradation products seen eluted near 28 minutes (the antibody was roughly ten years old at the time of this HPLC). This predominant peak was not seen in HPLC spectra of antibody after purification by filtration.

To assess the ability of the antibody to bind Ecgp96 post DOTA labeling, a binding study was performed using a Scatchard analysis followed by data modeling using a Langmuir Adsorption Isotherm. Scatchard analysis of receptor-ligand binding estimates both the dissociation constant, K_d, and the total number of receptor-binding sites, $[\star]_o$, in a given set of cells. Receptor-ligand binding and binding association constant K_a are given by the equations:

$$\star + \mathrm{L} \underset{k_{des}}{\overset{k_{ads}}{\rightleftharpoons}} \star L$$

$$K_a = \frac{k_{ads}}{k_{des}} = \frac{[\star L]}{[\star][L]}$$

$$K_d = \frac{1}{K_a}$$

When the binding of the ligand to the receptor has reached equilibrium then

$[\star]_o = [\star \mathrm{L}] + [\star]$. Simple rearrangement leads to:

$$\frac{[\star L]}{[L]} = K_a([\star]_o - [\star L]) \qquad (1)$$

which is a linear plot of slope $-K_a$ and x-intercept of $K_a[\star]_o$. Therefore, the binding association constant K_a and total binding sites $[\star]_o$ can be estimated from the linearized equation. Error propagation of the linearized data at low concentrations is large and distorts the actual parameter values. Untransformed data can be modeled in this case with a Langmuir adsorption isotherm, and parameters K_a and $[\star]_o$ can be determined by performing a non-linear regression using a software package. The Langmuir adsorption isotherm is derived from an alternative rearrangement of the above relations and yields:

$$[\star L] = \frac{[\star]_o K_a[L]}{1 + K_a[L]} \qquad (2)$$

MATlab function nlinfit, is a non-linear regression tool that was used to determine actual K_a and $[\star]_o$ parameters. Initial guesses are required by nlinfit, which

was initially provided by the Scatchard analysis, however a large range of reasonable initial values resulted in the same output (Figure 2.4 and Figure 2.5).

The binding study was performed by flow cytometry. HBMEC cells were detached from T75 flasks and fixed in BD Cytofix for 30 min at 4 ºC. Unmodified antibodies to Ecgp96 and DOTA labeled antibodies to Ecgp96 were labeled with AlexaFluor 488. Increasing concentrations of these fluorophore labeled antibodies (denoted as "Ecgp96" and "Ecgp96-DOTA" respectively) were added to the cells. An AlexaFluor labeled normal mouse antibody was used as a control. Cells were washed with 2% FBS in PBS and then analyzed by flow cytometry. Cells were appropriately gated based on forward and side scattering and bound antibody was measured by the geometric mean of the population fluorescent signal (Figure 2.5).

The nonlinear fit shows that when antibody is conjugated to DOTA, there is a weak decrease in binding strength and a small increase in the total amount of binding. Decrease in binding affinity was expected since DOTA conjugation was site unspecific and could mask the antibody-docking site for Ecgp96. The small increase in the total binding sites may be due to increased non-specific interaction of DOTA with HBMEC surface proteins, or due to errors in gating during data collection. Most importantly, this analysis shows the antibody to Ecgp96 does not appreciably lose its binding specificity or strength when coupled with DOTA. The normal mouse IgG control does not show binding to the HBMEC cells.

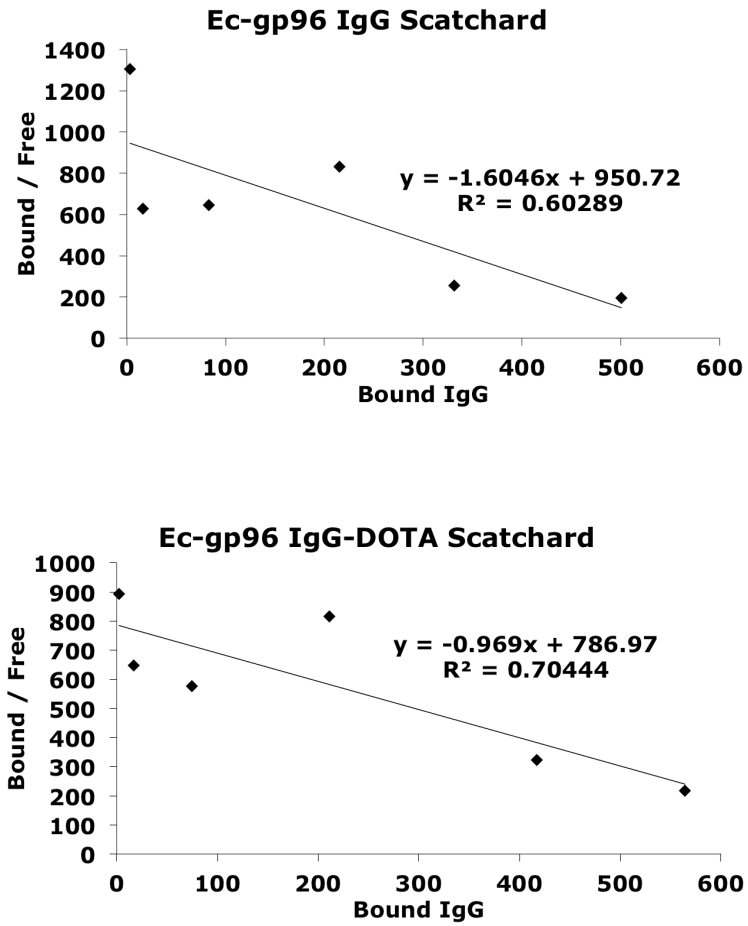

Figure 2.4: Scatchard analysis of HBMEC binding study to both unmodified antibody to Ecgp96 (top panel) and DOTA labeled antibody to Ecgp96 (bottom panel).

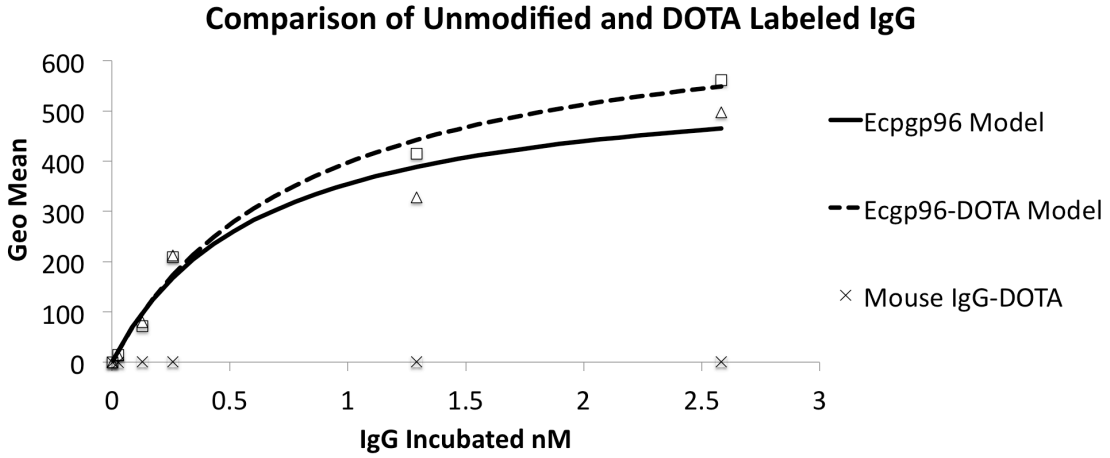

Figure 2.5: Geometric mean data generated from flow cytometry of HBMEC cells incubated with increasing concentrations of unmodified antibody to Ecgp96 and DOTA-labeled antibody to Ecgp96.

Radiochemistry and Imaging

Before injection and imaging, ^{64}Cu was incubated with the DOTA conjugated antibodies at 43 ^{o}C in a citrate buffer for 45 minutes (both antibody to Ecgp96 and a normal mouse antibody control were labeled with ^{64}Cu and injected into two separate mice). Unchelated ^{64}Cu was separated from the antibody by size exclusion using a Micro-bio-spin desalting column. Antibody labeling and purification were confirmed via instant thin layer chromatography (ITLC) using a Biodex tec-control ^{99m}Tc chromatograph strip. The IgG associated section 2 of the ITLC strip was separated from the free ^{64}Cu associated section 1, the activity of each section measured in an activity counter, and the percent labeling (%LE) calculated:

$$\%LE = \frac{\text{net counts section 2}}{\text{net counts section 1} + \text{ net counts section 2}} \qquad (3)$$

Post filtration, greater than 99.9% of activity was associated with the antibodies. Antibodies were immediately injected into C6 black adult mice (age 12-14 weeks) and two hour dynamic and 22 hour static images were taken. Images were taken at UCLA Crump Imaging Center under the direction of Dr. David Stout and Dr. Waldemar Ladno. Note there are no data for the mouse injected with normal mouse antibody at 22 hour as this mouse died overnight. According to Dr. Ladno this rarely occurred and he had no explanation for the cause of death.

Images were processed using Amide software, and the min and max threshold of

both the Ecgp96 probed and control mouse were set to the same levels. After two hours post injection, there was no clear signal in the brain of either the Ecgp96 probed mouse (Figure 2.6) or the control mouse (Figure 2.7).

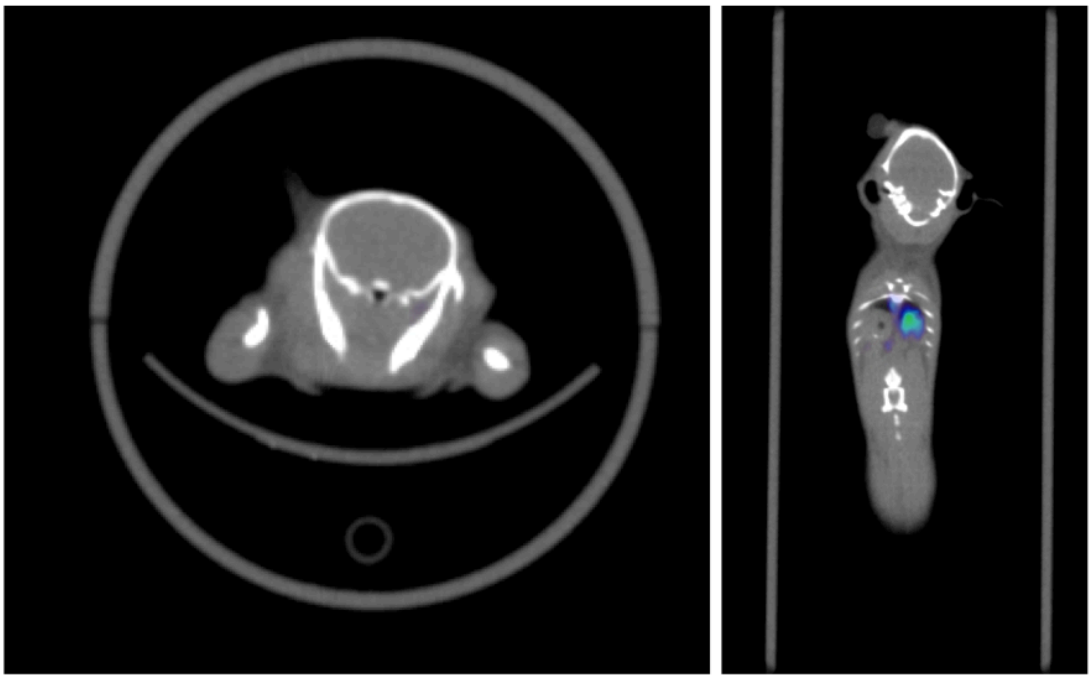

Figure 2.6: Transverse and coronal sections showing brain of a mouse injected with antibody against Ecgp96. There is no clear PET signal from the antibody in the brain.

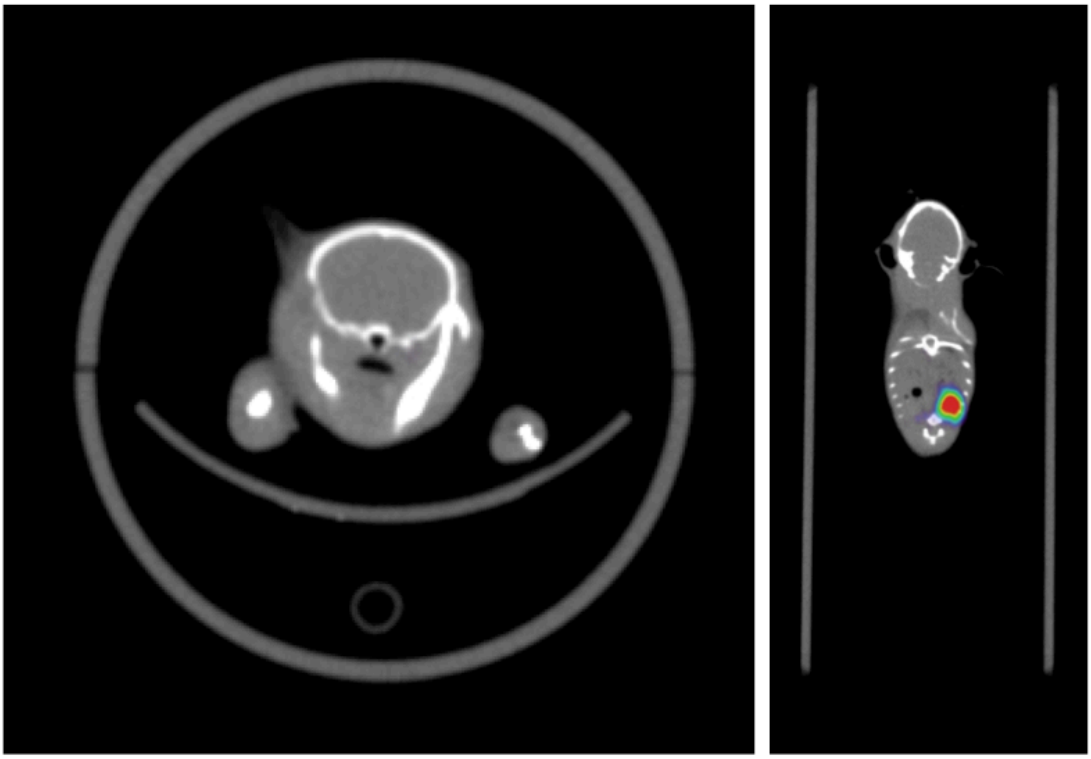

Figure 2.7: Transverse and coronal sections showing brain of a mouse injected with a normal mouse antibody. Again, there is no clear PET signal from the antibody in the brain.

Though clearly visible signal was not seen in the brain from either injected mouse, it was possible that there was a minute amount of signal that was present, but not seen due to the threshold settings input into the Amide software. Region of Interest (ROI) analysis in the Amide software was therefore employed to determine if accumulation of antibodies in the brain actually occurred. In this analysis, a three dimensional ellipsoid region of interest was placed in the brain and also in the heart to monitor the signal that is due to antibody circulating in the blood (Figure 2.8). The mean positron signal in the regions was tabulated over the dynamic scan period of two hours (Figure 2.9).

The mean positron signal from the brains of both the control mouse and Ecgp96 probed mouse closely follows the positron signal trend from the blood of both mice. In

the Ecgp96 probed mouse, it appears there is more signal in the blood than the brain, however it must be noted that the mean positron intensity in the brain was very small, and slight variations in the maximum signal used to normalize this curve could shift the curve closer to the values observed in the blood. Therefore, this analysis yielded negative results that the antibody significantly accumulated in the brain due to the presence of Ecgp96.

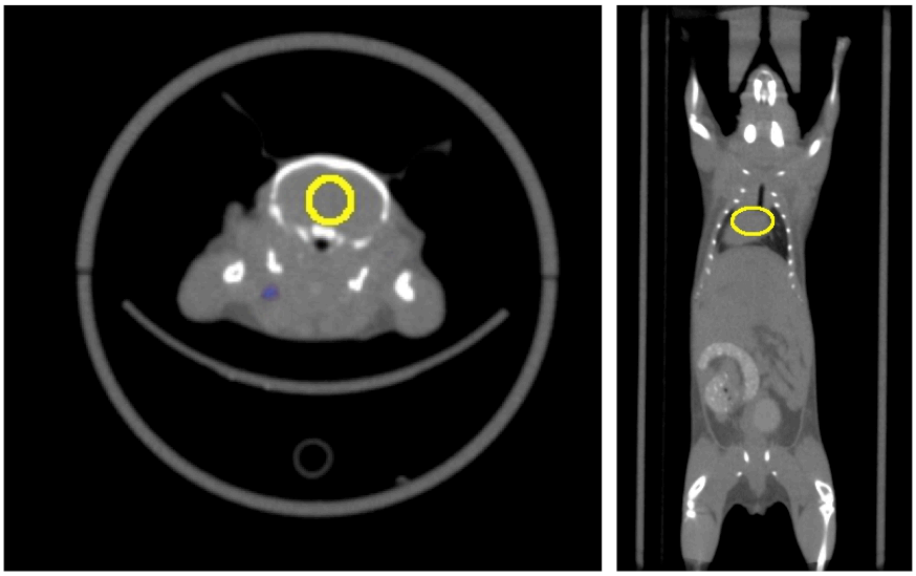

Figure 2.8: Region of Interest Analysis. Three-dimensional ellipsoid regions of interest were placed in the brain (left panel) and heart (right panel), and the mean positron signal in these regions was tabulated over the dynamic scan period of two hours.

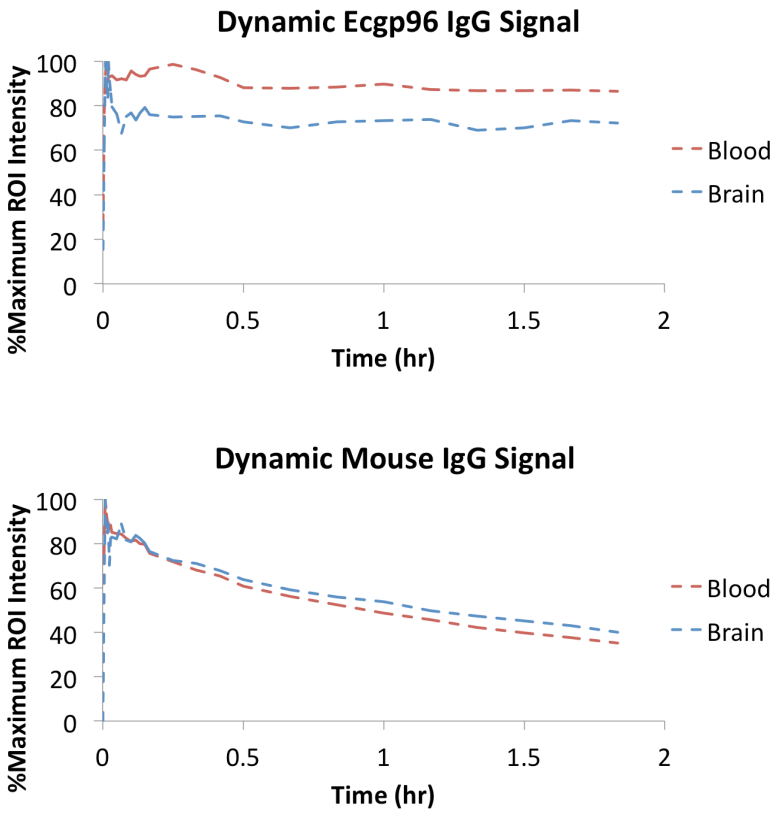

Figure 2.9: Dynamic ROI analysis. Mean positron intensities were tabulated for both the Ecgp96 probed mouse (top panel) and control mouse (bottom panel).

Though the PET scans demonstrated that Ecgp96 was likely not accessible to antibodies from the blood on the blood-brain barrier, an interesting observation was made in the eyes of the Ecgp96 probed mouse. That is, there was a significantly higher positron signal in the eyes of the Ecgp96 probed mouse than the control mouse (Figure 2.10). It was unclear if this signal was due to antibody circulating in the blood, or if the antibody had associated with Ecgp96, perhaps at the blood-retina barrier. Since the resolution of PET could not distinguish signal in retina from signal in blood, and since the ROI analysis was inconclusive, future plans for contrast enhancement MRI were made that could potentially spatially resolve these two regions (see next section).

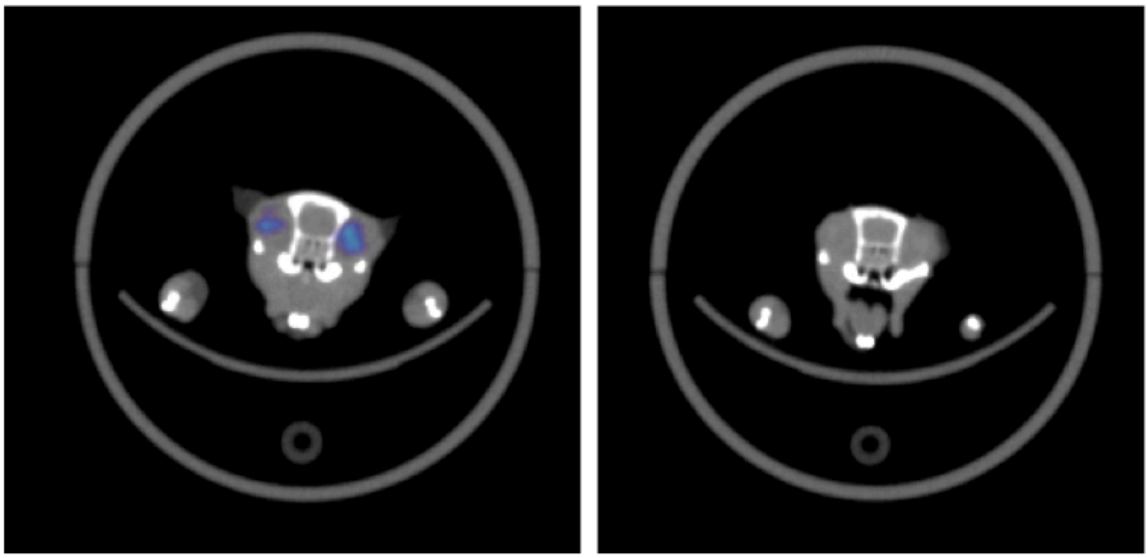

Figure 2.10: Two hours post injection, there was a significantly higher signal in the eyes of the Ecgp96 probed mouse (left panel) than the control mouse (right panel). The increased signal in the eye from the Ecgp96 antibody was also observed at 22 hours.

The PET scans did provide information that the majority of antibody (both antibody to Ecgp96 and normal mouse antibody) accumulated in the liver. At two hours, a significant amount of both antibodies stuck to the liver, though it appears more of the antibody to Ecgp96 remained in circulation than the normal mouse antibody (Figure 2.11).

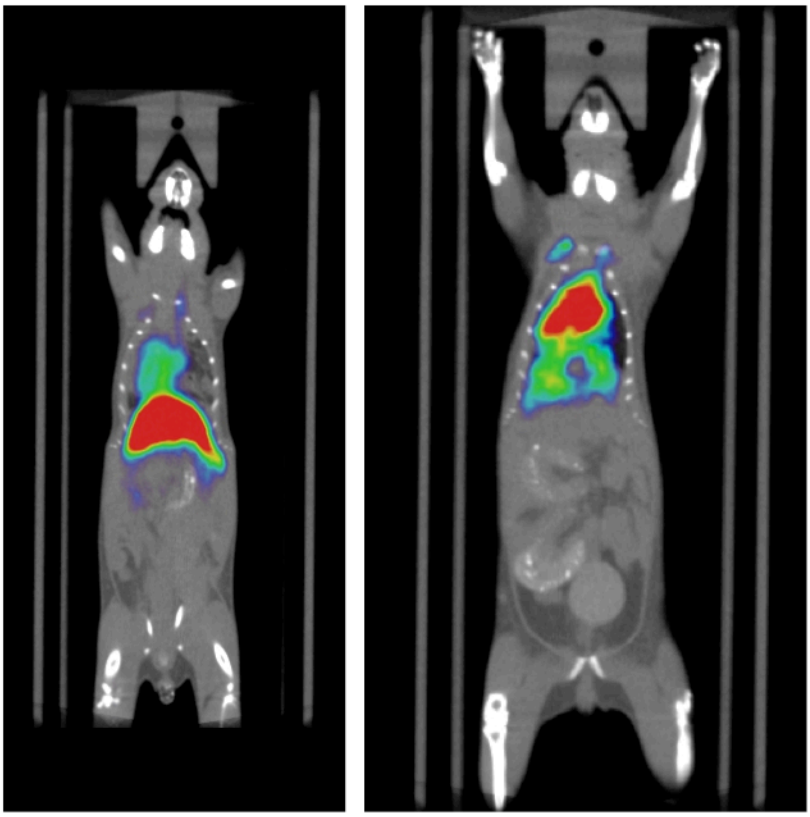

Figure 2.11: Normal mouse antibody (left panel) and antibody to Ecgp96 (right panel) two hours post injection. Normal mouse antibody accumulates in the liver more than antibody to Ecgp96, which significantly remains in the heart/circulation two hours post injection.

Conclusions for PET/CT imaging

These images provided the first evidence that Ecgp96 was not on the blood-brain barrier *in-vivo* as it was not accessible from the blood by a systemically injected antibody. Though the PET/CT images were a basis for understanding the biodistribution of Ecgp96, it was decided additional imaging was needed using other imaging modalities to confirm Ecgp96 was not present on the surface of blood-brain barrier endothelial cells *in-vivo*.

Gd Contrast MRI Imaging

Background - Searching for Ecgp96 with Increased Resolution in Eye

By PET, there was a significantly higher positron signal in the eyes of the Ecgp96 probed mouse than the control mouse, and it remained unclear if this signal was due to antibody circulating in the blood, or if the antibody had associated with Ecgp96 at the blood-retina barrier. PET was not capable of producing images that clearly resolved signal from retina as opposed to the blood or surrounding fat and glands. MRI has a spatial resolution much less than 1 mm, which is an advantage over PET; however, contrast enhanced MRI images require a concentration of imaging agents at least three orders of magnitude higher for MRI than for PET [13]. Giving up signal strength for resolution was necessary for in-vivo localization of the signal coming from the eye. Gadolinium (Gd) was selected as a contrast enhancing agent for MRI, which offers advantage over ^{64}Cu in that radioactivity is not involved - eliminating the need for radioactivity protocols and special handling procedures involved with radioactivity. Previous studies have successfully utilized DOTA-Gd labeled globulins for tumor imaging [17], and Gd-transferrin labeled gold nanoparticles which were shown to accumulate in the brain [18].

Gadolinium T1 Relaxation of Water

Gd complexes with DOTA, and the same DOTA conjugated antibodies that were used in the PET/CT scans were also used for the MRI scans. DOTA-labeled antibodies were incubated with a solution of gadolinium chloride in acetate buffer for at least an hour, and unbound gadolinium was removed by spin filtration. The arsenazo assay was

used to indirectly measure the amount of Gd chelated by DOTA (like copper, arsenazo also complexes with gadolinium [19]). To directly confirm Gd association with antibody, an NMR T1 relaxation study was employed. Gd has been used as a contrast-enhancing image agent in MRI and has been shown to decrease the T1 relaxation time of water through the relation [20]:

$$\frac{1}{T_1(C)} = \frac{1}{T_{1,0}} + \alpha_1 C \qquad (4)$$

A standard curve was generated of T1 relaxation times of water with increasing concentrations of free gadolinium. Antibodies previously loaded with Gd were measured for their associated T1 relaxation values and the standard curve was used to calculate the amount of Gd associated with the antibodies. Note this T1 relaxation quantification study may have limitations since Gd is complexed with DOTA and may not be fully accessible to water protons, which may effect the slope of equation (4).

Measurements were taken on the 600 MHz FID at the NMR facilities at Caltech using 95% H2O and 5% D2O (Figure 2.12). The arsenazo assay-based values of the Gd degree of labeling were consistent with the values obtained by the T1 relaxation study, providing both direct and indirect evidence that the antibodies were labeled with Gd through DOTA.

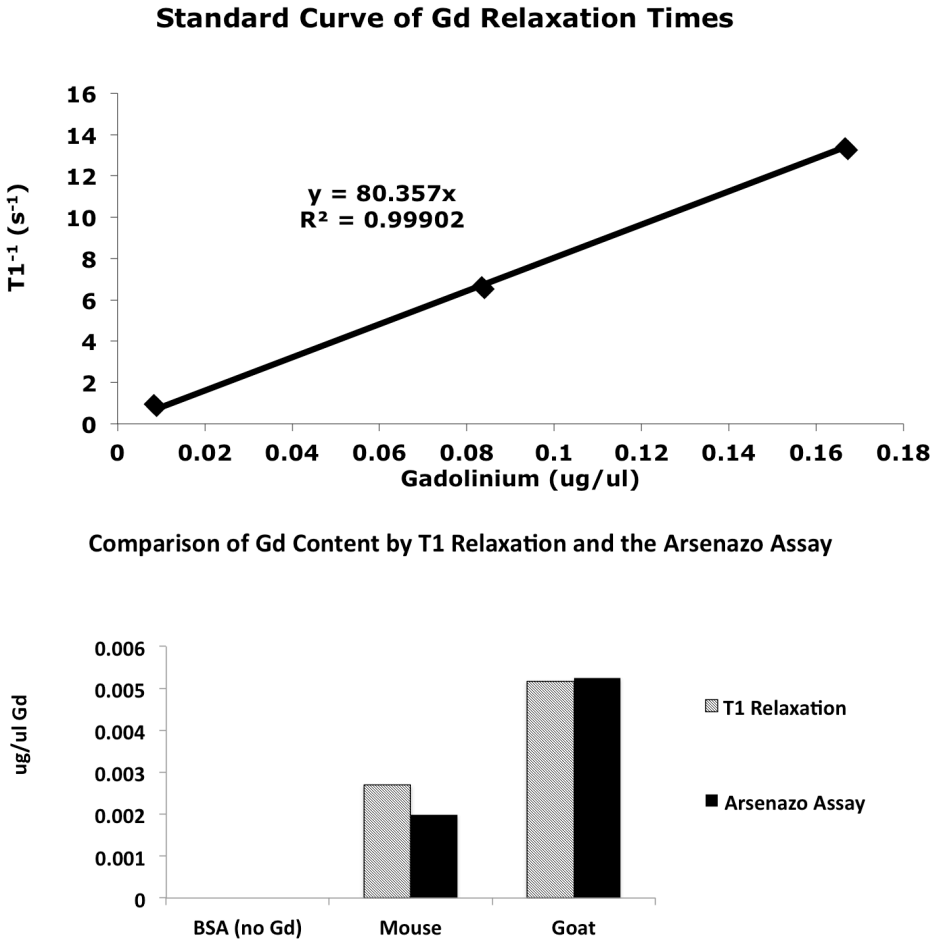

Figure 2.12. Confirmation of gadolinium loading of antibody. The T1 relaxation time of water increased with increasing concentration of free gadolinium (top panel). The concentration of gadolinium bound to antibodies in solution measured indirectly by the arsenazo assay agreed with the values obtained by direct measurement through the T1 relaxation study. Note that goat antibody 'Goat' was used in lieu of antibody to Ecgp96 as there was a limited amount of this valuable antibody left for injection. As a control the T1 relaxation of water due to bovine serum albumin (BSA) not loaded with gadolinium was measured (no measurable increased T1 relaxation of water due to protein alone).

Imaging

One mouse was injected with 5 mg/kg of the Gd labeled Ecgp96 antibody and imaged 2 hours, 4 hours, and 24 hours post injection. Figure 2.13 shows a comparison between the baseline cross-sectional image and the post-injection cross-sectional images.

There is little difference in the eye between the baseline image and the Gd contrast enhanced images and there is no clear accumulation of the Gd labeled antibody in the eye or brain. Unfortunately MRI proved to be an inadequate method for biodistribution studies - presumably due to the weak signal generated by T1 relaxation in comparison to the signal generated by ^{64}Cu in PET. There was no signal seen in brain, consistent with the PET scan.

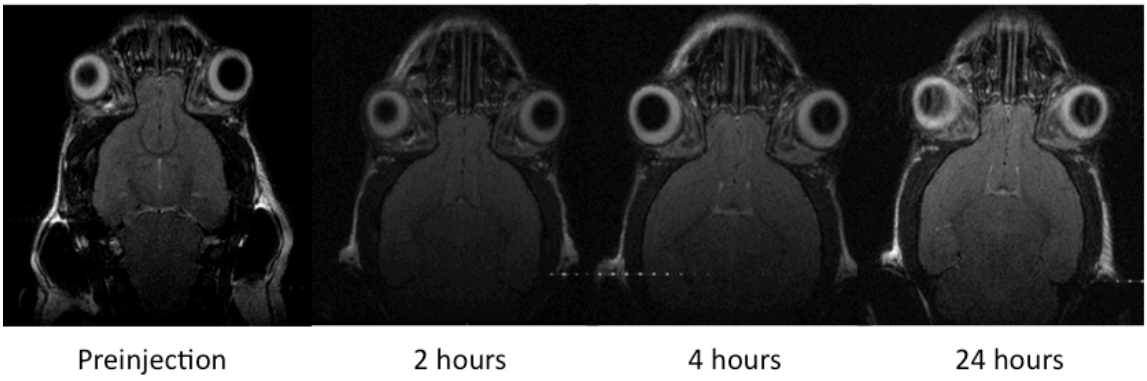

Figure 2.13: Cross sections of brain and eyes from mouse MRI images. Baseline, pre-injection (left panel) image is no different than the images taken two, four, and 24 hours (left to right) post injection of gadolinium labeled antibody to Ecgp96. There is no accumulated gadolinium signal in either the brain or the retina.

Fluorescence Xenogen Imaging and Ecgp96 Biodistribution

Motivation

Confirmation of the biodistribution trend seen in the PET/CT scans could be relatively easily accomplished through use of a fluorescence Xenogen imaging system which is capable of detecting signal of a fluorophore labeled antibody *in-vivo*. A capillary depletion method was used to determine amount of blood-brain barrier bound antibody that accumulated.

Fluorophore Conjugation

Antibodies were labeled with a near infra-red AlexaFluor at an appropriate degree of labeling (2 fluorophores per IgG) for in-vivo imaging as specified by Invitrogen SAIVI antibody labeling kit. This kit was developed specifically for labeling antibodies with near-infrared fluorophores that emit light with high tissue penetration depths for the purpose of in-vivo imaging by fluorescence Xenogen spectrophotometry.

Imaging

Two mice were shaved for fluorescence Xenogen imaging. One of the mice was injected with 4 mg/kg of AlexaFluor 680 labeled antibody to Ecgp96 while the second mouse remained un-injected, acting as an auto-fluorescence control. 24 hours post injection the mice were anesthetized with isofluorane, their right atrium was opened, and 10 ml of PBS were injected into the left ventricle. Confirmation of systemic perfusion was seen by the liver turning a whitish hue. PBS perfusion was employed to remove any antibody remaining in the blood that was not attached to the blood-brain barrier. After PBS perfusion, the brain, liver, heart, and eyes were resected and imaged simultaneously. During the analysis, the gain of the image processing software, Living Image, was adjusted so that the control organ was at the limit of detection for autofluorescence. The organ from the mouse injected with the fluorophore labeled antibody was then compared to see if there was increased fluorescence due to the accumulation of the injected antibody (Figure 2.14).

There was no increase in fluorescence signal in the brain of the injected mouse over the autofluorescence measured from the control mouse brain. This suggests that any

antibody in the brain was removed by the PBS perfusion and that no detectable antibody remained due to association with Ecgp96. This is consistent with the PET/CT ROI analysis that showed there was no increased antibody signal in the brain over the signal that was present in the blood.

There was a significant increase in the antibody-associated fluorescent signal of the liver in the injected mouse - consistent with the PET/CT scan. There was no signal seen in the eyes from the fluorophore labeled antibody, which suggests that the signal seen in the PET/CT scan may have been from the blood, or from surrounding fat or glands. There was increased signal due to the fluorophore-labeled antibody in the heart, which could possibly be from accumulation of the antibody there, or more likely from un-removed blood.

Most important to the goals of this this work, fluorescence Xenogen imaging was the second imaging modality that demonstrated there was no signal in the brain due to accumulation of antibody bound to Ecgp96. This gave the second most definitive evidence that Ecgp96 was not accessible on the blood-brain barrier to antibody from the blood.

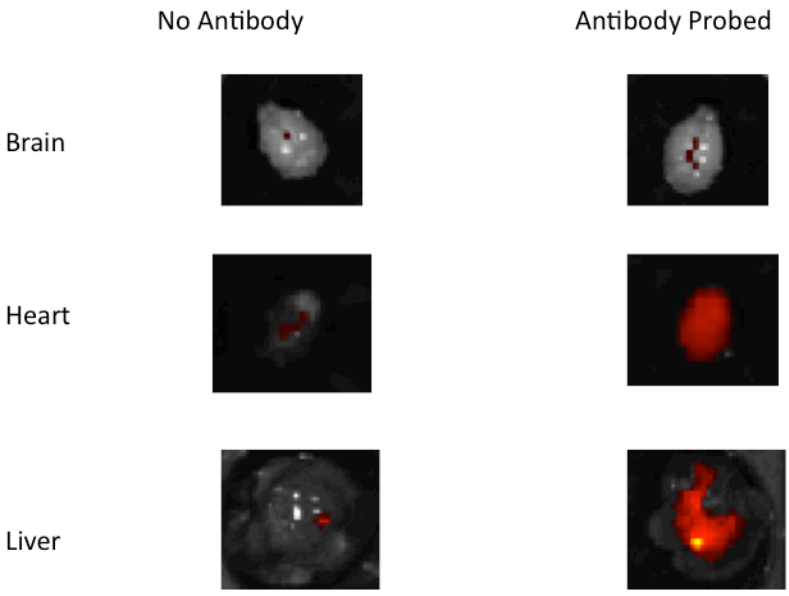

Figure 2.14: Fluorescence Xenogen Images of resected organs. The 'No Antibody' organs in the left column were from a mouse not injected with antibody. These organs were imaged directly next the organs that were resected from the mouse injected with the fluorophore labeled antibody to Ecgp96. The images from these organs are in the 'Antibody Probed' right column. During analysis, the gain of the software was increased until the 'No Antibody' organs showed first signs of autofluorescence signal. Any signal seen in the "Antibody Probed' organs is above autofluorescence and due to the fluorophore labeled antibody that was injected and remained post PBS perfusion.

SPECT/CT Imaging

Motivation

Ecgp96 was not on the surface of brain endothelial cells and accessible from the blood in adult mice. However OmpA+ E. coli have been shown to breach the blood-brain barrier through some Ecgp96-associated mechanism *in-vivo* when the studies were performed on three-day-old neonatal mice (personal communication with Dr. Prasadarao). This is consistent with E. coli meningitis being a disease of newly born infants. It was therefore hypothesized that Ecgp96 may be present on brain endothelial cells of neonatal mice, but not on the brain endothelial cells of adult mice. To test this hypothesis, a new

PET/CT biodistribution study for Ecgp96 in neonatal mice was proposed.

Injecting antibody into neonatal mice for the PET/CT studies is difficult as three-day-old mouse veins are small. To systemically administer agents into neonatal mice, Dr. Prasadarao and others [10] have used intracardiac injections. The PET/CT facilities at UCLA neither worked with neonatal mice nor performed intracardiac injections, therefore the proposed imaging studies could not be performed using PET/CT at UCLA. Dr. Prasadarao had experience with intracardiac injections and had approved protocols for working with neonatal mice at CHLA. Dr. Rex Moats at the CHLA Small Animal Imaging Research Center (SAIRC) had facilities that were willing to work with neonatal mice and image them by SPECT/CT. Therefore the proposed neonatal mouse experiments would be carried out using SPECT/CT as opposed to PET/CT.

Radiolabeling and Imaging

DOTA conjugation to IgG and radiolabeling along with confirmatory studies were performed with the same protocols used in preparation for PET/CT imaging, except that ^{111}In was used as the radioisotope for SPECT imaging in lieu of ^{64}Cu. ^{111}In is a gamma emitter with a half-life of just over two days which readily complexes with DOTA and is detectable by SPECT. Biodistribution studies of DOTA-^{111}In conjugates of different proteins have been previously performed by SPECT [21, 22].

An estimated 3 mg/kg of ^{111}In labeled antibody to Ecgp96 was injected into a C6 black adult mouse and imaged 24 hours post injection. A lead shield was placed around the body of the mouse to reduce signal from the torso allowing increased gain from brain without signal washout from non-brain regions such as the heart and liver. No signal

from the brain was observed at the maximum gain, confirming again that antibody to Ecgp96 does not accumulate in the brain of adult mice.

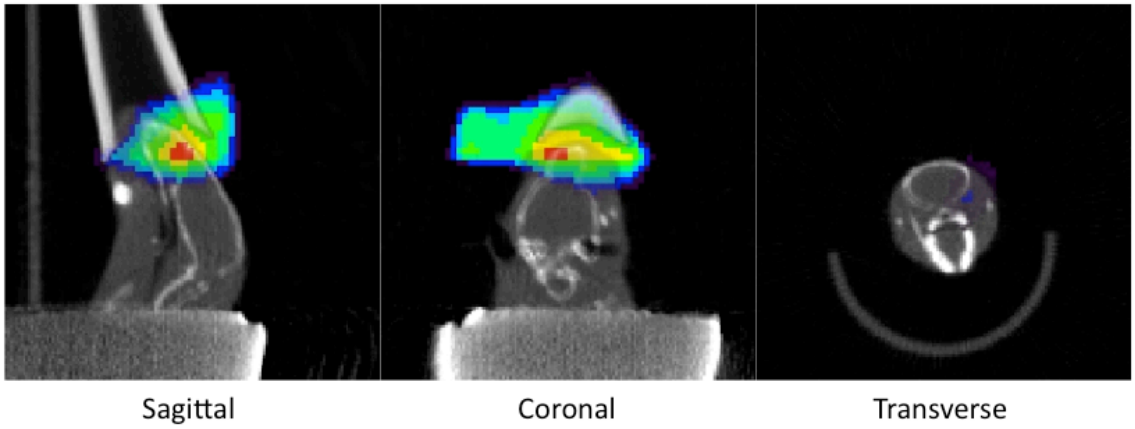

Figure 2.15: SPECT/CT images of Ecgp96 probed adult brain. The signal seen near the tip of the nose was taken when the gamma detector gain was set near saturation and is considered to be non-specific. The lead shield seen near the base of the sagittal and coronal sections eliminated signal from the heart and lung, and allowed imaging with high gamma-detection gain without signal washout in the brain from these organs. There was no detectable signal from the brain of the mouse before the gamma detector gain exceeded total signal saturation.

An estimated 3 mg/kg of ^{111}In labeled antibody to Ecgp96 was injected into a three-day old C6 black mouse and imaged 24 hours post injection. A lead shield was also placed around the body of the pup, again to reduce signal from the torso allowing increased gain from brain without signal washout from non-brain regions. Unfortunately, the technician taking the SPECT/CT scan moved the pup such that the head was not in the same position during the CT scan that it was in during the SPECT scan. It appears however that the SPECT signal is located near where the nose of the pup would have been had it not fallen out of the anesthesia tube (similar signal seen in the adult mouse brain). For the SPECT signal to be from brain, the head would have been completely inside the anesthesia tube, therefore it was assumed that the signal was not from the brain.

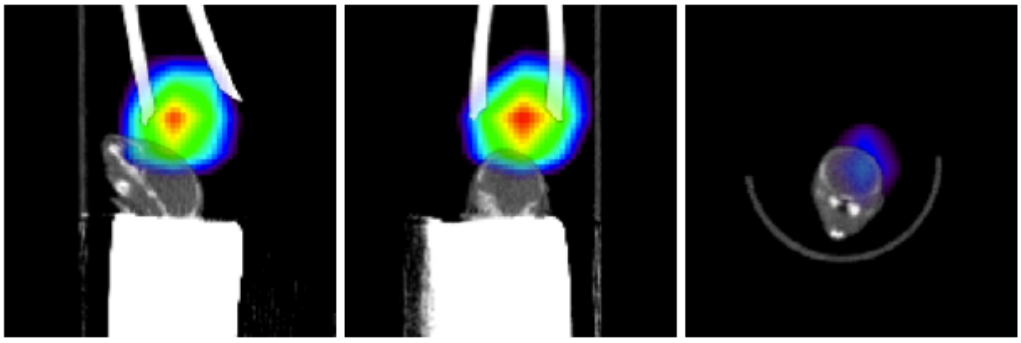

(a) pupsagittal (b) pupcoronal (c) PupTransverse

Figure 2.16: SPECT/CT images of Ecgp96 probed neonatal mouse brain. Like the adult mouse, the signal seen near the tip of the nose was taken when the gamma detector gain was set near saturation. There was no observable gamma signal in the brain of the neonatal mouse.

These results demonstrate that in normal neonatal mice there is no accumulation of antibody to Ecgp96 in the brain. Ecgp96 is therefore not present on the blood-brain barrier and accessible from the blood in three-day old mice.

Confocal Microscopy

Motivation

Ecgp96 was not detected on the blood-brain barrier *in-vivo*, however this did not conclusively rule out the possibility that Ecgp96 was not located within the endothelial cells *in-vivo*. As a final study to see if any signal could be detected in or on brain endothelium from antibody directed against Ecgp96, confocal microscopy was performed. Confocal microscopy has been validated as a method for detecting antibodies directed against blood-brain barrier receptors for up to 24 hours [23, 24]. Confocal may have advantages over PET and SPECT in that the confocal microscope can focus in on a small region of tissue possibly with a much higher sensitivity than PET or SPECT for local signal from the injected antibody.

Imaging

1.5 mg/kg of AlexaFluor 488 labeled antibody directed against Ecgp96 was injected into a six-week-old A/J mouse. 24 hours post injection the mouse was perfused with 40 ml PBS at 2 ml per min. The brain was resected, paraffin embedded, and mounted for confocal imaging. A second mouse was injected with 3.5 mg/kg of AlexaFluor 488 labeled antibody (normal mouse IgG from Santa Cruz Biotech) and similarly processed. No antibody signal was seen in the mouse antibody negative control or from sections taken from the Ecgp96 antibody injected mouse (Figure 2.17). Signal from the antibody was seen in liver consistent with the PET/CT and Xenogen experiments.

To determine if Ecgp96 was located inside the endothelial cells of the blood-brain barrier, a normal mouse brain was resected, and paraffin embedded tissue sections were stained with the antibody to Ecgp96 followed by a secondary antibody for signal enhancement. Signal from the Ecgp96 antibody was clearly observed from the blood vessels within this tissue section (Figure 2.17). Ecgp96 therefore exists in the blood vessels, however it is not accessible from the blood.

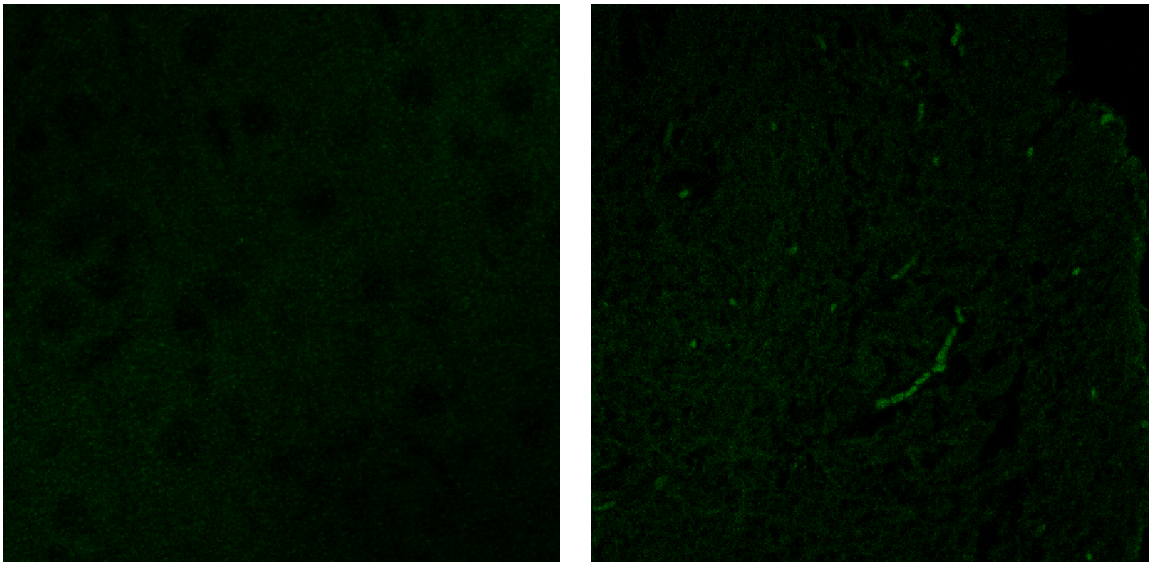

Figure 2.17: Confocal microscopy of mouse brain sections. Confocal images of the brain from the mouse injected with AlexaFluor labeled antibody to Ecgp96 show no specific signal above the background auto-fluorescence (left panel). Brains that were first resected followed by tissue staining with antibody to Ecgp96 followed by a fluorophore labeled secondary antibody show clear signal from Ecgp96 in the blood vessels (right panel).

In-vivo Studies Conclusion

In conclusion, the accumulated results from PET/CT, SPECT/CT, Fluorescence Xenogen imaging, MRI, and confocal microscopy indicate that Ecgp96 is located within the endothelial cells of the blood-brain barrier, however Ecgp96 is not accessible to antibodies from the blood. Confocal microscopy of sectioned brain tissue demonstrated that Ecgp96 did reside within the endothelial cells. PET/CT imaging demonstrated that there was no accumulation of antibodies to Ecgp96 in the brain, and ROI analysis confirmed that there was no significant accumulation of antibody in the brain above the signal observed from the blood.

SPECT/CT based biodistribution studies on neonatal mice demonstrated that Ecgp96 was also not accessible from the blood on the blood-brain barrier endothelial

cells of neonatal mice. Most importantly it was shown that Ecgp96 cannot be accessed from the blood on blood-brain barrier endothelial cells in adult mice and therefore it cannot serve as a target receptor for receptor-mediated transcytosis of nanoparticles across the blood-brain barrier.

In-vitro Studies of Ecgp96

Ecgp96 was found to be inaccessible from the blood on the blood-brain barrier *in-vivo*, however there is still evidence that Ecgp96 is expressed on the surface of brain endothelial cells *in-vitro*. HBMEC cells provided by Dr. Prasadarao were used in the binding studies of the DOTA conjugated antibody to Ecgp96, suggesting that the Ecgp96 is surface expressed on these cells, at least when they are grown in culture. The following in-vitro experiments were performed to help confirm that Ecgp96 was expressed on the surface of the HBMEC cell line and that Ecgp96 expression is increased in these cells when in the presence of E. coli-associated protein OmpA.

Confocal Microscopy of HBMEC Visualizing Surface Expression of Ecgp96

Ecgp96 has been shown to be surface expressed on HBMEC *in-vitro* through imaging of HBMEC cells incubated with E. coli and also through immunocytochemical staining and flow cytometry experiments [2-4, 11]. Since Ecgp96 is mainly an endoplasmic reticulum associated protein, it is necessary to confirm that the signal seen in the flow cytometry experiments is in fact associated with the membrane surface (and not due to endoplasmic reticulum-associated signal from cells with compromised membrane associated with cell processing). Confocal microscopy has been used in the literature to confirm surface expression of proteins [25, 26].

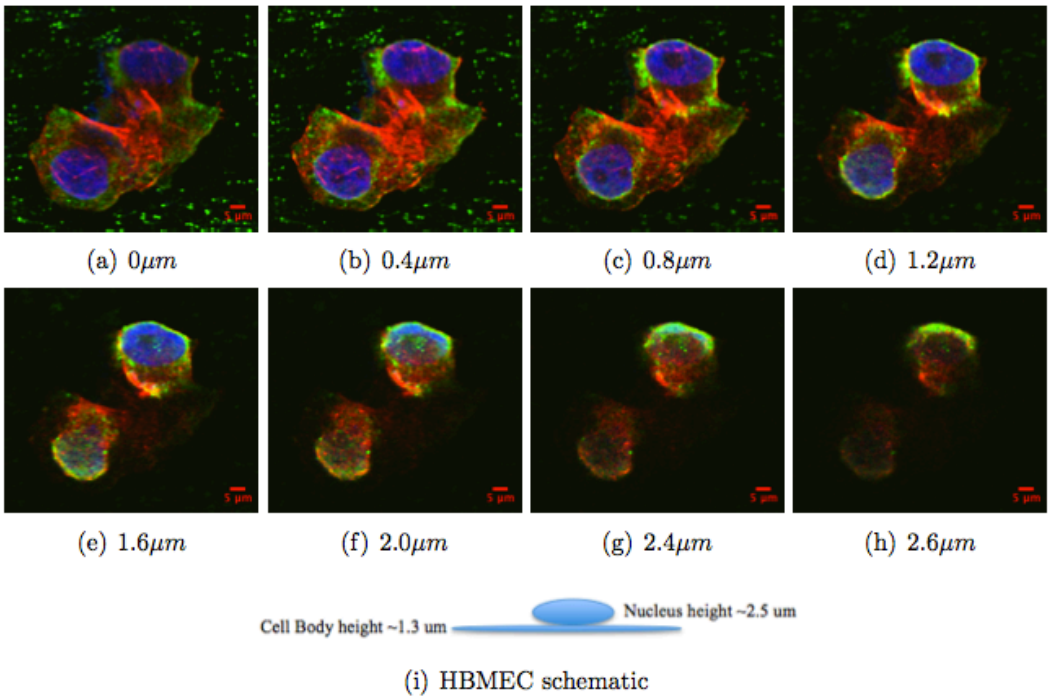

Figure 2.18: z-stack of confocal images of HBMEC cells with staining for actin (red), Ecgp96 (green), and cell nuclei (blue). Images begin at the glass slide (a) and move up by increments of 0.4 um. Passing through the bulk of the cell body near the glass slide it appears there is little to no signal from Ecgp96 colocalized with the actin signal (panels a-c) indicating there is likely no significant intracellular signal. There is clear Ecgp96 near the periphery of the cell (especially in panels c-h) indicating a strong possibility that Ecgp96 is located on the surface of the cell.

Signal for Ecgp96 appears to be on the surface of the cells, though it cannot be directly proven from these images (Figure 2.18). The optimal pinhole size (for the 488 nm laser on the LSM 510 Meta) collects light from 1 μm axially, and HBMEC cells were seen to be only 1.3 μm thick. The signal from the flattened region of the cells therefore could not be completely resolved through the z-axis to confirm signal was cell surface associated. Though signal around the area of the nucleus could be from membrane, it could also be from within the cell, in the perinuclear region of the cytoplasm where endoplasmic reticulum usually resides. The lateral resolution was only about 0.3 μm, and the signal from the nucleus (blue) is continuous with the signal from Ecgp96 (green).

This analysis shows that for thin cells (such as endothelial cells), it is difficult to determine surface expression by confocal microscopy. For cells much thicker than 1 μm, it would be easy to see a perimeter of surface-associated signal.

OmpA Induced Surface Expression of Ecgp96

Monitoring Ecgp96 surface expression of HBMEC has often involved incubation with OmpA positive E. coli [3, 11]. Our lab does not work with OmpA positive E. coli, and we have had difficulty observing Ecgp96 via flow cytometry without the HBMEC exposure to OmpA positive E. coli. It was therefore hypothesized that Ecgp96 surface expression on HBMEC cells is increased by some factor on the E. coli stimulating Ecgp96 delivery to the HBMEC cell surface. Since it has been shown there is little to no invasion of OmpA negative E. coli in HBMEC, but there is adhesion and invasion of OmpA positive E. coli into HBMEC, it was likely that OmpA was the E. coli protein responsible for the proposed mechanism of increased Ecgp96 surface expression. To independently confirm that OmpA may be in fact stimulating the surface expression of Ecgp96 on HBMEC cells (as opposed to other possibly confounding factors associated with E. coli), purified recombinant OmpA was purchased from a third party (Genway), and a flow cytometry based binding experiment was performed with OmpA pre-incubated cells.

One flask of HBMEC cells was incubated with 10 nM OmpA for one hour. Three flasks were placed on ice for 20 minutes (remaining on ice for the remainder of processing), and then cells were removed by scraping. The cells were then incubated in increasing concentrations of an Abcam GRP94 antibody for one hour. The cells were

washed and all cells were incubated in a 1:500 goat-anti-rabbit-AF488 antibody for 30 minutes. The cells were again washed and analyzed by flow cytometry. All forward and side scattering gating and voltage gain settings were set on the first measured sample and unchanged afterward. Primary antibody to intracellular antigen (bcl-2) acted as an isotype control that should not bind to the cell surface and that would serve as a control to confirm the cell membrane remained un-permeabilized during cell processing. Scatchard analysis was performed to determine the initial K_a and $[\star]_o$ guesses for nlinfit (Scatchard values are in parentheses in the table below).

	OmpA +	OmpA -	Bcl-2
K_a (pM^{-1})	60 (72)	88 (90)	16 (Small)
$[*]_o$	769 (664)	360 (335)	501 (Large)

Table 2.1. Binding strengths of GRP94 antibody to HBMEC associated Ecgp96 (K_a) and modeled total number of Ecgp96 binding sites on HBMEC cells $[\star]_o$.

These values suggest that by adding OmpA, the total number of GRP94 antibody binding sites significantly increases on HBMEC cells (very similar to the results reported by Mittal et al [11]). Also this data suggests that upon addition of OmpA, the binding affinity of Ecgp96 to the GRP94 antibody decreases, which is likely due to Ecgp96-OmpA interactions that reduce the antibody docking sites on Ecgp96. The isotype control showed almost no specific binding to the cells, however there was a small amount that did bind indicating there may have been some cell death and membrane permeabilization during processing for flow cytometry. Inserting $[\star]_o$ and K_a into a Langmuir Isotherm, the data can be well fit (Figure 2.19). Error bars indicate one standard deviation of the gated events.

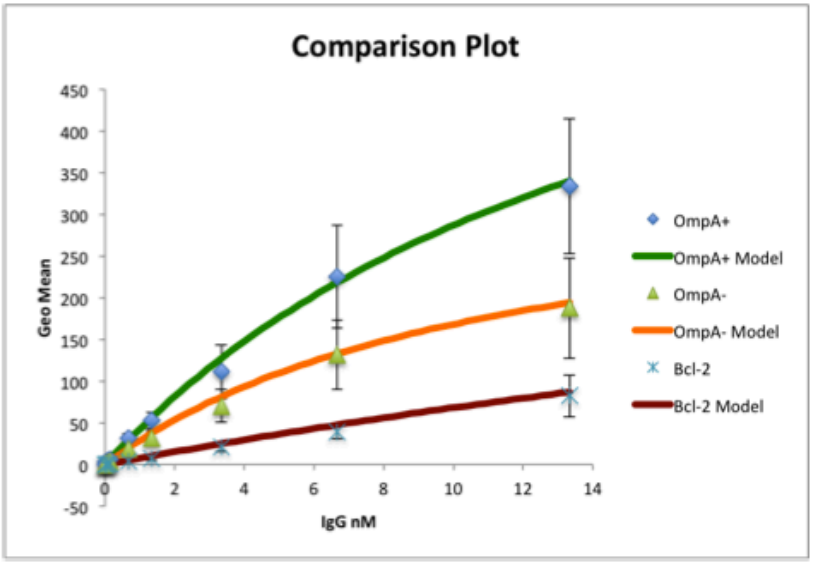

Figure 2.19: Flow Cytometry of HBMEC cells. Cells incubated with OmpA have increased expression of Ecgp96 receptor on their surface.

These results are significant since they show that the Ecgp96 receptor is more highly expressed on the surface of HBMEC cells when they are exposed to OmpA. Since OmpA increases the surface expression of Ecgp96 on the HBMECs in-vitro it may be that OmpA is necessary to stimulate the expression of Ecgp96 on the surface of brain endothelial cells in-vivo. Administration of OmpA expressing E. coli in-vivo may therefore stimulate the surface expression of Ecgp96 on brain endothelium.

Since E. coli meningitis is a disease of neonates and is predominantly due to OmpA positive E. coli, one interpretation of Dr. Prasadarao's studies in light of our *in-vivo* and *in-vitro* results is that neonatal (but not adult) blood-brain barrier endothelial cells *in-vivo* are stimulated by OmpA positive E. coli to express Ecgp96 on their surface at pathologically significant quantities. This may facilitate the interaction of OmpA with Ecgp96, and subsequently some mechanism occurs that allows the passage of the E. coli across the blood-brain barrier.

In-vitro Studies Conclusion

Studies of HBMEC cells in culture demonstrated that the expression of Ecgp96 on HBMEC cells in culture is directly related to the presence of the E. coli related protein, OmpA, without the presence of the E. coli itself. Since E. coli has been shown to infiltrate the central nervous system of neonatal mice, and that E. coli meningitis is predominantly a disease of neonatal infants, it was concluded that E. coli and related OmpA are likely necessary for the expression of Ecgp96 on the surface of blood-brain endothelial cells in neonatal mice. This would be consistent with OmpA positive E. coli as a stressor that causes the loss of Ecgp96 ER retention signal KDEL (which has been reported for cells under stress [3, 16]) and subsequent Ecgp96 transport to and accumulation at the site of OmpA positive E. coli binding.

Summary and Discussion

Our studies have demonstrated that Ecgp96 cannot be accessed at the blood-brain barrier from the blood *in-vivo* in adult and neonatal mice under normal, non-pathological conditions. These results conclusively demonstrate Ecgp96 cannot be used as a receptor at the blood-brain barrier for receptor-mediated nanoparticle delivery to the brain. These results also help direct future work to be performed by infectious disease labs to further understand the mechanism of E. coli mediated neonatal meningitis, and in particular how Ecgp96 is involved in this process. The *in-vivo* results from this work suggest there must be an alternative mechanism that explains how OmpA positive E. coli are more able to penetrate the blood-brain barrier than OmpA negative E. coli. In particular future work is

needed with focus on how OmpA may be necessary for the expression of Ecgp96 on the surface of blood-brain barrier endothelial cells in neonatal mice when E. coli are present in the blood at pathologic levels.

For the purposes of our lab and targeted drug delivery, it is undesirable to target a receptor that cannot be visualized without stimulation by an E. coli meningitis-associated protein such as OmpA. Though academically interesting, it would be clinically impractical to develop a therapeutic that would either require a pre-injection of OmpA in humans or incorporate a possibly harmful OmpA molecule on the nanoparticle surface to make the nanoparticle capable of crossing the blood-brain barrier. A more practical solution to delivering nanoparticles into the brain would be to target a blood-brain barrier receptor that is widely accepted to be on blood-brain barrier endothelial cells and is associated with receptor mediated transcytosis. The transferrin receptor has both of these advantages and already has a clinically approved recombinant protein for human application that can be used for receptor targeting. The transferrin receptor is therefore much better suited for investigation than Ecgp96.

References

1. National Center for Health Statistics. NCHS Data Brief 90, Number 88, March 2012. 1–8 (2012).
2. Prasadarao, N., Wass, C. & Kim, K. Identification and characterization of S-fimbria-binding sialoglycoproteins on brain microvascular endothelial cells. *Infection and Immunity* **65,** 2852–2860 (1997).
3. Prasadarao, N. Identification of Escherichia coli outer membrane protein A receptor on human brain microvascular endothelial cells. *Infection and Immunity* **70,** 4556 (2002).
4. Prasadarao, N. *et al.* Cloning and expression of the Escherichia coli K1 outer membrane protein A receptor, a gp96 homologue. *Infection and Immunity* **71,** 1680 (2003).
5. Csermely, P., Schnaider, T., Soti, C., Prohaszka, Z. & Nardai, G. The 90-kDa molecular chaperone family: Structure, function, and clinical applications. A comprehensive review. *Pharmacol Therapeut* **79,** 129–168 (1998).
6. Robert, J., Menoret, A. & Cohen, N. Cell surface expression of the endoplasmic reticular heat shock protein gp96 is phylogenetically conserved. *J Immunol* **163,** 4133–4139 (1999).
7. Kang, S. H. & Welch, W. J. Characterization and purification of the 94-kDa gluocose-regulated protein. *J Biol Chem* **266,** 5643–5649 (1991).
8. Altmeyer, A. *et al.* Tumor-specific cell surface expression of the -KDEL containing, endoplasmic reticular heat shock protein gp96. *Int J Cancer* **69,** 340–349 (1996).

9. Ahmed Khan, N. Outer membrane protein A and cytotoxic necrotizing factor-1 use diverse signaling mechanisms for Escherichia coli K1 invasion of human brain microvascular endothelial cells. *Microbial Pathogenesis* **35,** 35–42 (2003).

10. Wang, Y. & Kim, K. S. Role of OmpA and IbeB in Escherichia coli K1 invasion of brain microvascular endothelial cells in vitro and in vivo. *Pediatr Res* **51,** 559–563 (2002).

11. Mittal, R. & Prasadarao, N. V. Nitric oxide/cGMP signalling induces Escherichia coli K1 receptor expression and modulates the permeability in human brain endothelial cell monolayers during invasion. *Cellular Microbiology* **12,** 67–83 (2010).

12. Nag, S., Kapadia, A. & Stewart, D. J. Review: Molecular pathogenesis of blood-brain barrier breakdown in acute brain injury. *Neuropathology and Applied Neurobiology* **37,** 3–23 (2011).

13. Smith, S. Molecular imaging with copper-64. *Journal of Inorganic Biochemistry* **98,** 1874–1901 (2004).

14. Bartlett, D. W., Su, H., Hildebrandt, I. J., Weber, W. A. & Davis, M. E. Impact of tumor-specific targeting on the biodistribution and efficacy of siRNA nanoparticles measured by multimodality in vivo imaging. *P Natl Acad Sci Usa* **104,** 15549–15554 (2007).

15. Al-Ejeh, F., Darby, J. M., Thierry, B. & Brown, M. P. A simplified suite of methods to evaluate chelator conjugation of antibodies: effects on hydrodynamic radius and biodistribution. *Nuclear Medicine and Biology* **36,** 395–402 (2009).

16. Brady, E. D., Chong, H. S., Milenic, D. E. & Brechbiel, M. W. Development of a

spectroscopic assay for bifunctional ligand-protein conjugates based on copper. *Nuclear Medicine and Biology* **31,** 795–802 (2004).

17. Tan, M., Wu, X., Jeong, E.-K., Chen, Q. & Lu, Z.-R. Peptide-targeted nanoglobular Gd-DOTA monoamide conjugates for magnetic resonance cancer molecular imaging. *Biomacromolecules* **11,** 754–761 (2010).
18. Korkusuz, H. *et al.* Transferrin-coated gadolinium nanoparticles as MRI contrast agent. *Mol Imaging Biol* (2012). doi:10.1007/s11307-012-0579-6
19. Nagaraja, T. N. *et al.* Application of arsenazo III in the preparation and characterization of an albumin-linked, gadolinium-based macromolecular magnetic resonance contrast agent. *J Neurosci Methods* **157,** 238–245 (2006).
20. Curtet, C. *et al.* Selective modification of NMR relaxation time in human colorectal carcinoma by using gadolinium-diethylenetriaminepentaacetic acid conjugated with monoclonal antibody 19-9. *P Natl Acad Sci Usa* **83,** 4277–4281 (1986).
21. Virgolini, I. *et al.* Indium-111-DOTA-lanreotide: Biodistribution, safety and radiation absorbed dose in tumor patients. *Journal of Nuclear Medicine* **39,** 1928–1936 (1998).
22. Jalilian, A. Preparation, quality control and biodistribution studies of two [111In]-rituximab immunoconjugates. *Sci Pharm* **76,** 151–170 (2008).
23. Paris-Robidas, S., Emond, V., Tremblay, C., Soulet, D. & Calon, F. In vivo labeling of brain capillary endothelial cells after intravenous injection of monoclonal antibodies targeting the transferrin receptor. *Mol. Pharmacol.* **80,** 32–39 (2011).

24. Yu, Y. J. *et al.* Boosting brain uptake of a therapeutic antibody by reducing its affinity for a transcytosis target. *Science Translational Medicine* **3,** 1–8 (2011).

25. Jiang, W., Kim, B. Y. S., Rutka, J. T. & Chan, W. C. W. Nanoparticle-mediated cellular response is size-dependent. *Nature Nanotech* **3,** 145–150 (2008).

26. Na, X., Kim, H., Moyer, M. P., Pothoulakis, C. & Lamont, J. T. gp96 is a human colonocyte plasma membrane binding protein for Clostridium difficile toxin A. *Infection and Immunity* **76,** 2862–2871 (2008).

Chapter 3: Formulation and Characterization of Transferrin Containing Gold Nanoparticles*

Introduction

Once it was established Ecgp96 was not a good candidate target receptor at the blood-brain barrier for achieving receptor mediated transcytosis, a decision was made to attempt to deliver nanoparticles to the brain through the transferrin receptor. The transferrin receptor is responsible for internalizing iron carrying protein transferrin, it is expressed throughout the body, it is well accepted to exist on the blood-brain barrier [1], and it has been widely studied for its potential ability to deliver entities across the blood-brain barrier (historically by monoclonal antibody OX26) [2]. Usage of transferrin receptor enables further investigations of different nanoparticle designs that may cross the blood-brain barrier by receptor-mediated transcytosis. A well-defined set of nanoparticle designs of varying size and transferrin content are formulated and characterized here in order to carry out meaningful *in-vivo* experiments.

The objective of this work was to investigate whether the blood-brain barrier transcytosis behavior of transferrin-targeted nanoparticles was similar to the blood-brain barrier transcytosis behavior of antibodies reported by Yu et al. [3] in the sense that the avidity (or nanoparticle effective binding strength to multiple receptors) must be appropriately modulated in order to allow receptor binding from the blood, transcytosis across the blood-brain barrier, and release from the receptors into the brain parenchyma.

---

* Excerpts of this chapter are reproduced with permission from "Transcytosis and brain uptake of transferrin-containing nanoparticles by tuning avidity to transferrin receptor." Wiley, D. T., Webster, P., Gale, A., & Davis, M. E. *Proc. Natl. Acad. Sci. USA*. (2013).

Our expectation was that in order to effectively undergo blood-brain barrier transcytosis the nanoparticles would need proper avidity, size and surface charge. Designs of varying nanoparticle size and avidity with fixed zeta potentials are studied here.

Our research group has been involved in translating two nanoparticles from the laboratory into clinical trials [4-5]. These nanoparticles are below 100 nm in size for many reasons including their ability to move through tissues. Here, we restrict our investigations to nanoparticles in this size range. After the completion of our experimental studies, it was reported that nanoparticles in the sub-100 nm range can, in fact, move through brain tissue [6]. Additionally, it is known that nanoparticle zeta potentials that are slightly negative to near neutral are desirable, as highly negatively and positively charged nanoparticles are known to: (i) disrupt the BBB [7], (ii) facilitate formation of protein coronas that may mask or alter the function of the targeting ligand [8], and (iii) elicit unwanted immune responses and faster blood clearances via increased uptake through the mononuclear phagocyte system (MPS) [9].

It is well known that the avidity and receptor selectivity of targeted nanoparticles can be tuned by the choice of targeting ligand and its number density (multivalent nanoparticles can engage multiple cell surface receptors at the same time) [10, 11]. When an individual targeting ligand is conjugated to a nanoparticle, the affinity of the ligand to the receptor is reduced. However, if the receptor density is such that multiple targeting ligands on the nanoparticle can simultaneously bind to the receptors, then the targeted nanoparticle avidity [12] and selectivity [11] can be increased. These effects have been illustrated in several investigations; for example, Choi et al. reported the interactions of transferrin-containing gold nanoparticles on both cancer cells in-vitro and

tumors in-vivo in mice [12]. These authors showed that the animal whole body biodistribution of transferrin containing gold nanoparticles of ca. 70 nm diameter was independent of the transferrin content, but that the amount of nanoparticles localizing in the cancer cells of solid tumors 24 hours after injection increased with increasing transferrin content. Thus, the targeting ligand acts as a cell entrance facilitator rather than altering the biodistribution of the nanoparticles. This effect is now being reported for a number of different types of targeted nanoparticles.

Transferrin-containing gold nanoparticles were chosen as a model nanoparticle system to engage the transferrin receptor at the blood-brain barrier. Human transferrin has already been used as a targeting agent on nanoparticles in human clinical trials [4, 13], and it is a recognized ligand for the well established transferrin receptor at the blood-brain barrier. Human transferrin that is fully loaded with iron (holo-transferrin) binds strongly to transferrin receptor (K_d = 1-10 nM) [14], and, after vesicle acidification and iron release, the subsequent apo-transferrin has a reduced binding strength to transferrin receptor (K_d > 700 nM) [14] at physiologic pH. Mouse transferrin was not employed for reasons provided below.

Gold nanoparticles were chosen for this work due to their ease of synthesis, surface modification through reactions with thiol groups, quantification by inductively coupled plasma–mass spectroscopy (ICP-MS), and imaging by TEM. Additionally, we found that gold nanoparticles are convenient for studies of the blood-brain barrier because they can be visualized inside and outside the vasculature by light microscopy through silver enhancement. The silver enhancement of gold nanoparticles is a highly sensitive detection technique, and has been used to detect zeptomolar concentrations of

nanoparticles in immune assays [15]. Furthermore, silver enhancement has been used to visualize gold nanoparticles in kidney and tumor through light microscopy [16, 17].

Experimental Results

Transferrin was coupled to gold nanoparticles through an NHS-PEG_{5k}-OPSS linker, where the NHS-ester reacts with transferrin through primary amines on lysine groups (preferred PEG coupling method to transferrin [18]), and OPSS reacts with gold surfaces through gold-thiol dative bonding (Figure 3.1). Mono-PEGylated transferrin was highly purified before coupling to the gold nanoparticles (Figure 3.2), as di-PEGylated transferrin can cause a small degree of particle aggregation. Gold cores of increasing sizes (5 nm, 20 nm, and 50 nm) were reacted with increasing amounts of Tf-PEG_{5k}-OPSS (transferrin – Tf), and afterward, methoxy-PEG_{5k}-SH (PEGylation) was added to the nanoparticle surface to increase nanoparticle stability in high ionic solutions such as blood. Attempts to use mouse transferrin for nanoparticle assembly failed. For unknown reasons, mouse transferrin does not appear to be as stable as human transferrin to these types of physical and chemical manipulations.

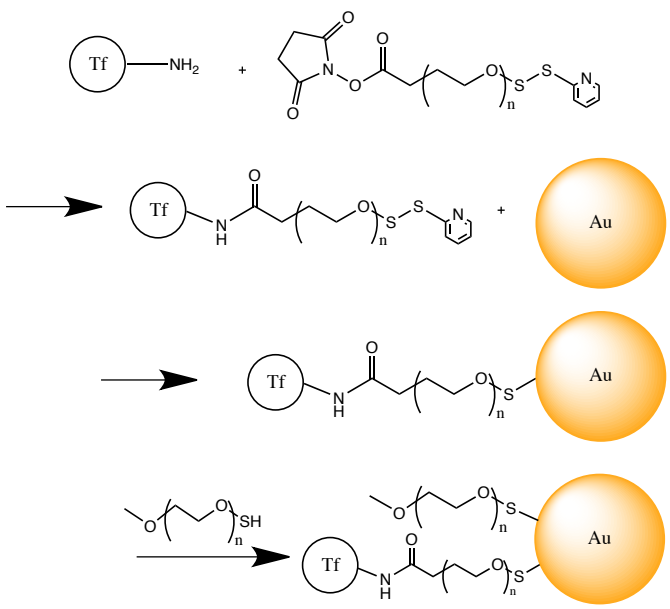

Figure 3.1: Representation of targeted nanoparticle assembly process (n ~ 120, PEG MW of 5,000 Da).

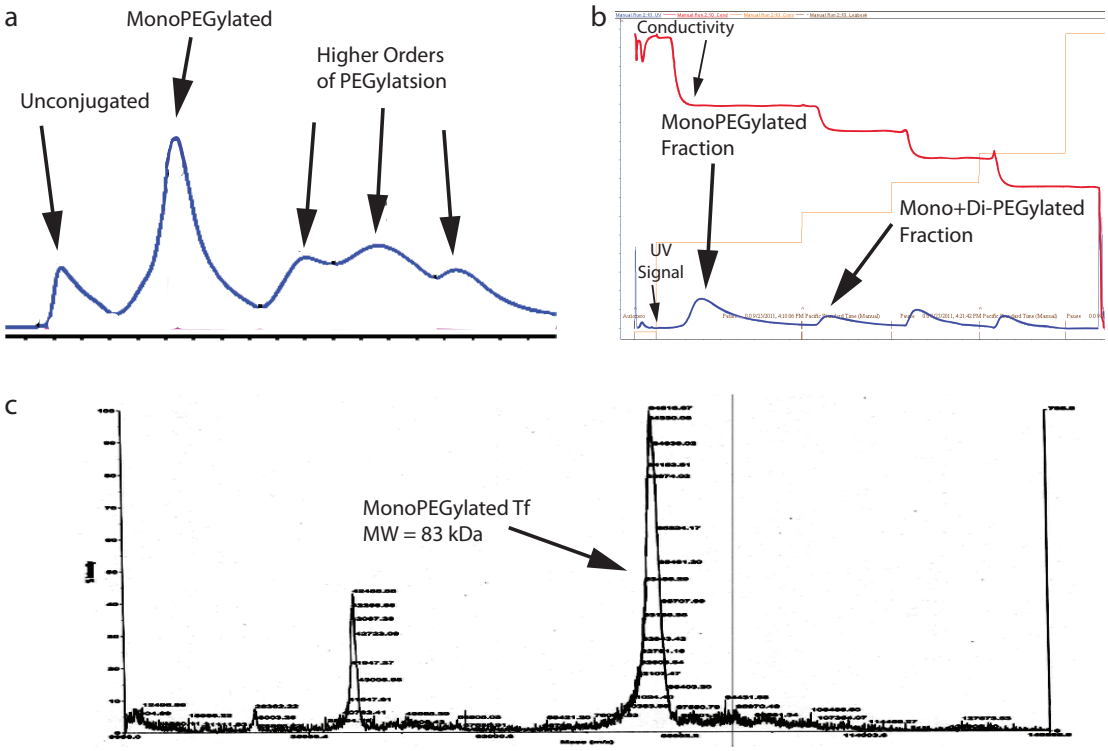

Figure 3.2. **a**, High Pressure Liquid Chromatography (HPLC) data with an impure monoPEGylated fraction eluting at the second peak. All unconjugated transferrin eluted in the first peak. **b**, Hydrophobic Interaction Chromatography (HIC) performed post HPLC with a pure monoPEGylated fraction eluting from the first peak. **c**, Matrix

Assisted Laser Desorption-Ionization Time of Flight (MALDI-TOF) Mass Spectroscopy demonstrating a monoPEGylated fraction was obtained (MW = 83 kDa); unPEGylated transferrin had a MALDI-TOF peak at 78 kDa.

Nanoparticle sizes were measured with dynamic light scattering (DLS) and Nanoparticle Tracking Analysis (NTA) technologies. NTA methods allow direct visualization of individual nanoparticles and can provide nanoparticle size distributions within a sample. All NTA sizes listed in Table 3.1 are from unimodal size distributions, indicating a single population of similarly sized nanoparticles. Unfortunately, the smaller sized nanoparticles cannot be detected by this method. Since the NTA size distributions were unimodal, DLS was employed, and the sizes listed in Table 3.1. For those nanoparticles measured by both NTA and DLS methods, the sizes were essentially the same. All the nanoparticles synthesized had zeta potentials between -15 mV and -5 mV, when measured in 1.5 mM KCl (Table 3.1). Zeta potential distributions were measured for the ca. 80 nm nanoparticles using NTA methods. The full width at half maximum (FWHM) values obtained from the zeta potential distributions did not vary with transferrin content. These data would be consistent with a similar Poisson-type distribution of transferrin over the nanoparticle population for each formulation.

Transferrin content on the nanoparticles was directly measured by: (i) apo-Tf-PEG-OPSS chelation of ^{64}Cu, (ii) nanoparticle formulation with ^{64}Cu-Tf-PEG-OPSS, and (iii) measurement of nanoparticle associated gamma activity (Cu chelation method modified from [19]). The average transferrin contents of some of the nanoparticle formulations are listed in Table 3.1. The nanoparticles were formulated so that there was a wide range of transferrin on the surface of the nanoparticles; each size having a formulation with very little transferrin, and a formulation approaching the maximum

number of possible transferrin molecules on each particle. The theoretical maxim density of transferrin on the surface of the nanoparticle was estimated based on the total surface area of the particle (from the surface area of a sphere), and an estimate of the amount of surface each transferrin molecule could cover (hydrodynamic radius approximately 4 nm per transferrin [20]). Note that as the attempted loading of transferrin increased (amount listed in column one of Table 1), the fraction of transferrin that actually was on the nanoparticle decreased, most likely due to steric crowding.

More critical than the precise number of transferrin on each nanoparticle formulation is the nanoparticle avidity and how it changes with transferrin content. Yu et al. performed competitive binding assays with mouse transferrin receptor in order to provide a relative ranking of the antibodies used in their study [3], while Friden et al. used purified human transferrin receptor and the human K562 cell line to measure transferrin and antibody binding [21]. Here, in order to provide a relative ranking of nanoparticle avidity, binding isotherms were obtained using Neuro2A cells as a model cell type with mouse transferrin receptor (Figure 3.3, K_d values listed in Table 3.1). The K_d values have an inverse relationship with transferrin content (Figure 3.4a). There is a clear increase in avidity with transferrin content within each formulation size (Figure 3.4b). Within the limited number of nanoparticles used in this study, it appears that there is a weak effect of size on avidity (Figure 3.4b). Previous reports that included much smaller nanoparticle sizes similarly observed that increasing the size and antibody content of antibody-coated nanoparticles increased their avidity to cell surface receptors [22].

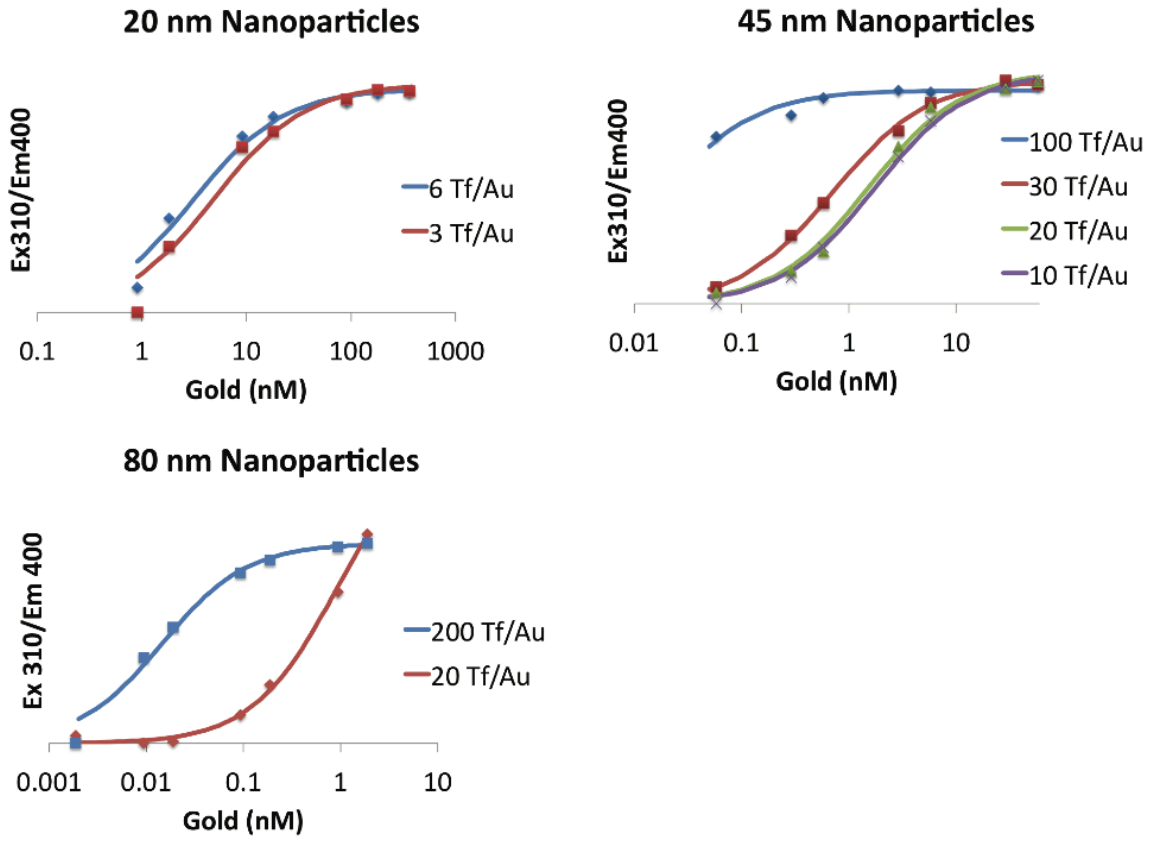

Figure 3.3: Binding isotherm data for each nanoparticle formulation on Neuro2A cells. The model curves are based on Langmuir isotherms, where K_d and B_{max} values were numerically determined by Matlab nlinfit.

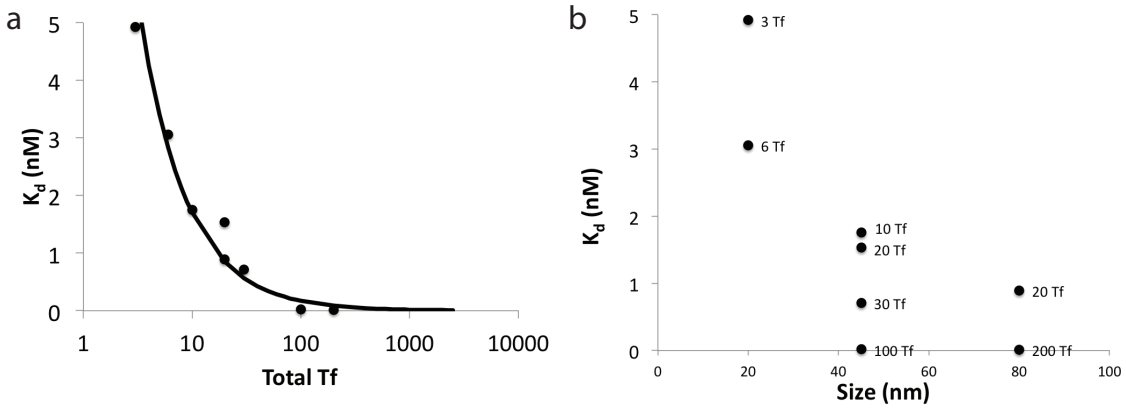

Figure 3.4: Binding data of gold nanoparticle formulations on Neuro2A cells. **a,** Effects of nanoparticle transferrin content on the binding dissociation constant of the nanoparticle to Neuro2A transferrin receptors. **b,** Effects of nanoparticle size and transferrin content on binding dissociation constant of the nanoparticle to Neuro2A transferrin receptors.

Formulations (Core + no. of Tf)	Tf measured from ^{64}Cu Experiment	Nanoparticle Diameter (DLS)	Nanoparticle Diameter (NTA)	Zeta Potential in KCl (mV)	Binding Constant, K_d (nM)
5 nm + mPEG	0	21.6 ± 0.2	n.d.	-11.4 ± 1.3	-
5 nm + 3 Tf	3.2	21.0 ± 2.5	n.d.	-12.9 ± 0.3	4.9
5 nm + 6 Tf	4.6	25.3 ± 2.5	n.d.	-10.0 ± 1.9	3.1
20 nm + mPEG	0	46.1 ± 2.7	n.d.	-8.3 ± 0.8	-
20 nm + 10 Tf	7.4	44.6 ± 3.2	n.d.	-14.4 ± 2.2	1.7
20 nm + 20 Tf	9.5	43.6 ± 4.6	n.d.	-6.8 ± 0.4	1.5
20 nm + 30 Tf	n.d.	48.3 ± 2.9	n.d.	-14.1 ± 1.4	0.71
20 nm + 100 Tf	49.9	46.3 ± 1.3	n.d.	-10.2 ± 2.3	0.018
50 nm + mPEG	0	78.8 ± 3.1	72.0 ± 1.7	-5.7 ± 1.1	-
50 nm + 20 Tf	n.d.	78.1 ± 2.8	69.7 ± 2.3	-5.3 ± 2.0	0.89
50 nm + 200 Tf	107.3	85.4 ± 2.9	73.3 ± 2.1	-6.3 ± 0.4	0.014

Table 3.1. Nanoparticle formulations and characterizations.

Methods

Tf-PEG-OPSS Synthesis. Human holo-transferrin (Sigma, 100 mg, 2 mg/ml) was added to 8 molar excess NHS-PEG$_{5k}$-OPSS (Creative PEGworks) in a 10 mM sodium phosphate buffer, pH 9.0. The reaction proceeded for 90 minutes under gentle rocking at room temperature. Excess PEG was removed and the transferrin was concentrated in a 50 kDa MWCO centrifugal filter (Amicon, Millipore) after which the monoPEGylated fraction was separated by HPLC (1200 series, Agilent, using two TOSOH TSK gel G3000swxl columns in series) followed by Hydrophobic Interaction Chromotography (HIC) (using an AKTA prime plus FPLC system (GE Healthcare) and a 5 ml HiTrap Phenyl column (GE Healthcare)). HIC was run with a high salt buffer of 1 M Ammonium Sulfate with 50 mM Sodium Phosphate (pH 7.0), and a low salt buffer of the former only. MonoPEGylated fractions from HIC were confirmed by Matrix Assisted Laser Desorption Ionization Time-Of-Flight mass spectroscopy – MALDI-TOF (Voyager DE PRO PerSeptive Biosystems) using a sinapic acid matrix. Iron citrate (2.5 mole excess) in 100 mM sodium bicarbonate was added to the monoPEGylated fraction and

incubated with gentle stirring for 2.5 hours at room temperature. The excess iron was removed with six washes of 100 mM sodium bicarbonate through a 50 kDa centrifugal filter. The iron loading content of transferrin was measured by UV-VIS through the ratio of A_{465}/A_{280} and was compared to the same ratio of the original non-processed holo-transferrin. A_{465}/A_{280} ratios above 0.8 were considered to be adequate evidence for iron loading. Tf-PEG-OPSS was stored at 4 ^{o}C in a 50 mM sodium bicarbonate buffer pH 8.0.

Au-PEG-Tf Synthesis. Tf-PEG-OPSS was added in the indicated molar fraction (e.g. 10 mole excess transferrin added to gold for a 10 transferrin per particle formulation) to gold cores of 5 nm, 20 nm, and 50 nm (BBI International). The reaction was stirred for at least 90 minutes, and a large excess (~10,000 molar excess) of 5 kDa mPEG-SH (Laysan Bio) was added for a remaining 90 minutes. The resulting 45 nm and 80 nm nanoparticles were pelleted at 20,000 g for 10 minutes, and the pellets were resuspended in 1 ml of water, sonicated for 10 minutes, and repelleted. This washing procedure was repeated two times. In lieu of centrifugation for the 20 nm nanoparticles, a 100 kDa MWCO spin filter (Amicon) was used to removed excess PEG and concentrate the nanoparticles.

Dynamic Light Scattering (DLS): Particle sizes and zeta potentials were measured with a Brookhaven Instruments DLS and ZetaPALS. Hydrodynamic diameters were measured in PBS and averaged from three runs at two minutes each. Zeta potentials were run in 1.5 mM KCl (pH 7.0) and averaged from three runs at a target residual of 0.02. Measurements were reported as the average +/- one standard deviation.

Nanoparticle Tracking Analysis (NTA): NTA measurements were performed with a NanoSight NS500 (NanoSight). All measurements were taken in 50 mM sodium phosphate (pH 7.0) over a time of 60 s with manual shutter and gain adjustments. The data is reported as the mode with one standard deviation of three runs on the same sample.

Nanoparticle-Cell Binding Assay. Neuro2A cells (ATCC) were cultured for at least one week in DMEM, 10% FBS and PEN/STREP. Cells were washed once with cold PBS, scraped from the flask and suspended in cold PBS, fixed for 15 minutes in cold BD Cytofix (BD Biosciences) and resuspended in PBS with 4% BSA. Increasing concentrations of nanoparticles were incubated with 5 x 10^6 cells at 2.5 x 10^7 cells/ml for 90 minutes. Cells were pelleted at 300 g for 4 minutes, the supernatant/nanoparticles were removed, and the cells were resuspended in PBS. Post incubation with the gold nanoparticles, the cells were washed twice with 15 ml of PBS, stained with silver enhancement solution, and measured for gold content in a 96 well plate reader (Tecan, Infinite M200) (Excitation – 310 nm, Emission – 400 nm). The data were fit to a Langmuir binding isotherm with B_{max} and K_d nonlinearly fit with Matlab nlinfit.

Nanoparticle Transferrin Content. Iron was dechelated from Tf-PEG-OPSS by incubating in sodium maleate solution (pH 5.0) for one hour and removing unbound iron with 50 MWCO spin filters (Amicon). Iron removal was confirmed by measuring A_{465}/A_{280} and comparing to A_{465}/A_{280} of holo-transferrin. Tf-PEG-OPSS was resuspended in 50 mM sodium bicarbonate (pH 8.0) to which 4 mCi of ^{64}Cu (obtained from Isotope Production Group at Washington University, Saint Louis) was mixed and incubated for 90 minutes at room temperature. Tf-PEG-OPSS was concentrated in the 50

MWCO spin filter, and unbound copper was removed with a citrate based (pH 7.0) Micro Bio-Spin column (Bio-rad). ^{64}Cu labeling of transferrin was tested and confirmed by instant thin layer chromatography (ITLC) (Biodex, Tec-Control). The concentration of the radiolabeled Tf-PEG-OPSS was determined using a Nanodrop 2000 (Thermo), and the Tf-PEG-OPSS was stirred at room temperature with the indicated ratio of gold nanoparticles for at least one hour. Unbound transferrin was removed by pelleting the nanoparticles through centrifugation and removing the transferrin-laden supernatant. The nanoparticles were sonicated and washed with 1.5 ml of water. Gamma Activities of each particle formulation were counted with a gamma counter (Wizard, Perkin Elmer) and a standard curve of Tf-PEG-OPSS was generated to determine the bulk amount of transferrin attached to the gold.

Discussion and Conclusion

A well-defined set of nanoparticles was created that is critical for clearly understanding the *in-vivo* studies that follow. Dynamic Light Scattering was employed with nanoparticle tracking analysis to size the nanoparticles, and the results obtained from these two modalities yield sizes that are essentially the same. NTA demonstrated that the nanoparticle population was unimodal (only one size of nanoparticle present in each formulation), which gave confidence the DLS measurement were within reason. Zeta potentials as measured by Brookhaven's ZetaPals were all within -5 mV to -15 mV and satisfy the requirement that the nanoparticles be slightly negative to near neutral, to avoid blood-brain barrier disruption, protein corona formation, and MPS uptake.

Also, NTA zeta potential analysis gave first insights into the distribution of transferrin over the associated nanoparticle population. A unimodal Poisson distribution

was seen across each nanoparticle formulation. This is important to assure the zeta potentials and transferrin content of the nanoparticle population is homogeneous and that the nanoparticles within the population will act similarly in crossing the blood-brain barrier.

Nanoparticle transferrin content was directly measured by labeling transferrin with positron emitting ^{64}Cu, formulating the nanoparticles with the radiolabeled transferrin, and measuring the nanoparticle associated gamma signal. This gave the first direct measurement of transferrin content on gold nanoparticles as previous measurements utilized methods such as ELISA that only indirectly measured nanoparticle transferrin content through mass balances [12].

Finally this was the first report of a cell binding study that utilizes silver enhancement fluorescence for quantification of nanoparticles. This binding assay has provided the first data that clearly shows an increase in binding avidity to cell-associated receptors with increasing ligand content within a nanoparticle size. These data demonstrated size effects of binding to the cell and the nanoparticle ligand content effects of binding avidity to the cell surface receptors. It was found that within the nanoparticle size range studied that nanoparticle size has a weak effect on binding, and that nanoparticle ligand content has a strong relationship with binding avidity.

References

1. Paris-Robidas, S., Emond, V., Tremblay, C., Soulet, D. & Calon, F. In vivo labeling of brain capillary endothelial cells after intravenous injection of monoclonal antibodies targeting the transferrin receptor. *Mol. Pharmacol.* **80,** 32–39 (2011).
2. Bickel, U., Yoshikawa, T. & Pardridge, W. Delivery of peptides and proteins through the blood-brain barrier. *Advanced Drug Delivery Reviews* **10,** 205–245 (1993).
3. Yu, Y. J. *et al.* Boosting brain uptake of a therapeutic antibody by reducing its affinity for a transcytosis target. *Science Translational Medicine* **3,** 1–8 (2011).
4. Davis, M. The first targeted delivery of siRNA in humans via a self-assembling, cyclodextrin polymer-based nanoparticle: from concept to clinic. *Molecular Pharmaceutics* **6,** 659–668 (2009).
5. Davis, M. E. Design and development of IT-101, a cyclodextrin-containing polymer conjugate of camptothecin. *Advanced Drug Delivery Reviews* **61,** 1189–1192 (2009).
6. Nance, E. A. *et al.* A Dense Poly(Ethylene Glycol) Coating improves penetration of large polymeric nanoparticles within brain tissue. *Science Translational Medicine* **4,** 149ra119–149ra119 (2012).
7. Lockman, P. R., Koziara, J. M., Mumper, R. J. & Allen, D. D. Nanoparticle surface charges alter blood-brain barrier integrity and permeability. *Journal of Drug Targeting* **12,** 635–641 (2004).
8. Lundqvist, M. *et al.* Nanoparticle size and surface properties determine the protein

corona with possible implications for biological impacts. *Proceedings of the National Academy of Sciences* **105,** 14265–14270 (2008).

9. Xiao, K. *et al.* The effect of surface charge on in vivo biodistribution of PEG-oligocholic acid based micellar nanoparticles. *Biomaterials* **32,** 3435–3446 (2011).
10. Montet, X., Funovics, M., Montet-Abou, K., Weissleder, R. & Josephson, L. Multivalent effects of RGD peptides obtained by nanoparticle display. *J. Med. Chem.* **49,** 6087–6093 (2006).
11. Martinez-Veracoechea, F. J. & Frenkel, D. Designing super selectivity in multivalent nano-particle binding. *Proceedings of the National Academy of Sciences* **108,** 10963–10968 (2011).
12. Choi, C. H. J., Alabi, C. A., Webster, P. & Davis, M. E. Mechanism of active targeting in solid tumors with transferrin-containing gold nanoparticles. *Proceedings of the National Academy of Sciences* **107,** 1235–1240 (2010).
13. Davis, M. E. *et al.* Evidence of RNAi in humans from systemically administered siRNA via targeted nanoparticles. *Nature* **464,** 1067–1070 (2010).
14. Dautry-Varsat, A., Ciechanover, A. & Lodish, H. F. pH and the recycling of transferrin during receptor-mediated endocytosis. *Proceedings of the National Academy of Sciences* **80,** 2258–2262 (1983).
15. Hou, S. Y., Chen, H. K., Cheng, H. C. & Huang, C. Y. Development of zeptomole and attomolar detection sensitivity of biotin−peptide using a dot−blot goldnanoparticle immunoassay. *Anal. Chem.* **79,** 980–985 (2007).
16. Choi, C. H. J., Zuckerman, J. E., Webster, P. & Davis, M. E. Targeting kidney mesangium by nanoparticles of defined size. *Proceedings of the National Academy*

of Sciences **108,** 6656–6661 (2011).

17. Perrault, S. D., Walkey, C., Jennings, T., Fischer, H. C. & Chan, W. C. W. Mediating tumor targeting efficiency of nanoparticles through design. *Nano Lett* **9,** 1909–1915 (2009).

18. Bellocq, N. C., Pun, S. H., Jensen, G. S. & Davis, M. E. Transferrin-containing, cyclodextrin polymer-based particles for tumor-targeted gene delivery. *Bioconjug Chem* **14,** 1122–1132 (2003).

19. Mangani, S. & Messori, L. EXAFS studies on copper transferrin. *Journal of Inorganic Biochemistry* **48,** 33–40 (1992).

20. Armstrong, J. K., Wenby, R. B., Meiselman, H. J. & Fisher, T. C. The hydrodynamic radii of macromolecules and their effect on red blood cell aggregation. *Biophysical Journal* **87,** 4259–4270 (2004).

21. Friden, P. M., Olson, T. S., Obar, R., Walus, L. R. & Putney, S. D. Characterization, receptor mapping and blood-brain barrier transcytosis of antibodies to the human transferrin receptor. *J Pharmacol Exp Ther* **278,** 1491–1498 (1996).

22. Jiang, W., Kim, B. Y. S., Rutka, J. T. & Chan, W. C. W. Nanoparticle-mediated cellular response is size-dependent. *Nature Nanotech* **3,** 145–150 (2008).

Chapter 4: In-vivo Blood-Brain Barrier Study of Transferrin Containing Nanoparticles*

Introduction

Recently it has been reported that antibodies with high affinity to the transferrin receptor strongly attach to the receptor and do not readily detach from the receptor and enter the brain parenchyma. It was shown that these antibodies, when designed to have reduced affinity to the receptor, can engage the receptor on the blood side of the blood-brain barrier and release from the receptor on the brain side of the blood-brain barrier [1].

Inspired by this study, nanoparticles of varying avidities to transferrin receptors were created to test whether this behavior was also true for nanoparticles targeted to transferrin receptors. Here, we report that transferrin-containing gold nanoparticles can reach the brain parenchyma from systemic administration in mice through a receptor mediated transcytosis pathway. This transport is aided by tuning the nanoparticle avidity to transferrin receptor, that is correlated to the nanoparticle size and total number of transferrin decorating the nanoparticle surface. Nanoparticles of both 45 nm and 80 nm diameter reach the brain parenchyma, and their accumulation there (visualized by silver enhancement light microscopy in combination with transmission electron microscopy imaging) is observed to be dependent on transferrin content (avidity): nanoparticles with large amounts of transferrin remain strongly attached to brain endothelial cells, while nanoparticles with less transferrin are capable of both interacting with transferrin receptor on the luminal side of the blood-brain barrier and detaching from transferrin receptor on

* Excerpts of this chapter are reproduced with permission from "Transcytosis and brain uptake of transferrin-containing nanoparticles by tuning avidity to transferrin receptor." Wiley, D. T., Webster, P., Gale, A., & Davis, M. E. *Proc. Natl. Acad. Sci. USA*. (2013).

the brain side of the blood-brain barrier. The necessity of nanoparticles to have proper avidity in order to reach brain parenchyma is consistent with recent behavior observed with transcytosing antibodies that bind to transferrin receptor [1].

Results

Accumulation of Targeted Nanoparticles in the Brain Parenchyma is Dependent on Transferrin Amount.

The formulations listed in Table 3.1 were administered to mice by lateral tail vein injection. One mouse was injected per each formulation of the ca. 20 nm nanoparticles (after analysis of the tissues (vide infra) a decision was made not to inject additional mice with these formulations because the resulting images were conclusively negligible relative to the images taken of the ca. 45 nm and 80 nm nanoparticle treated mice). Three mice were injected per 45 nm and 80 nm formulations, and at eight hours post injection the brains were resected and processed for silver enhanced imaging.

Nanoparticles in the parenchyma of each image were quantified and compiled into the box plots of Figure 4.1a. These data illustrate how nanoparticle accumulation in the brain parenchyma was altered by both nanoparticle size and transferrin content. Nanoparticles in the 45 nm and 80 nm size range were observed in the brain parenchyma, and statistically significant maximums were obtained within the formulations studied for both sizes. Nanoparticles of ca. 20 nm as well as all formulations with mPEG-only were not clearly seen in the parenchyma.

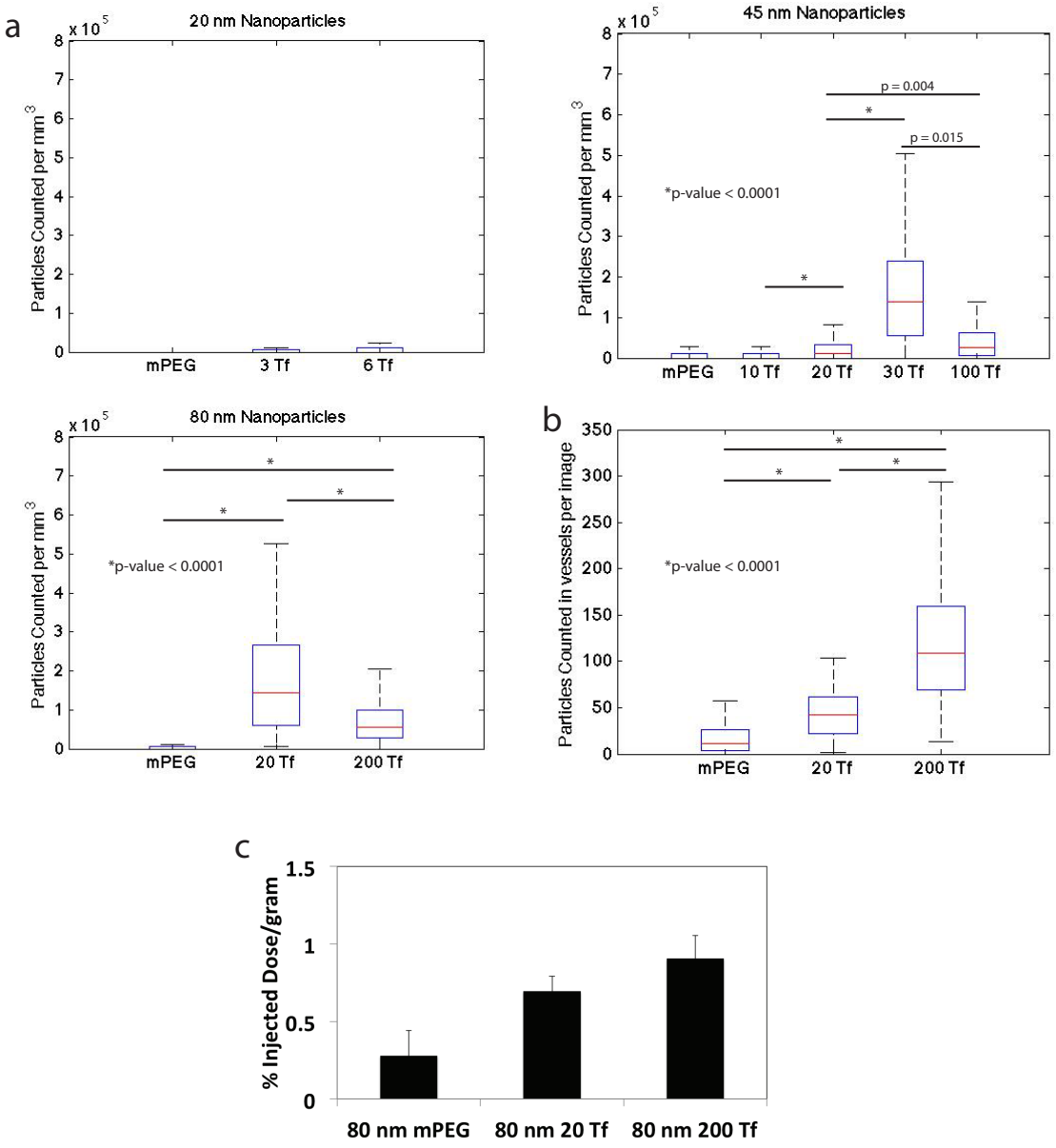

Figure 4.1: **a**, Quantitation of the nanoparticles observed in the brain parenchyma after tail vein injection. **b**, Quantitation of 80 nm formulations in the blood vessels. p-values calculated from non-normal distributions by Mann-Whitney U test (Wilcoxon rank sum test) of compiled data from all mice investigated in each nanoparticle formulation. **c**, ICP-MS data of bulk brain gold content from the 80 nm formulations.

In some regions of a few tissue sections, silver enhancement deposited in a pattern that we classified as not specific to nanoparticles. Also, several areas with silver enhancement characteristic of nanoparticles were observed and classified as not due to

receptor-mediated transcytosis (Figure 4.2). These events were documented but not included in the quantitative analysis. One brain from a mouse not injected with nanoparticles was stained with hematoxylin and silver enhancement solution, and some background signal due to silver enhancement was rarely seen in this section (Figure 4.3). These non-specific events due to silver enhancement are clearly distinguishable from signal in the parenchyma due to gold nanoparticles.

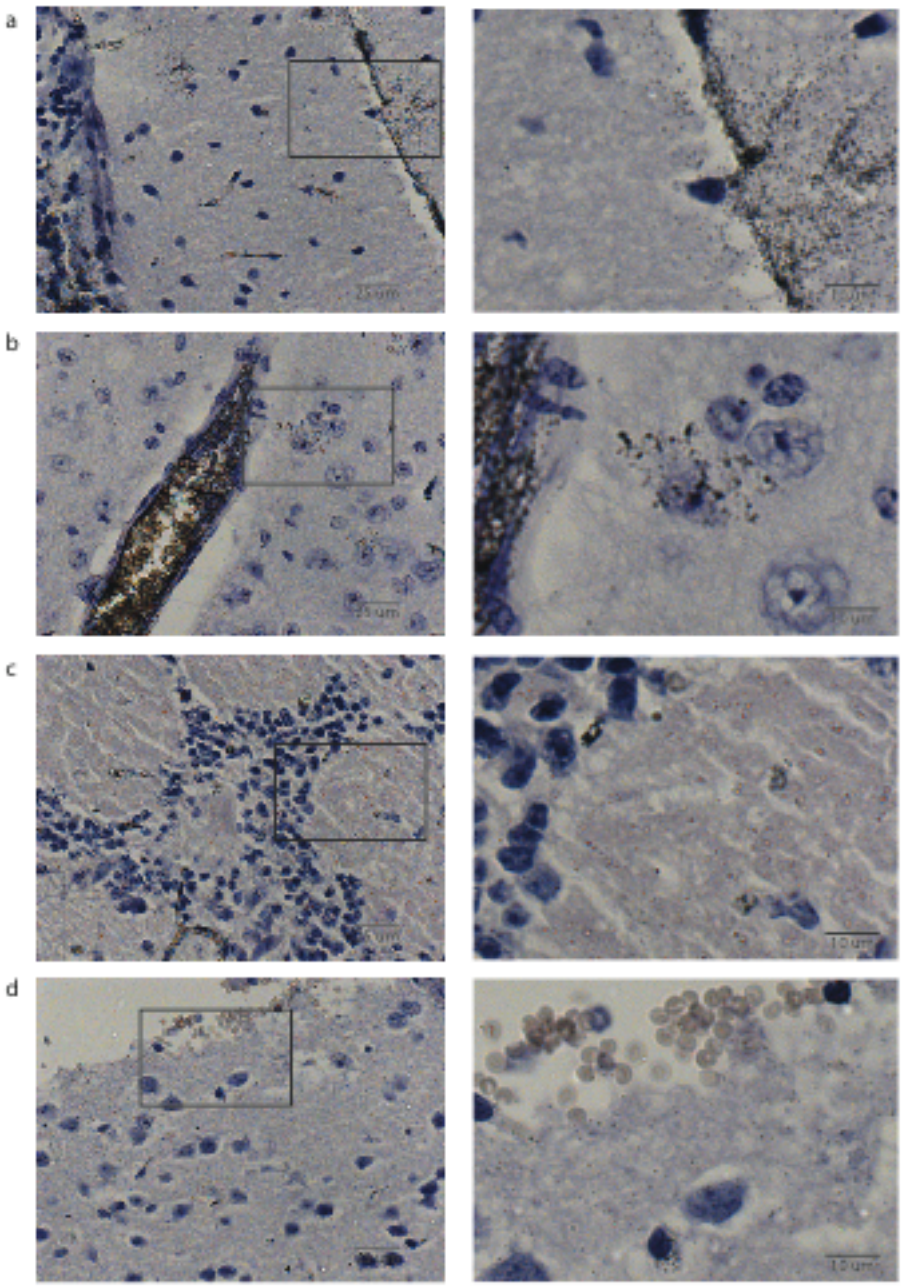

Figure 4.2: Examples of silver enhancement signal observed in the brain parenchyma that were not considered to be specific to nanoparticle accumulation due to receptor mediated transcytosis. **a**, Some large vessels had an excessive amount of silver enhancement signal adjacent to the vessel; likely due to tissue processing. **b**, Rarely, blotching was seen (also seen in the untreated brain) due to silver enhancement deposition in the tissue. **c**, A silver enhancement signal unique to the rostral cortex, the olfactory glomerulus, and the cerebellum was observed in some (but not all) sections. When this staining pattern was seen it was difficult to identify nanoparticles, and therefore these nanoparticles were not included in the quantitative analysis in order to avoid miscounting. **d**, At some of the

bordering regions of the brain (both in the ventricles and outer periphery of the brain) silver enhancement signal that looked to be from gold nanoparticles was present. It was not certain this signal was from receptor mediated transcytosis or artifact from tissue processing, and therefore was not included in the quantitative analysis.

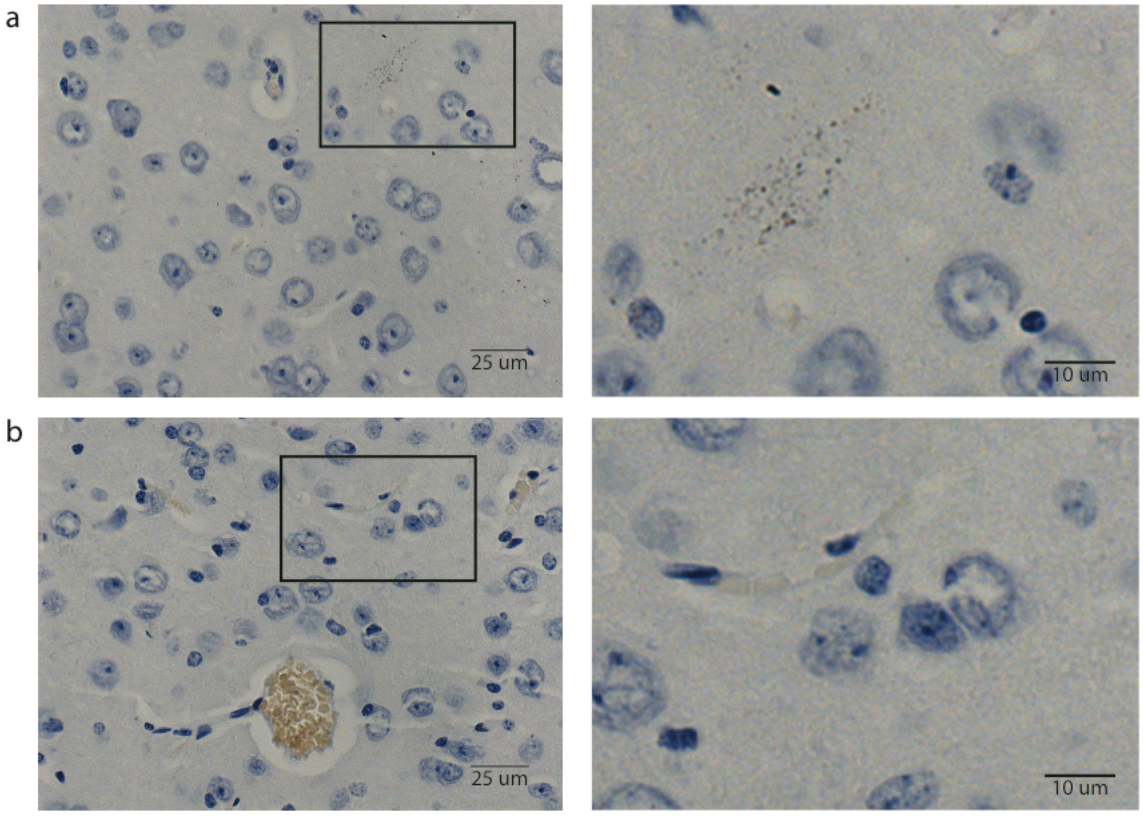

Figure 4.3: Images from the brain of the untreated mouse. **a**, Very rarely, some silver enhancement deposited in the tissue resulting in non-specific blotching. **b**, Most of the brain is clean of silver enhancement deposition in the large vessels, capillaries and parenchyma.

Figure 4.4 presents representative images from a number of the formulations studied (full, unmagnified images can be seen in Figures 4.6-4.8). Vessel staining is most clear in the images of nanoparticles of the ca. 20 nm formulations that remain largely in the vasculature (vessels stained black with a lack of clearly visible nanoparticles outside the vasculature). The images of the 45 nm, 30 Tf and 80 nm, 20 Tf formulations are representative of the majority of images taken with clear nanoparticle signal in the parenchyma. The arrow in the 80 nm, 200 Tf image points to a nanoparticle that is out of

focus. Within 5 μm tissue sections, it was impossible to consistently take images where all nanoparticles were in focus. These out-of-focus nanoparticles were also included in the quantitative analysis.

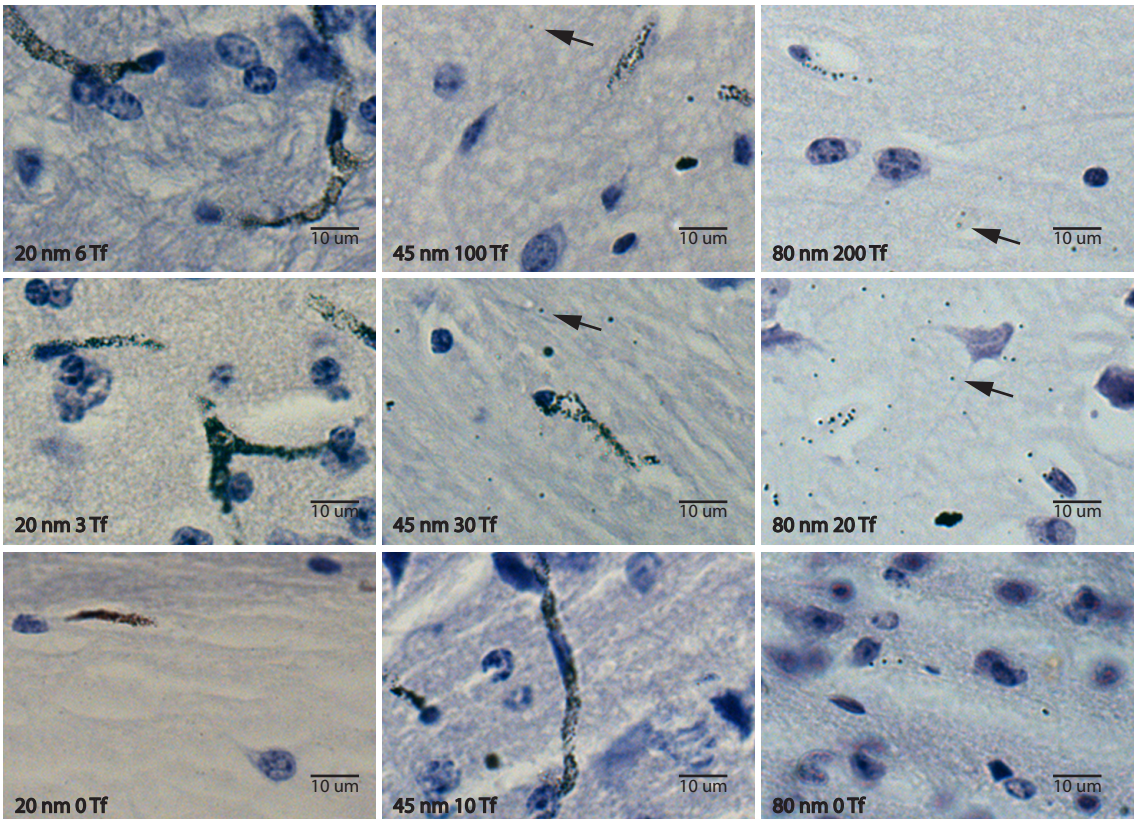

Figure 4.4. Sample images from hematoxylin stained and silver enhanced brain sections. Included are images from a range of nanoparticle formulations injected systemically with brains resected and processed eight hours later. Black arrows accentuate clearly visible nanoparticles. Left column: 20 nm nanoparticles with 6 Tf, 3 Tf, and no Tf (images from top to bottom). Center column: 45 nm nanoparticles with 100 Tf, 30 Tf, and 10 Tf (images from top to bottom). Right column: 80 nm nanoparticles with 200 Tf, 20 Tf, and no Tf (images from top to bottom).

High Transferrin Content Nanoparticles Have Increased Association with Brain Endothelial Cells.

High binding avidity with high nanoparticle transferrin content reduces the parenchymal accumulation of the 45 nm and 80 nm nanoparticles (Table 3.1, Figures 4.1 and 4.4). Additionally, high avidity 80 nm nanoparticles (with 200 Tf) consistently

remained associated with the blood vessels more than the untargeted 80 nm nanoparticles. To quantify this phenomenon, at eight hours post injection we homogenized two brains containing mPEG-only nanoparticles and three brains each of the 80 nm nanoparticles containing 20 Tf and 200 Tf, and we measured the total brain gold content by ICP-MS (Figure 4.1c). Additionally, the 80 nm nanoparticle silver enhancement signal appeared discrete in the blood vessels (unlike the continuous signal of the 20 nm and 45 nm nanoparticles in the vessels), and this vessel-associated nanoparticle signal was quantified for each 80 nm formulation and the data compiled in Figure 4.1b.

Consistent with the vessel-associated nanoparticle content quantified from the images, more gold was detected in the bulk brain (vessels and parenchyma) with higher nanoparticle transferrin content by ICP-MS. The combination of the vessel analysis, ICP-MS analysis, and the parenchymal quantitative imaging analysis indicates more 80 nm nanoparticles remain in the bulk of the brain with increasing transferrin, not because they are entering the brain parenchyma, but because they are largely stuck in or on the endothelial cells of the vasculature.

TEM Images Show that Nanoparticles Undergo Receptor Mediated Transcytosis and are Present in Brain Parenchyma.

The 80 nm formulations accumulated in the brain to the greatest extent, so these nanoparticles were chosen for additional TEM analysis (Figure 4.5). All sample images were taken from the cerebral cortex. No untargeted 80 nm nanoparticles were found in the endothelial cells or brain parenchyma after several hours of imaging, though they were seen in the vessel lumen – consistent with the light microscopy data. Nanoparticles

with low (20Tf/nanoparticle) and high (200 Tf/nanoparticle) amounts of transferrin were both observed in endothelial cells, as well as in the parenchyma (Figures 4.5a-d). Nanoparticles visualized inside endothelial cell vesicles (e.g., Figure 4.5b), suggest a trans-cellular route of delivery to the brain parenchyma. Untargeted nanoparticles were not observed inside endothelial cells, and all 80 nm formulations had similar zeta potentials, suggesting that the transferrin coated nanoparticles entered into the endothelial cells via a transferrin receptor-mediated process. Note the reduced quality of tissue microstructures in these images that can be attributed to the method of tissue processing needed to see extracellular nanoparticles (mice underwent CO_2 asphyxiation followed by brain resection and immediate submersion in formalin solution). Higher quality cellular microstructures are preserved with a perfusion fixation technique (Figures 4.5e-i).

Nanoparticle-associated toxicity has been suggested to degrade the blood-brain barrier [2], that may be a contributing factor to nanoparticle access to the brain parenchyma. Cardiac perfusion-fixation with a solution of fixative containing blood-brain barrier impermeable TEM contrast agent lanthanum nitrate has previously been used to ensure the blood-brain barrier integrity is intact [3]. Each 80 nm nanoparticle formulation was injected, and cardiac-perfusion fixation was performed eight hours post injection. In all three brains, lanthanum remained exclusively within the vasculature (strongly staining glycocalyx on the surface of the endothelial cells with partial interendothelial cleft staining) and no sub-endothelial staining was seen (e.g., Figure 4.5f-g). Additionally, no nanoparticles were observed in the lumen of the vessels after vascular perfusion, though transferrin coated nanoparticles were again localized in the endothelial cells and parenchyma (Figure 4.5h-i). The blood-brain barrier therefore

remains intact and is not permeabilized to large ions after exposure to the 80 nm gold nanoparticle formulations. An intact blood-brain barrier that only allows transferrin-associated nanoparticles to reach the parenchyma demonstrates the transferrin targeted nanoparticles reach the brain through a receptor-mediated transcytosis pathway.

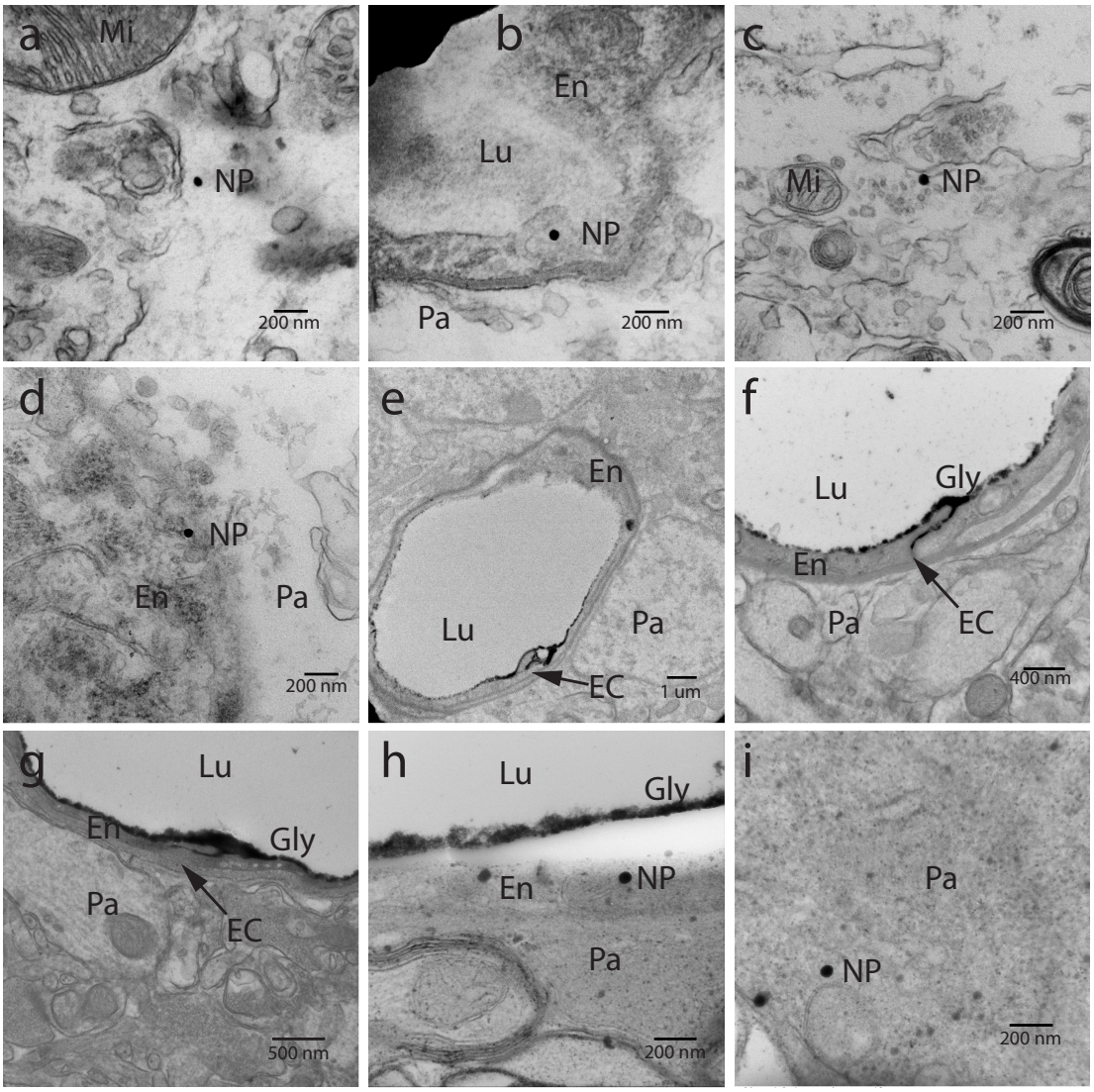

Figure 4.5. (Mi-Mitochondria, Lu-Lumen, En-Endothelial Cell, Pa-Parenchyma, EC-Endothelial Cleft, NP-Nanoparticle, Gly-Glycocalyx) a, 80 nm, 20 Tf nanoparticle in the parenchyma. b, 80 nm, 20 Tf nanoparticle inside a vesicle of the blood-brain barrier endothelial cell. c, 80 nm, 200 Tf nanoparticles in the parenchyma. d, 80 nm, 200 Tf nanoparticle near the basal surface of an endothelial cell. e, Perfusion fixation with lanthanum nitrate showing lanthanum penetrating the interendothelial cleft with no subendothelial staining. f,g, 80 nm particles injected followed by perfusion fixation eight hours post injection. Both the 20 Tf/Au formulation (f) and the 200 Tf/Au formulation (g) do not degrade the blood-brain barrier tight junctions to lanthanum nitrate as the same interendothelial cleft penetration with no subendothelial staining is seen. h, 80 nm, 200 particle inside, and near the apical surface of the endothelial cell. (Note: The lanthanum nitrate-stained glycocalyx separated from the cell surface due to the use of the electron beam during imaging.) i, 80 nm, 200 Tf particle found within the brain parenchyma after perfusion fixation.

Methods

Animal Studies. All animals were treated according to the NIH Guidelines for Animal Care and Use as approved by the Caltech Institutional Animal Care and Use Committee. Female Balb/c mice (Jackson Laboratory) received i.v. doses of nanoparticles in 150 ul of PBS through the lateral tail vein. Injected doses were as follows: 20 nm gold = 5×10^{13} nanoparticles/mouse, 45 nm gold = 2.9×10^{12} nanoparticles/mouse, 80 nm gold = 4.5×10^{11} nanoparticles/mouse. When processing for light microscopy and TEM imaging, the mice were euthanized by CO_2 overdose. For TEM perfusion fixation analysis, mice were deeply anesthetized with 3% isoflurane, the skin over the ventral thorax was incised and the thorax opened to expose the heart. The right atrium was clipped and the left ventricle was perfused with 10% sucrose followed by the fixative (4% paraformaldehyde, 0.05% glutaraldehyde, 5% lanthanum nitrate in 100 mM sodium cacodylate buffer, pH 7.2) at 300 mm Hg using a Perfusion One perfusion pump system (Leica Neurolabs). After fixation, the brain was removed and placed in 4% paraformaldehyde for further tissue processing.

Transmission Electron Microcopy: 500 μm vibratome sections were additionally fixed in 2.5% glutaraldehyde (in 0.1 M sodium cacodylate, pH = 7.4) for 2 hours, stained by 1% OsO_4 on ice for two hours, and 0.9% OsO_4 and 0.3% $K_4Fe(CN)_6$ at room temperature for 2 hours. Gradual dehydration with ethanol and propylene oxide enabled tissue embedding in Epon 812 resins (Ted Pella). Vibratome sections of the fixed brains were flat embedded in order to select specific regions of the brain for further sampling. Cerebral sections of the brains were cut from the epoxy block with a diamond wire hand saw and re-embedded in epoxy resin for ultramicrotome sectioning. 180 nm thick

sections were deposited on carbon and formvar-coated, 200-mesh, copper grids (Electron Microscopy Sciences) and stained with 3% uranyl acetate and Reynolds lead citrate (15 minutes each) for visualization under a 80 kV TF30UT transmission electron microscope (FEI, Tecnai).

Light Microscopy: Resected tissues were fixed in fresh 4% paraformaldehyde (in PBS pH 7.0) overnight, dehydrated in increasing concentrations of ethanol (3 x 30 minutes each), equilibrated in xylenes (3 x 30 minute washes) and equilibrated in 50% xylene/50% molten paraffin (30 minutes). The tissues were placed in pure molten paraffin (3 x 1 hour), placed in a paraffin mold, allowed to cool, and 5 μm sections were obtained. Sections were deparafinized with xylenes, rehydrated with serial dilutions of ethanol. To visualize gold nanoparticles, the silver enhancement kit for light and electron microscopy (Ted Pella) was used as indicated by the manufacturer – silver enhancement was allowed to incubate on the tissue section for approximately 20 minutes. After hematoxylin counterstaining, the sections were re-dehydrated with ethanol and xylenes, and mounted with Permount (Fisher). All light microscopy images were taken on an Olympus IX50 microscope with a 40x objective using QCapture Pro imaging software (QImaging).

Image Analysis, Particle Counting, and Statistics: All images were taken from sections as close to the mid sagittal plane as possible (one section imaged per brain). 40 images were taken of each tissue section, with images taken from throughout four regions of the brain (10 images per region): rostral, dorsal, and ventral regions, and the cerebellum. Within each region the images were acquired with a sequential random sampling method: beginning from a randomly chosen starting point images were taken at

set intervals using transverse scans that spanned most of the tissue section. Nanoparticles visualized in the parenchyma and 80 nm nanoparticles visualized in the vessels were manually counted and the data was binned in Matlab. Pairwise comparison groups (e.g. 80 nm 20 Tf vs. 80 nm 200 Tf) of the non-normal distributions were analyzed for statistically significant differences using a Mann-Whitney U test (Wilcoxon rank sum test) and p-values reported in Figure 4.1. Image brightness and contrast were adjusted using "Levels" and "Curves", and all adjustments were applied to the whole image. In some instances (H&E images), color was adjusted using "Levels" to match the other images in the figure. This adjustment was applied to the whole image. All adjustments were made using Adobe PhotoShop.

ICP-MS. Brains were microwaved in aqua regia (70% HNO_3 and 30% HCl in a 3:1 volume ratio) until they were fully homogenized. 20.5 mL of deionized water were added and the sample was centrifuged at 3200 g for 15 min to remove cell debris. The supernatant was analyzed for gold content using an HP 4500 ICP-MS (Agilent). Nebulization occurred with a flow of 1.3 L/min of argon using a Babbington type nebulizer in a Pyrex Scott-type spray chamber. The argon plasma power was 1200 W with a flow of 15 L/min and an auxiliary flow of 1.1 L/min. A calibration curve of various concentrations of unmodified gold nanoparticles was used to measure the gold content, using 2.5% HNO3 and 0.42% HCl as the blank solvent. Reported values are expressed as the percent of injected dose per gram of brain tissue. Error bars represent the standard error from the measurements taken from each group of mice.

Supplemental Figures

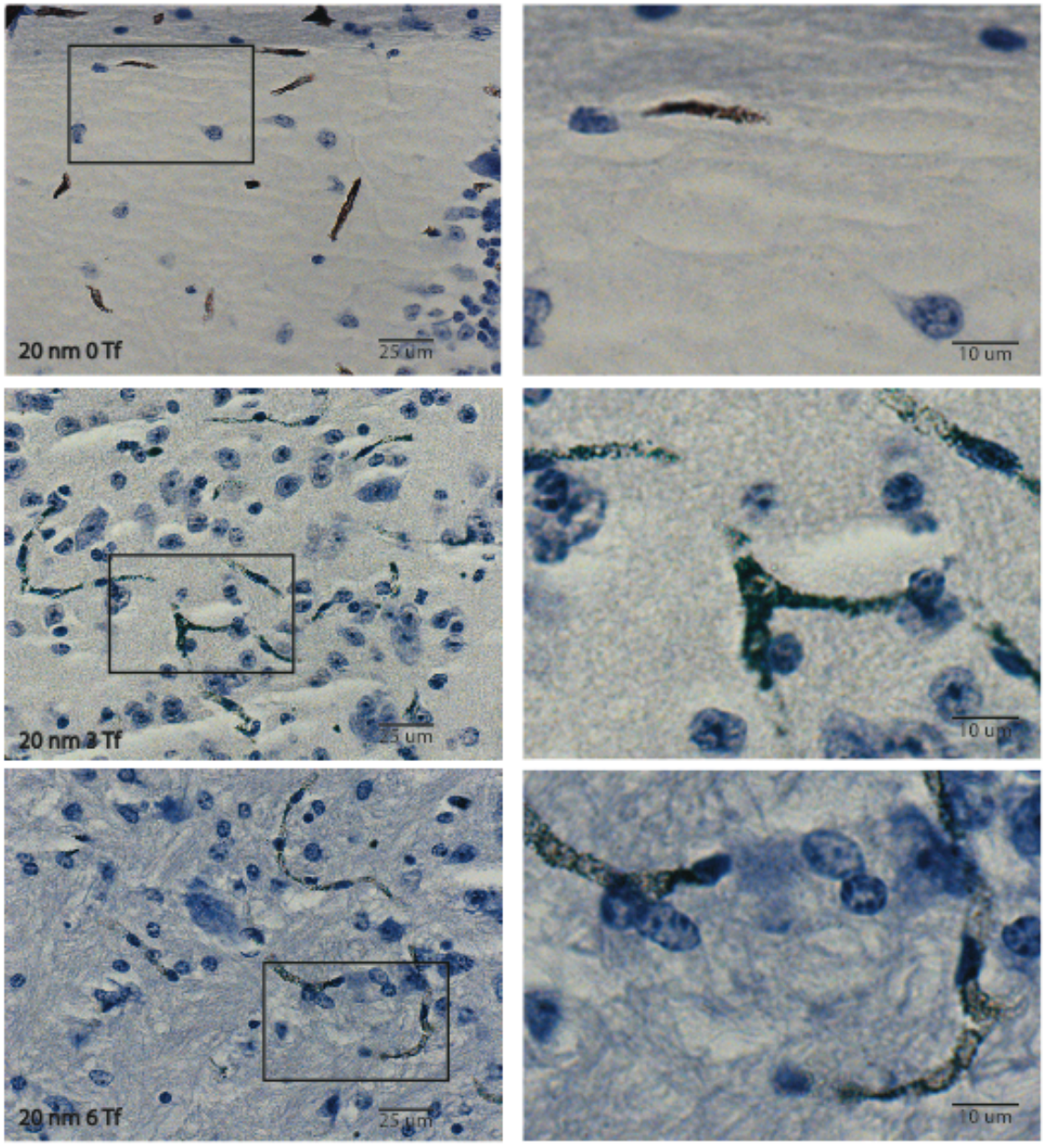

Figure 4.6. Low and high magnification images of 20 nm nanoparticles. Left column: low magnification images; right column: high magnification images. Top row: 0 Tf; center row: 3 Tf; bottom row: 6 Tf.

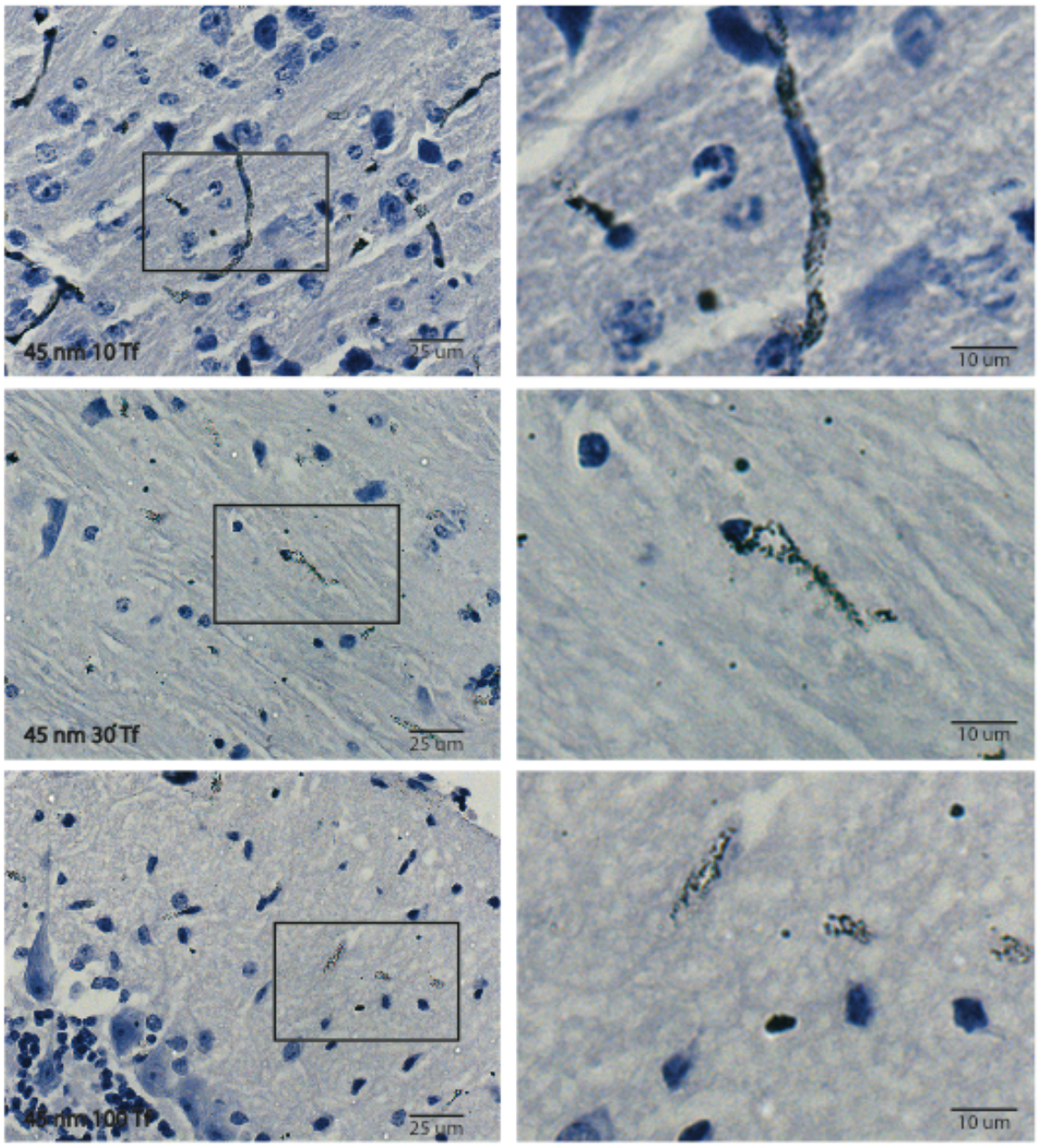

Figure 4.7. Low and high magnification images of 45 nm nanoparticles. Left column: low magnification images; right column: high magnification images. Top row: 10 Tf; center row: 30 Tf; bottom row: 100 Tf.

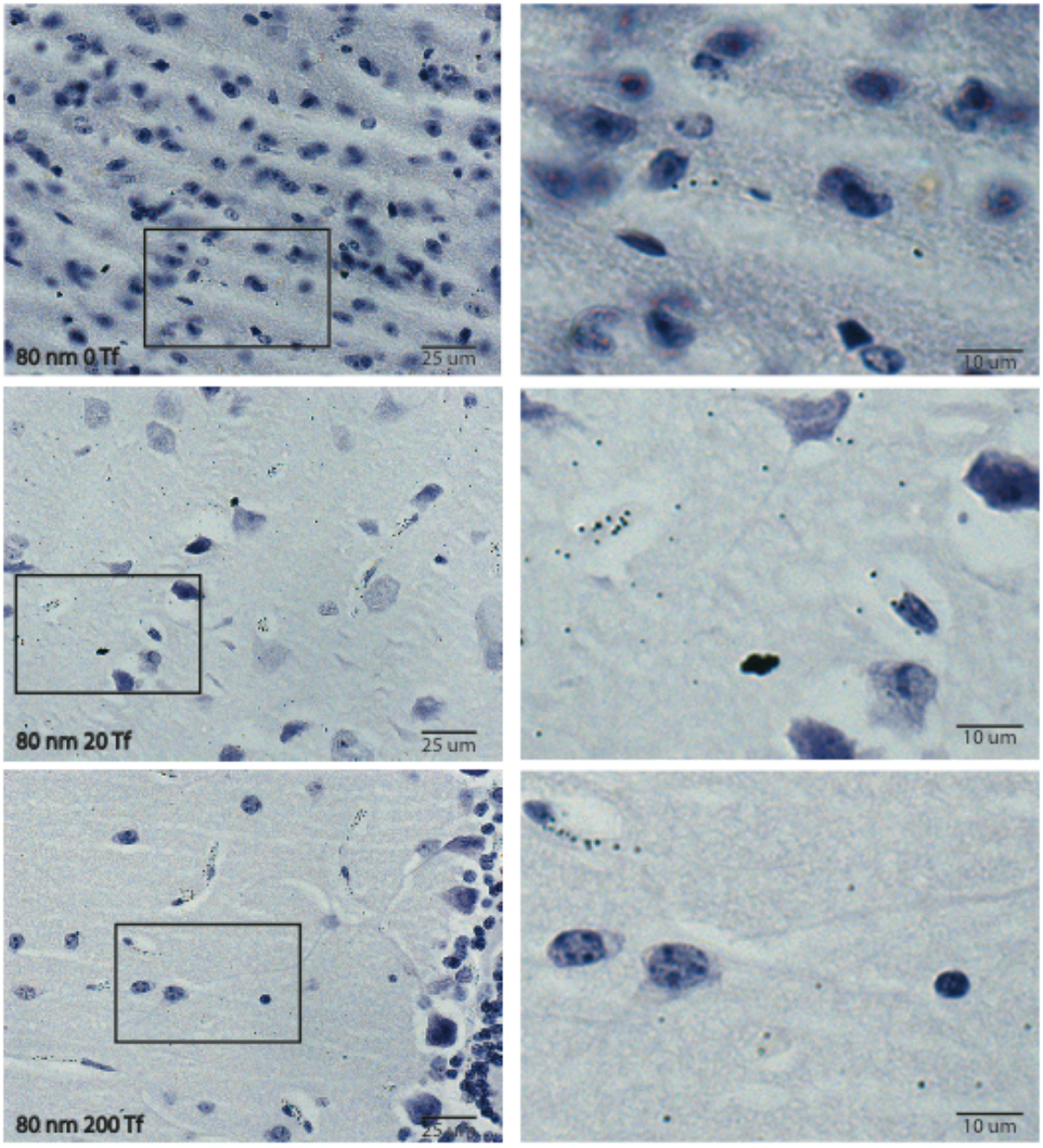

Figure 4.8. Low and high magnification images of 80 nm nanoparticles. Left column: low magnification images; right column: high magnification images. Top row: 0 Tf; center row: 20 Tf; bottom row: 200 Tf.

Discussion

Nanoparticles in the sub-100 nm diameter size range have now been shown to be able to move through brain tissue [4]. Thus, if these nanoparticles can transcytose across the intact blood-brain barrier, they may be very useful in delivering a broad spectrum of

therapeutic and imaging agents. Of major importance is to show that it is truly the nanoparticle that is reaching the brain parenchyma, and that it is doing so without damaging the blood-brain barrier. Motivated by the results of Yu et al. [1], and by the fact that the avidity of nanoparticles can be altered by targeting ligand choice and number density, we prepared a series of targeted nanoparticles that had a range of avidities for the transferrin receptor. The results from measuring the avidities for the transferrin receptors on Neuro2A cells showed that avidities were altered by both the nanoparticle size and the total number of transferrin molecules decorated on the nanoparticle surface. This set of targeted nanoparticles was investigated for their ability to interact with and transcytose across the blood-brain barrier in mice. Our results show that nanoparticle avidity does play a significant role in the transcytosis behavior. Nanoparticles with the highest avidities were bound to the blood-brain barrier but had reduced accumulation in the brain parenchyma relative to nanoparticles with reduced avidities. If the avidity is too low, then nanoparticles did not engage the blood-brain barrier.

The necessity for having a particular avidity to allow transcytosis of targeted nanoparticles is consistent with behavior observed with transcytosing antibodies to transferrin receptor [1]. Nanoparticles with high avidity can have similar binding dissociation constants to typical antibodies, and much like the antibodies of high affinity, these nanoparticles engage the blood-brain barrier but do not appreciably enter the brain parenchyma. Nanoparticles with lesser avidities were able to reach the brain parenchyma most likely due to the release of the nanoparticles upon transcytosis. If the avidity is too low, the nanoparticles in circulation do not engage transferrin receptors on the blood-brain barrier as the nanoparticles are likely out competed by the inherent mouse

transferrin in blood for the available transferrin receptors. These results show that targeted nanoparticles can be prepared and their avidities tuned to allow for transcytosis across the blood-brain barrier. The avidity, along with nanoparticle size and surface charge, need to be controlled in order to have intact nanoparticle transcytose across the blood-brain barrier without alteration of its properties. Currently, we are exploring these nanoparticle design rules to prepare targeted nanoparticles with therapeutic agents.

References

1. Yu, Y. J. *et al.* Boosting brain uptake of a therapeutic antibody by reducing its affinity for a transcytosis target. *Science Translational Medicine* **3,** 1–8 (2011).
2. Lockman, P. R., Koziara, J. M., Mumper, R. J. & Allen, D. D. Nanoparticle surface charges alter blood-brain barrier integrity and permeability. *Journal of Drug Targeting* **12,** 635–641 (2004).
3. Wolburg, H. *et al.* Epithelial and endothelial barriers in the olfactory region of the nasal cavity of the rat. *Histochem Cell Biol* **130,** 127–140 (2008).
4. Nance, E. A. *et al.* A Dense poly(ethylene glycol) coating improves penetration of large polymeric nanoparticles within brain tissue. *Science Translational Medicine* **4,** 149ra119–149ra119 (2012).

Chapter 5: Summary and Conclusion

Inspired by the increasing rates of brain disease morbidity and mortality the nation will face over the next 50 years, a national initiative was created to develop new strategies for treating brain diseases such as Alzheimer's disease [1, 2]. In order to successfully treat diseases of the brain, therapeutics must cross the blood-brain barrier so they can reach the site of pathology and enact a therapeutic benefit. Most therapeutics do not cross the blood-brain barrier [3], and many therapeutics currently being developed will not be successful in treating their target disease not because they lack functionality, but simply because they cannot reach the brain. As an example, dopamine cannot access the brain for the treatment of Parkinson's disease, however the dopamine analogue, L-DOPA, is able to cross the blood-brain barrier and be converted into dopamine by brain-associated decarboxylases [4, 5]. Usage of nanoparticles as drug delivery vehicles for therapeutics will allow future investigators the freedom to create new therapeutics independent of blood-brain barrier permeability considerations. These nanoparticles can encapsulate the therapeutics, and deliver them across the blood-brain barrier.

The blood-brain barrier has been a major bottleneck in the development of new therapeutics for brain diseases [3]. Nanoparticles may be able to deliver therapeutics across the blood-brain barrier regardless of the therapeutic size or chemical composition (e.g. [6]). Nanoparticles may be able to be delivered to the brain through receptor mediated transcytosis by creating nanoparticles that attach to receptors on the blood brain barrier that transcytose [7]. In this work, Ecgp96, a receptor that reportedly is only accessible from the blood at the blood-brain barrier [8] and is thought to be capable of facilitating receptor-mediated transcytosis, was studied as a receptor that could

potentially deliver nanoparticles only to the brain. Additionally, nanoparticle designs and the understanding of how to optimize these designs to facilitate receptor-mediated transcytosis across the blood-brain barrier were investigated here. Gold nanoparticles were synthesized with varying sizes and varying targeting ligand contents. The nanoparticles were systemically injected into mice in order to determine their interactions with and transcytosis behaviors at the blood-brain barrier. These studies provided information on how to properly design nanoparticles that safely and efficiently cross the blood-brain barrier.

Though many receptors have been shown to be located at the blood-brain barrier and facilitate receptor mediated transcytosis of their endogenous ligands [7, 9-14], most of these traditionally targeted receptors are accepted to be ubiquitously expressed and would indiscriminately deliver the nanoparticles into cells throughout the body. Motivated by collaborators that work on infectious diseases, focus was placed on designing nanoparticles that are inspired by bacteria that are known to cause infections of the brain (such as OmpA positive E. coli [15, 16]). A strategy was proposed to target nanoparticles to the same receptors at the blood-brain barrier that these pathogens reportedly used to cross into the brain. One such receptor associated with neonatal E. coli meningitis was E. coli glycoprotein 96 (Ecgp96) that was reported to be only accessible from the blood at the blood-brain barrier [8], and that could potentially deliver nanoparticles into and across endothelial cells only at the blood-brain barrier.

The accumulated results from the PET/CT, SPECT/CT, Fluorescence Xenogen imaging, MRI, and confocal microscopy studies indicated that Ecgp96 is located within the endothelial cells of the blood-brain barrier; however Ecgp96 is not accessible to

antibodies from the blood. PET/CT imaging demonstrated that there was no gross accumulation of antibodies to Ecgp96 in the brain, and ROI analysis confirmed that there was no measurable accumulation of antibody in the brain beyond the levels of antibody found in the blood. Confocal microscopy studies of sectioned brain tissue demonstrated that Ecgp96 did reside within the endothelial cells at the blood-brain barrier but was not located on the surface of the endothelial cells.

Because E. coli meningitis is a disease of newborn infants, SPECT/CT based biodistribution studies were performed on neonatal mice to determine if Ecgp96 was located on the endothelial cells of newly born mice. These SPECT/CT studies demonstrated that Ecgp96 was also not accessible from the blood on the blood-brain barrier endothelial cells of three-day-old mice. Most importantly it was shown that Ecgp96 cannot be accessed from the blood on blood-brain barrier endothelial cells in mice and therefore it cannot serve as a target receptor for receptor-mediated transcytosis of nanoparticles across the blood-brain barrier.

Though it was determined that Ecgp96 was not accessible from the blood, these studies provided new information about the possible pathogenesis of E. coli meningitis in newborn infants. Confocal microscopy and flow cytometry studies of cultured brain endothelial cells showed that Ecgp96 may be located on the surface of cultured cells and that the presence of OmpA in culture may increase the expression of Ecgp96 on the surface of the cells. The *in-vivo* studies demonstrate that Ecgp96 is not normally located on the surface of blood-brain barrier endothelial cells *in-vivo*, however the *in-vitro* studies suggest that the presence of OmpA positive E. coli may cause the endothelial cells to transport Ecgp96 to the cell surface, which is consistent with reports of Ecgp96

on the cell surface after loss of endoplasmic reticulum retention sequence KDEL [17]. If OmpA stimulates the expression of Ecpg96 on the surface of the endothelial cell *in-vivo,* further E. coli OmpA-Ecgp96 interactions may help facilitate the passage of the E. coli into the brain through some undetermined mechanism. Confirmatory *in-vivo* studies remain to be performed by an infectious disease lab.

In order to move forward with determining how to design nanoparticles that can cross the blood-brain barrier, a receptor was chosen that is known to exist on the blood-brain barrier and facilitate the transport of its ligand to the brain. The receptor chosen was the transferrin receptor which facilitates the transport of iron into the brain through its carrier protein, transferrin. The transferrin receptor has been used for multiple blood-brain barrier transcytosis studies of antibodies [7, 18-19] and nanoparticles [20-22]. Recently it has been reported that antibodies with high affinity to the transferrin receptor strongly attach to the receptor and do not readily detach from the receptor and enter the brain parenchyma. It was shown that these antibodies, when designed to have reduced affinity to the receptor, can engage the receptor on the blood side of the blood-brain barrier and release from the receptor on the brain side of the blood-brain barrier [19, 23].

Inspired by the antibody study, nanoparticles of varying avidities to transferrin receptors were created to test whether this behavior was also true for nanoparticles targeted to transferrin receptors. Nanoparticles of varying sizes and transferrin contents were created and their sizes, zeta potentials, transferrin contents and binding avidities to mouse cell transferrin receptors were measured. Within a nanoparticle size, it was shown that nanoparticle binding strength to mouse transferrin receptors is directly related to the transferrin content of the nanoparticle. Also, within the size range reported, it was shown

there was only a weak effect of size on the nanoparticle binding strength to the cells.

Many nanoparticle-based studies do not quantify the amount of nanoparticle that reaches the brain (e.g. [6]), and many that do utilize a capillary depletion method that does not clearly distinguish nanoparticle that remains stuck in or on the endothelial cells as opposed to nanoparticle that enters the brain parenchyma [24]. A silver-enhancement method was developed in this work that can clearly visualize nanoparticles under light microscopy and can clearly distinguish vessel-associated nanoparticles from parenchyma-associated nanoparticles. These images are taken on an appropriate size scale for counting multiple nanoparticles within a single field of view. This silver enhancement quantification method provided information on how many nanoparticles remained associated with the vessels in comparison to how many nanoparticles released from the vessels and entered the brain parenchyma. It was found that nanoparticles of both 45 nm and 80 nm diameter reached the brain parenchyma, and their accumulation there was observed to be dependent on transferrin content. Nanoparticles with large amounts of transferrin remain strongly attached to brain endothelial cells, while nanoparticles with less transferrin are capable of both interacting with transferrin receptor on the luminal side of the blood-brain barrier and detaching from transferrin receptor on the brain side of the blood-brain barrier.

The silver enhancement quantification method was also useful for counting the number of 80 nm nanoparticles that remained associated with the blood vessels after eight hours of circulation. The nanoparticles with large amounts of transferrin remained more highly associated with the vessels, which is consistent with the ICP-MS studies of the bulk brain gold content (gold in both vessels and parenchyma) that showed more

nanoparticle remained in the bulk of the brain with higher nanoparticle transferrin content. In combination these studies indicate more 80 nm nanoparticles remain in the bulk of the brain with increasing transferrin, not because they are entering the brain parenchyma, but because they are largely stuck in or on the endothelial cells of the vasculature. This finding is consistent with the analysis provided by Paris-Robidas [25] and the results of the antibody based study by Yu et al. [19].

Furthermore, TEM imaging studies of 80 nm nanoparticles demonstrated that transferrin-containing nanoparticles entered the endothelial cells of the blood-brain barrier and entered the brain parenchyma, but untargeted nanoparticles did not. A lanthanum nitrate blood-brain barrier permeability study after systemic injection of the nanoparticle formulations demonstrated that the nanoparticles did not degrade the blood-brain barrier integrity and that the nanoparticles did not access the brain through the paracellular route, but were transported into the brain through transferrin-receptor mediated transcytosis.

This study is critical for understanding how to properly design nanoparticles that can safely and efficiently enter the brain parenchyma to deliver a therapeutic payload. Most importantly, it was concluded that the avidity of the nanoparticle to the receptors must be tuned to maximize the amount of nanoparticle that reaches the brain parenchyma. This avidity can be mildly adjusted by the nanoparticle size (within the 20 nm to 100 nm size scale), and can be mainly tuned by the total ligand content of the nanoparticle.

This study also provides insight into the current state of nanoparticle delivery to the brain. Very little of the injected dose of the optimized nanoparticle formulation reached the brain parenchyma. Less than 1% of the injected dose per gram entered the

bulk of the brain as measured by ICP-MS, and only a fraction of that amount exited the vessels and entered the brain parenchyma as observed in the silver enhanced light microscopy images. These amounts are very small and consistent with the amounts of optimized antibodies that reached the brain parenchyma as reported by Yu et al. [19]. Further work needs to be done to increase the amount of nanoparticles reaching the brain.

References

1. Adamec, C. 2012 facts figures fact sheet. *alz.org* 1–2 (2012).
2. Khachaturian, Z. S., Khachaturian, A. S. & Thies, W. The draft "National Plan" to address Alzheimer's disease - National Alzheimer's Project Act (NAPA). *Alzheimers Dement* **8,** 234–236 (2012).
3. Pardridge, W. M. The blood-brain barrier: bottleneck in brain drug development. *NeuroRx* **2,** 3–14 (2005).
4. Wade, L. A. & Katzman, R. Synthetic amino acids and the nature of L-DOPA transport at the blood-brain barrier. *J Neurochem* **25,** 837–842 (1975).
5. Gilbert, J. A., Frederick, L. M. & Ames, M. M. The aromatic-L-amino acid decarboxylase inhibitor carbidopa is selectively cytotoxic to human pulmonary carcinoid and small cell lung carcinoma cells. *Clin Cancer Res* **6,** 4365–4372 (2000).
6. Ulbrich, K., Hekmatara, T., Herbert, E. & Kreuter, J. Transferrin and transferrin receptor antibody modified nanoparticles enable drug delivery across the blood–brain barrier (BBB). *European Journal of Pharmaceutics and Biopharmaceutics* **71,** 251–256 (2009).
7. Jones, A. & Shusta, E. Blood–brain barrier transport of therapeutics via receptor-mediation. *Pharm Res* **24,** 1759–1771 (2007).
8. Prasadarao, N., Wass, C. & Kim, K. Identification and characterization of S-fimbria-binding sialoglycoproteins on brain microvascular endothelial cells. *Infection and Immunity* **65,** 2852–2860 (1997).
9. Deane, R., Zheng, W. & Zlokovic, B. V. Brain capillary endothelium and choroid

plexus epithelium regulate transport of transferrin-bound and free iron into the rat brain. *J Neurochem* **88,** 813–820 (2004).

10. Burdo, J. R. & Connor, J. R. Brain iron uptake and homeostatic mechanisms: an overview. *Biometals* **16,** 63–75 (2003).
11. Pardridge, W. M., Eisenberg, J. & Yang, J. Human blood-brain barrier insulin receptor. *J Neurochem* **44,** 1771–1778 (1985).
12. Duffy, K. R. & Pardridge, W. M. Blood-brain barrier transcytosis of insulin in developing rabbits. *Brain Research* **420,** 32–38 (1987).
13. Rooy, I. *et al.* Identification of Peptide Ligands for Targeting to the Blood-Brain Barrier. *Pharm Res* **27,** 673–682 (2010).
14. Wang, X. X., Cho, Y. K. & Shusta, E. V. Mining a yeast library for brain endothelial cell-binding antibodies. *Nat Meth* **4,** 143–145 (2007).
15. Ahmed Khan, N. Outer membrane protein A and cytotoxic necrotizing factor-1 use diverse signaling mechanisms for Escherichia coli K1 invasion of human brain microvascular endothelial cells. *Microbial Pathogenesis* **35,** 35–42 (2003).
16. Wang, Y. & Kim, K. S. Role of OmpA and IbeB in Escherichia coli K1 invasion of brain microvascular endothelial cells in vitro and in vivo. *Pediatr Res* **51,** 559–563 (2002).
17. Altmeyer, A. *et al.* Tumor-specific cell surface expression of the -KDEL containing, endoplasmic reticular heat shock protein gp96. *Int J Cancer* **69,** 340–349 (1996).
18. Lee, H. J., Engelhardt, B., Lesley, J., Bickel, U. & Pardridge, W. M. Targeting rat anti-mouse transferrin receptor monoclonal antibodies through blood-brain barrier

in mouse. *J Pharmacol Exp Ther* **292,** 1048–1052 (2000).

19. Yu, Y. J. *et al.* Boosting brain uptake of a therapeutic antibody by reducing its affinity for a transcytosis target. *Science Translational Medicine* **3,** 1–8 (2011).
20. Hu, K. *et al.* Lactoferrin conjugated PEG-PLGA nanoparticles for brain delivery: Preparation, characterization and efficacy in Parkinson's disease. *International Journal of Pharmaceutics* **415,** 273–283 (2011).
21. Huang, R. *et al.* Lactoferrin-modified nanoparticles could mediate efficient gene delivery to the brain in vivo. *Brain Research Bulletin* **81,** 600–604 (2010).
22. Korkusuz, H. *et al.* Transferrin-coated gadolinium nanoparticles as MRI contrast agent. *Mol Imaging Biol* (2012). doi:10.1007/s11307-012-0579-6
23. Atwal, J. K. *et al.* A therapeutic antibody targeting BACE1 inhibits amyloid-production in-vivo. *Science Translational Medicine* **3,** 84ra43–84ra43 (2011).
24. Triguero, D., Buciak, J. & Pardridge, W. M. Capillary depletion method for quantification of blood-brain barrier transport of circulating peptides and plasma proteins. *J Neurochem* **54,** 1882–1888 (1990).
25. Paris-Robidas, S., Emond, V., Tremblay, C., Soulet, D. & Calon, F. In vivo labeling of brain capillary endothelial cells after intravenous injection of monoclonal antibodies targeting the transferrin receptor. *Mol. Pharmacol.* **80,** 32–39 (2011).